Axon Initial Segment Plasticity in Mouse Models of Amyotrophic Lateral Sclerosis

John W. Smerdon

Submitted in partial fulfillment of the requirements
for the degree of Doctor of Philosophy
in the Graduate School of Arts and Sciences

Columbia University

2019

Abstract

Axon Initial Segment Plasticity in Mouse Models of Amyotrophic Lateral Sclerosis

John W. Smerdon

Amyotrophic Lateral Sclerosis (ALS) is a debilitating and fatal neurodegenerative disease affecting upper and lower motor neurons. Though studied for over two decades since the first ALS-associated genetic mutation was discovered, researchers have yet to uncover the pathological processes that lead to progressive degeneration of motor neurons in ALS, or to develop effective treatments. One prominent hypothesis proposes that excitotoxicity caused by increased motor neuron firing plays a role in ALS pathogenesis. While prior studies reported increased action potential firing in early postnatal ALS-model motor neurons *in vivo*, it remains unknown whether the increased activity stems from increased intrinsic excitability of ALS motor neurons or from increased excitatory drive, and whether these changes are transient or persist into adulthood, when ALS symptoms emerge.

In this thesis, I circumvented the difficulties in standard measurement of electrophysiological properties of adult spinal motor neurons *in vivo* by relying on the visualization of the axon initial segment, a subcellular structure known to undergo compensatory structural changes in response to perturbations in excitatory input. I discovered that cultured motor neurons derived from stem cells of the $SOD1^{G93A}$ mouse model of ALS display shortened axon initial segments and hypoexcitable electrophysiological properties. The shortening of the axon initial segment is compensatory, as ALS motor neurons receive increased numbers of excitatory inputs and manifest increased spontaneous activity. Remarkably, similar shortening of the axon initial segment was detected in early presymptomatic spinal motor neurons *in vivo*. The shortened axon initial segment persists into the symptomatic stages and is particularly

pronounced in motor neurons containing p62 immunoreactive aggregates and neurons exhibiting swollen mitochondria, two signs of stress and neurodegeneration in the disease. Based on these observations I propose that early in the presymptomatic stages of the disease, spinal motor neurons recruit excessive excitatory inputs, resulting in their increased activity that is in part compensated by shortening of the axon initial segment. This state persists and becomes even more pronounced in motor neurons exhibiting biochemical changes preceding neurodegeneration.

While these observations support the potential role for excitotoxic stress in spinal ALS motor neurons, I paradoxically observed the opposite phenotype in ALS-vulnerable cranial motor neurons in the brainstem of the $SOD1^{G93A}$ animals, raising the possibility that the cellular stress that drives the neurodegeneration in ALS is motor neuron subtype specific.

Table of Contents

List of Figures ..... **v**

Acknowledgments ..... **ix**

Dedication ..... **xii**

Chapter 1: Introduction **1**

I. Amyotrophic Lateral Sclerosis **2**

II. Mechanisms of Pathogenesis in the SOD1^{G93A} Mouse Model of ALS **6**

III. Spinal motor neuron subtypes in ALS **10**

IV. Vulnerable and resistant populations of cranial motor neurons in ALS **16**

V. Electrophysiological Battlefield in ALS **20**

VI. The Axon Initial Segment **29**

Chapter 2: Length changes in the axon initial segment is induced prior to p62 pathology and mitochondrial swelling in a mouse model of Amyotrophic Lateral Sclerosis **35**

Summary **35**

Introduction **36**

Results **38**

Activity modifications in motor neurons induce plastic changes in axon initial segment length 38

The axon initial segment of vulnerable motor neurons shortens in presymptomatic ALS mice 41

Axon initial segment shortening succeeds spinal circuit maturation 44

Axon initial segment shortening is persistent and progressive 44

p62 pathology marks vulnerable α-motor neurons and precedes vacuole invasion of the soma 46
Increased excitation leads to early stress in ALS motor neurons 48
Discussion 50
Methods 55
Chapter 3: Heterogeneity of ALS phenotypes between cranial motor nuclei and spinal motor neurons 60
Summary 60
Introduction 61
Results 63
Dynamic and heterogeneous plasticity of the axon initial segment in cranial motor nuclei 63
p62 aggregation is heterogeneous across vulnerable cranial motor nuclei 67
ALS-vulnerable cranial motor neurons exhibit minimal somal invasion of vacuoles 69
Aggregation of misfolded SOD1 succeeds p62 pathology and accompanies somal vacuole invasion in spinal motor neurons 71
Oculomotor neurons maintain reduced SOD1 signal and resist aggregation 75
Misfolded SOD1 aggregation lines vacuoles of the neuropil in vulnerable cranial motor neurons 77
Discussion 79
Methods 81
Chapter 4: Aberrant synaptic input drives axon initial segment plasticity in an *in vitro* model of ALS 83
Summary 83
Introduction 84
Results 87

Reduction of the axon initial segment integrity *in vitro* disrupts normal action potential properties 87

Axon initial segment length correlates with action potential firing frequency in *in vitro* motor neurons 89

An *in vitro* model of ALS shows marked structural plasticity in the axon initial segment and reduction of intrinsic excitability 91

An *in vitro* model of ALS reveals an early increase in spontaneous action potential firing . 93

Spontaneous action potential output increases with maturation in *in vitro* $SOD1^{G93A}$ motor neurons 95

Increased spontaneous activity in *in vitro* $SOD1^{G93A}$ motor neurons is mediated by a cell-autonomous mechanism 97

Calcium permeability of AMPA receptors is reduced in *in vitro* $SOD1^{G93A}$ motor neurons.. 99

Increased spontaneous action potential firing is driven by increased excitatory synaptic input 103

VGluT2-possitive synapses are increased onto *in vitro* $SOD1^{G93A}$ motor neurons 105

V3 interneurons may be selectively enriched onto *in vitro* $SOD1^{G93A}$ motor neurons 107

Discussion 109

Methods 113

Chapter 5: Increasing STEM access to underprivileged high school students through the Science Matters Research Internship (SMRI) 119

Summary 119

Introduction 121

Results 124

Discussion 126

Chapter 6: Conclusions and Future Directions 127

References **137**

List of Figures

Chapter 1: Introduction

Figure 1.1: Motor neuron degeneration in Amyotrophic Lateral Sclerosis 3

Figure 1.2: Clinical and pathological phenotypes reported in the high expresser SOD1^{G93A} mouse on the hybrid B6SJL background. 5

Figure 1.3: Spinal motor neuron subtypes and their sensitivity to ALS 11

Figure 1.4: The fusimotor system 13

Figure 1.5: Spinal motor and oculomotor units 19

Figure 1.6: The axon initial segment and neuronal excitability 27

Figure 1.7: Plasticity in the axon initial segment 32

Chapter 2: Length changes in the axon initial segment is induced prior to p62 pathology and mitochondrial swelling in a mouse model of Amyotrophic Lateral Sclerosis

Figure 2.1: Activity-induced changes in motor neuron axon initial segments reflect adaptation of intrinsic excitability 40

Figure 2.2: Axon initial segment length is reduced in α-motor neurons of young adult ALS mice 43

Figure 2.3: Axon initial segment length is unchanged in α and γ-motor neurons of neonatal ALS mice, though markedly longer than their adult equivalents 45

Figure 2.4: Axon initial segment length changes are persistent in α-motor neurons of adult ALS mice and present in γ-motor neurons as the disease progresses 47

Figure 2.5: Axon initial segment shortening is an early phenotype in ALS, emerging prior to p62 aggregation and vacuolization 49

Figure 2.6: Axon initial segment shortening is restricted to motor neurons that display phenotypic markers of stress 51

Chapter 3: Heterogeneity of ALS phenotypes between cranial motor nuclei and spinal motor neurons

Figure 3.1: Visualizing cranial motor neurons in ALS 64

Figure 3 2: Changes in the axon initial segment in cranial motor neurons 66

Figure 3.3: p62 aggregation is less abundant in ALS-vulnerable cranial motor neurons as compared to spinal motor neurons 68

Figure 3.4: Vacuole localization in cranial motor neurons differs from localization in spinal motor neurons 70

Figure 3.5: Abundant vacuole formation in the neuropil of cranial motor neurons in $SOD1^{G93A}$ mice 72

Figure 3.6: A timeline of misfolded human SOD1 aggregation in spinal motor neurons of $SOD1^{G93A}$ mice 74

Figure 3.7: Misfolded human SOD1 aggregates are not present in ALS-resistant oculomotor neurons of $SOD1^{G93A}$ mice 76

Figure 3.8: Misfolded human SOD1 aggregation follows the pattern of vacuole formation found in cranial motor neurons 78

Chapter 4: Aberrant synaptic input drives axon initial segment plasticity in an *in vitro* model of ALS

Figure 4.1: Disruption of the axon initial segment alters action potential firing in motor neurons 86

Figure 4.2: Action potential firing properties effected by axon initial segment disruption 88

Figure 4.3: Axon initial segment length correlates with frequency of activity 90

Figure 4.4: *In vitro* SOD1^{G93A} stem cell-derived motor neurons exhibit intrinsic hypoexcitability and reduced axon initial segment length 92

Figure 4.5: *In vitro* SOD1^{G93A} stem cell-derived motor neurons display increased calcium transient frequency as compared to SOD1^{WT} 94

Figure 4.6: Loose patch electrophysiological recordings produce single action potential resolution and can mitigate issues that arise with calcium imaging 96

Figure 4.7: *In vitro* SOD1^{G93A} stem cell-derived motor neurons have persistently higher activity and develop higher burst frequencies 98

Figure 4-8: Increased activity in *in vitro* SOD1^{G93A} stem cell-derived motor neurons is mediated by a cell-autonomous mechanism 100

Figure 4.9: Fewer calcium-permeable AMPA channels may be present in *in vitro* SOD1^{G93A} stem cell-derived motor neurons 102

Figure 4.10: Further evidence of calcium-permeable AMPA channel reductions in *in vitro* SOD1^{G93A} stem cell-derived motor neurons 104

Figure 4.11: Increased numbers of excitatory synapses are found on *in vitro* SOD1^{G93A} stem cell-derived motor neurons 106

Figure 4.12: Increased numbers of VGluT2-possitive puncta are found on *in vitro* SOD1^{G93A} stem cell-derived motor neurons 108

Figure 4.13: *In vitro* SOD1^{G93A} stem cell-derived motor neurons exhibit axon initial segment shortening in response to enrichment of V3 interneurons in the surrounding culture 110

Chapter 5: Increasing STEM access to underprivileged high school students through the Science Matters Research Internship (SMRI)

Figure 5-1: Website for the Science Matters Research Internship 120

Figure 5-2: Sample syllabus for the SMRI Bio Bootcamp..... 123

Acknowledgments

Using bowling as a metaphor, the path I chose to get to graduate school did not resemble that perfect B-line strike right down the center of the lane. Nor was it that nice curve that swayed smoothly to one side and then gracefully drifted back to the center of the pins. No, it was more like the kind of throw a child makes with the bumpers up on the side, where it bounces back and forth until somehow finding that center pin in what looks like a feat of chance. Well, Linus Pauling once said, “The best way to have a good idea is to have a lot of ideas”. Hopefully that applies here, though a “good idea” may not be so easy to define. Nevertheless, I’ve ended up having a lot of ideas throughout my life that took me in many directions before I ended up getting to graduate school. The first of which was to become an auto mechanic after graduating high school rather than heading off to college. I have no regrets about that choice, and the knowledge I gained during that decade of my life has proven incredibly useful in and out of the laboratory. It took many years to reach the decision to go back to college though, and that brings me to my first acknowledgment, my parents and family. They have been supportive throughout all of my life decisions and I cannot thank them enough for everything they have done for me. However, I can try, so thanks to my Mom and Dad, and to my brother Jason and sister Amy!

I kicked off the transition back into academic pursuits by attending Spokane Falls Community College, at the Pullman WA campus. I thank them for their support, education, and then later employment while I finished my undergraduate degrees. Really in the end, it was the Psych 101 course I took during that first year at Community College that piqued my interest in Neuroscience, changing my course toward that discipline while at Washington State University, my undergraduate alma mater. On that note, the stellar Schools of Integrated Physiology and Neuroscience and Molecular Biosciences at WSU had a great impact on my future career in

Neuroscience, instilling an invaluable toolbox of knowledge to draw upon and I thank all of the instructors, advisors, and support staff that took part in that training.

This brings me to Graduate School at Columbia University. All of the past and present members of the Office of Graduate Affairs have provided stellar support throughout my time at Columbia. The Department of Physiology and Cellular Biophysics drew my interest in coming to perform my graduate school research and they have been amazingly supportive throughout my time here. In particular, I would like to thank all of the past and present administrative staff that has helped navigate this process, namely Karen Allis, Castalia Sanchez, Mathew Wallace, Dawn La Salle, Janice Savage and Dionida Ryce. I thank the Chair, Dr. Andrew Marks, and the graduate program directors past and present, Drs. Filippo Mancia, Jane Dodd, Ellen Lumpkin, and Henry Colecraft. Thanks also go to my cohort of Physiology and Cellular Biophysics students from 2012, Dr. Meagan Belcher-Dufrisne, Mike Holsey and Johnathan Kim. You have all been amazing friends and confidants navigating this crazy path we all have chosen!

One of my interviews on recruitment weekend was with Dr. Amy MacDermott where her excitement and expertise for electrophysiological techniques and their utility in investigating the pathophysiology of ALS shown through. She was a large part of my choice to come to Columbia and she became an unofficial co-mentor for the first two years of my graduate training. I thank her, and her lab for allowing me to come and train as an electrophysiologist. Amy, and post-doc Dr. Damian Williams patiently worked with me during weekly journal clubs and through the learning of multiple techniques to prepare me to continue electrophysiological analyses throughout my graduate career. Though Amy has retired and Damian moved on to further academic endeavors, they have continued to engage in many discussions regarding science and life, and have truly been remarkable mentors and friends.

This brings me to Dr. Hynek Wichterle, my advisor and mentor during my time at Columbia. Fortuitously, I ended up first meeting Hynek through his collaboration with Dr. Amy

MacDermott, and my subsequent interest in their project. Hynek was enthusiastic to continue our work together and I could not have been more fortunate than to have joined his lab. Not only has his enthusiasm for research been contagious, he has fostered many collaborations throughout Columbia and the broader scientific community. The broad focuses of his lab and these collaborations have provided me with exposure to a large range of techniques and input that has grown my skill and compelled me to be a more versatile scientist. I cannot thank Hynek enough for guiding my maturation as a researcher, offering superlative feedback and advice, and for providing me with the flexibility to partake in multiple endeavors. This includes the instillation of the Science Matters Research Internship, for that would not have been possible without Hyenk's support, and of course, the diligent efforts of the two other co-founders of SMRI, Drs. Katherine Xu and Elena Abarinov – I thank you both! Hynek has also aided in my development as a mentor, where I have taken on multiple interns and students over the years. In particular, I want to thank Alexandrina Danilov and Paul Kay, who were fantastic undergraduate students and who helped in the acquisition of a significant amount of data in this thesis. Finally, the Wichterle lab has provided a fantastic environment and I want to thank all of the past and present members for their support, feedback and camaraderie over the years.

I also want to thank my amazing committee members, my committee chair, Dr. George Mentis, the committee body, Drs. Franck Polleux, Neil Shneider, and Henry Colecraft and the past members, Drs. Attila Losonczy and Wes Grueber. All of my committee members have been incredibly helpful in guiding my project, providing tremendous feedback on my thesis, and building my knowledge as a scientist. I will greatly miss our fruitful discussions and the collegial environment you all created.

Lastly, I thank my wife, Dr. Kim Tjoelker. She has been a humbling source of inspiration, and her desire for knowledge has been abundantly motivating. Thank you for being my best friend, sharing a passion for life and adventure in the best of times, and helping me to laugh and love, even in the toughest of times.

For my wife, Kim,
and our families

Chapter 1: Introduction

The ultimate purpose of the central nervous system is to orchestrate precisely timed sequences of electrical signals, termed action potentials, to control voluntary movement, communicate ideas, regulate internal organs and to manifest basic instinctive behaviors. Motor neurons are the principal output unit and the final neuron in the motor circuit. Motor neurons relay signals to muscles that govern internal systems such as digestion and respiration, as well as allow movement and interactions with the outside world, controlling 320 bilateral pairs of skeletal muscles (Brooks, 2003). In order to generate the dynamic and distinct contractile properties of these muscles that are required to create a complex range of movement, specialization of the motor neurons must exist. Specialization in motor neurons is typically exposed by their patterns and speed of action potentials, and can be categorized into subtypes.

Many types of neurodegenerative diseases selectively affect particular subtypes of neurons, including Amyotrophic Lateral Sclerosis that affects subtypes of motor neurons. What drives the progressive degeneration of motor neuron subtypes remains an unanswered question for neuroscientists. Principally, it is unknown how the electrical tuning in neuronal subtypes and the neuronal constituents to which they are connected, leads to unique action potential properties and, in turn, makes them selectively vulnerable to human diseases. Although the abundant diversity in the central nervous system has made the illumination of these mechanisms a daunting undertaking, great insights have been made through studies of neuropathology, where perturbations to this finely tuned system have uncovered minute, though important physiological niches. With hope, these discoveries will lead to mechanism-based therapies and ultimately cures to these devastating diseases.

I. Amyotrophic Lateral Sclerosis

Amyotrophic Lateral Sclerosis (ALS), also known in the United States as Lou Gehrig's disease, is a devastating disorder that is clinically characterized by signs of progressive neurological deterioration of corticospinal and somatic motor neurons of the spinal cord and brainstem (Figure 1.1). ALS is typically fatal 3-5 years after symptom onset (Vucic et al., 2014), and death most often the result of denervation of the respiratory muscles (Rothstein, 2009). Although ALS was first medically described by Charcot almost 150 years ago (Vucic et al., 2014) and the first mouse model of the disease was created over 20 years ago (Gurney et al., 1994), the pathogenic pathways are still unknown and neither prophylactic nor curative treatments exist. Only two drugs for ALS are currently on the market, the first of which, Riluzole only extends life by a few months (Bensimon et al., 1994), and the second, Edaravone, shows a similarly limited treatment scope though not enough time has elapsed to understand its true effectiveness on survival (Oskarsson et al., 2018). Thousands of Americans are diagnosed with ALS each year resulting in a staggering impact on the United States economy, costing annually $256 to $433 million (Larkindale et al., 2014). According to the Centers for Disease Control, ALS prevalence in the United States was 5 cases per 100,000. Diagnosis of ALS is typically through identification of progressive weakness, spasticity, atrophy and eventual paralysis of skeletal muscles, as well as analysis of electromyograms and nerve conduction studies.

Hereditary genetic mutations account for about 10% of ALS diagnoses (familial ALS, or FALS), leaving 90% of the cases with no known genetic cause (sporadic ALS or SALS) (Li et al., 2015). Though FALS cases only account for roughly 10% of the ALS patients, there are strong links between phenotypes observed in FALS and SALS cases (Rakhit et al., 2004; Bosco et al., 2010; Haidet-Phillips et al., 2011; Guareschi et al., 2012), suggesting that treatments developed using FALS models might impact many ALS patients. More than 16 ALS-associated gene loci have been reported (Vucic et al., 2014), one of these, copper/zinc ion-binding

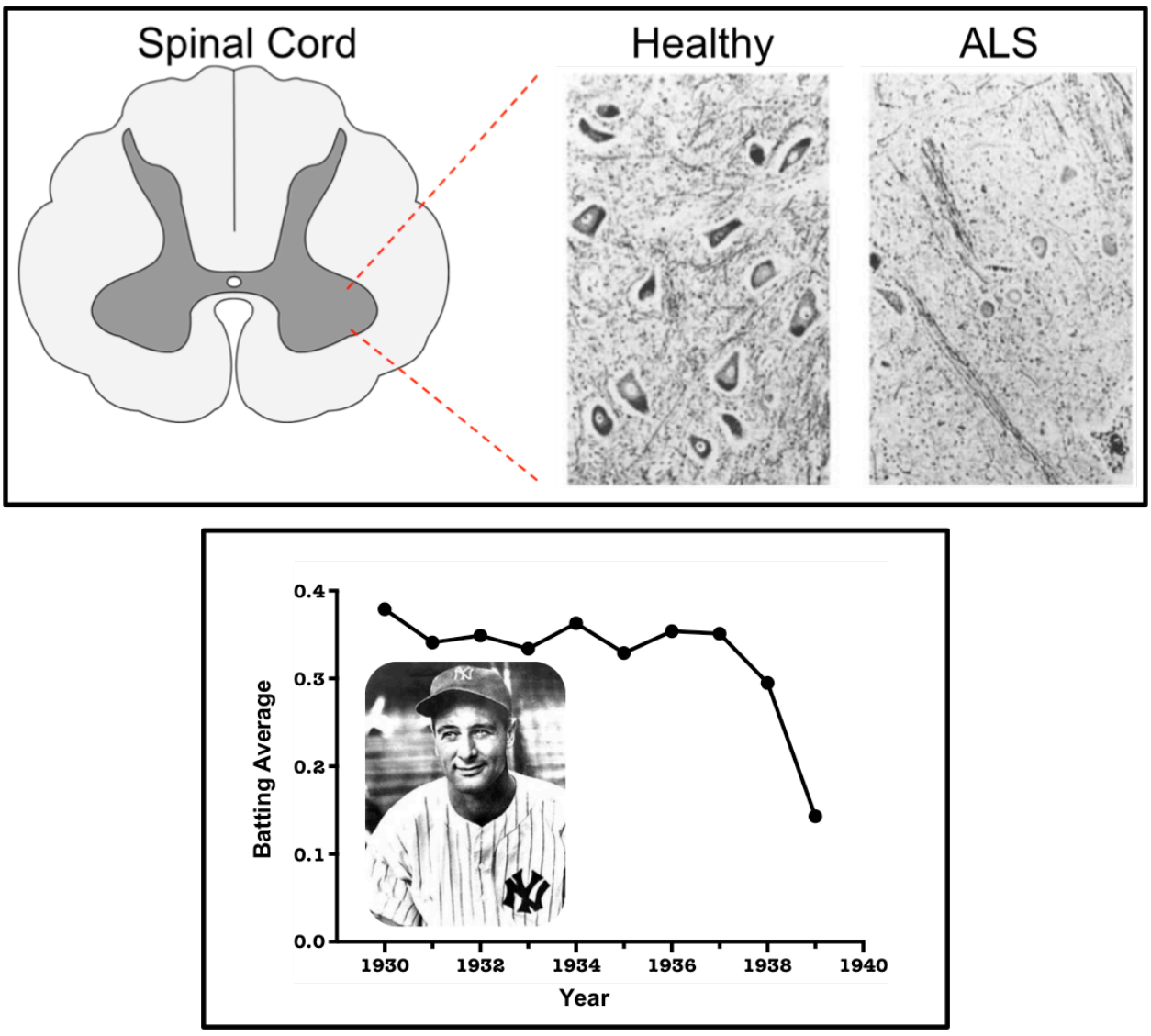

Figure 1-1: Motor neuron degeneration in Amyotrophic Lateral Sclerosis

Top – Parafin-embedded, Klüver-Barrera-stained postmortem anterior horn sections from the fourth lumbar segment of a control patient and an ALS patient (Terao et al., 1994). The large, dark cells in the control are motor neurons, clearly missing in the ALS patient.

Bottom – Yearly batting averages plotted vs. time for the last decade of Lou Gehrig's carrier. Demonstrating both the absence of symptoms prior to disease onset, as well as the rapid decline after symptom onset. Lou Gehrig succumbed to ALS in 1941.

Superoxide Dismutase 1 (SOD1) (Esteban et al., 1994; Gurney et al., 1994), has been widely studied in ALS research and accounts for 20% of the FALS cases (Kiernan et al., 2011). Over 150 mutations in SOD1 have been linked to ALS (Kiernan et al., 2011). One in particular, the glycine to alanine mutation at position 93 (G93A), was introduced in the first mouse model of ALS (Gurney et al., 1994) and is the most commonly used model for the disease (van Zundert et al., 2012). The construct in this model encoded for human SOD1 through 12-15 kb genomic fragments and was driven off of the endogenous promoter, and there are 18 copies of the transgene in the G1 mouse from the original report (Gurney et al., 1994).

Clinical events in the mice closely match those seen in ALS patients (Turner and Talbot, 2008). By 90 days of age, the mice develop tremors in their hindlimbs, as well as other locomotor shortfalls and muscle weaknesses (Figure 1.2). These symptoms progress into paralysis and death 30 days later, where postmortem analysis of the spinal cord and brainstem revel massive loss of motor neurons and reactive gliosis (Dal Canto and Gurney, 1994; Turner and Talbot, 2008). After this original mouse model was created, multiple ALS mouse models with various SOD1 mutations were created (Lutz, 2018) and all overexpressed the mutant human SOD1 gene. Though the models differ in onset, presentation and disease course, all have reduced lifespans and display clinical phenotypes of ALS, as well as undergo motor neuron degeneration, motor axon denervation, and show signs of protein aggregation.

For the $SOD1^{G93A}$ mouse, neuromuscular junctions degenerate at ~50 days and appears to first occur in fast-fatigable muscles (Kanning et al., 2010). By 80 days, 60% of the axons in the ventral root are lost and at least half of the motor neurons have degenerated by 100 days (Fischer et al., 2004). Though it is still unclear where the pathogenesis originates, the loss of the neuromuscular junction prior to complete loss of the motor neuron has helped to create a “dying-back” hypothesis. However, it is possible that denervation is a downstream event after initiation of stress in the motor neuron. There is evidence that motor neuron death is a slower event than what is seen in the canonical apoptotic or necrotic pathways, it may instead occur

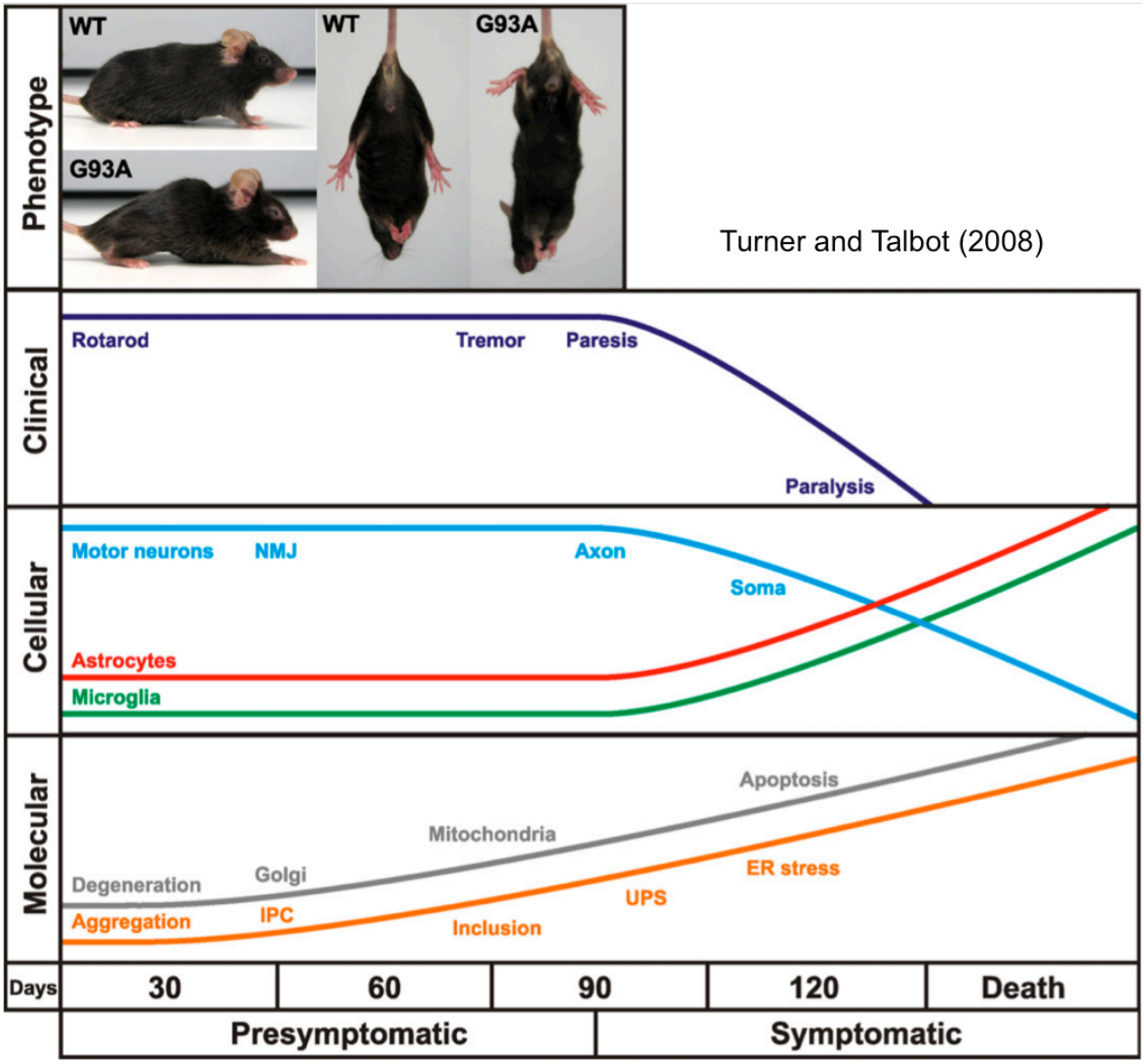

Figure 1-2: Clinical and pathological phenotypes reported in the high expresser SOD1^{G93A} mouse on the hybrid B6SJL background.

At 90 days postnatal, mice become symptomatic, presenting with tremors, weakness, and locomotor deficits. One month after symptom onset, significant muscle wasting and paralysis mark the end-stage symptoms, coupled to motor neuron lose and reactive gliosis. Preceding symptom onset, synaptic retraction from neuromuscular junctions and distal axonal degeneration is observed. As early as 30 days postnatal, increases in endoplasmic reticulum stress is observed (Saxena et al., 2009). Progressively through end-stage, mutant human SOD1 aggregation, ubiquitinated inclusion bodies, and mitochondrial dysfunction have been reported. Adapted from (Turner and Talbot, 2008).

over great amounts of time, albeit with necrotic-like signatures (Martin et al., 2007; Martin, 2010). Ultimately, these SOD1^{G93A} mice on the B6SJL hybrid background succumb to the disease at around 130 days. In the works presented in this thesis, I have used the SOD1^{G93A} mouse on the C57BL/6J inbred background that has slightly delayed disease duration where 50% survival is ~160 days, though disease onset occurs at a similar age (Kaplan et al., 2014). A caveat here is that the timeline of phenotypic presentation in the inbred line is far less well characterized, though assumed to be similar to the hybrid line.

II. Mechanisms of Pathogenesis in the SOD1^{G93A} Mouse Model of ALS

Though the pathophysiology of ALS remains unknown, many hypotheses have been proposed, however, none have lead to a clear understanding of the disease pathogenesis. Some of the difficulties arise from the inability to separate between the cell autonomous and non-autonomous mechanisms in the disease. Glial cells and inflammatory mechanisms have been implicated in ALS pathogenesis (Di Giorgio et al., 2007; Frakes et al., 2014; Re et al., 2014), evidence of non-autonomous contributions to the disease, and yet, only some motor neuron subtypes are selectively vulnerable to degeneration (Kihira et al., 1997; Lewinski and Keller, 2005; Brockington et al., 2013; Kaplan et al., 2014; Comley et al., 2015; Venugopal et al., 2015a), an indication of cell autonomous mechanisms at play. Given the high subtype specificity of the disease, where most of the neurons of the central nervous system (CNS) are spared, it may be most effective to focus on cell-autonomous mechanisms as a target for ALS treatments.

There are multiple mouse models in existence today (Lutz, 2018) that provide valuable insight to pathological mechanisms across diverse genetic backgrounds. Commonalities between these models may provide a truer picture of ALS pathogenesis. However, as these

models are relatively new, the breadth of research describing their phenotypic profiles is still far behind that of the SOD1 mouse models. For the purposes of this thesis, I will focus on the mechanisms presented in the SOD1 model. As described above, the SOD1 mouse model nicely recapitulates ALS clinical presentations. Additionally, there is hope that when the pathophysiology is uncovered in the SOD1 mouse model, it will have broader functional importance to many other types of familial and sporadic ALS cases (Rakhit et al., 2004; Bosco et al., 2010; Haidet-Phillips et al., 2011; Paré et al., 2018).

In the short few years following the initial creation of the $SOD1^{G93A}$ mouse model, it was determined that the loss of motor neurons was not due to a loss-of-function in SOD1, but instead due to a toxic gain-of-function. This was demonstrated in two seminal studies, the first of which utilized the creation of a SOD1 knockout mouse and showed that these animals maintained normal development and motor control well into adulthood and no signs of pathology in the spinal cord (Reaume et al., 1996). Nevertheless, these knockout mice notably have been shown to undergo chronic oxidative stress, where lifespan is reduced by 30% (Flood et al., 1999; Muller et al., 2006; Fischer et al., 2012). The second study utilized the $SOD1^{G85R}$ transgene on a normal mouse background, homozygous for endogenous SOD1, and on top of a $SOD1^{-/-}$ mouse (Bruijn et al., 1998) to show no difference in survival time in the two conditions. This would argue that endogenous SOD1 activity has little involvement in the pathophysiology of ALS.

As the $SOD1^{G93A}$ mutation does not effect normal catalytic activity of SOD1, one hypothesis surrounding the toxic gain-of-function has pointed to the protein becoming more susceptible to misfolding and aggregation (Banci et al., 2008). High molecular weight SOD1 aggregates are found across multiple SOD1 models and are isolated to the neuromuscular system (Bruijn et al., 1998; Wang et al., 2002; Turner et al., 2003). It was hypothesized that these aggregates are causing toxicity in ALS. Recently, it was discovered that large aggregates do not confer toxicity, instead, small soluble trimeric aggregates of SOD1 impact motor neuron

health (Zhu et al., 2018). However, it is still unclear how these moieties impart neurotoxic effects. Potential pathways may involve increased stress on the mitochondria, where SOD1 has been shown to accumulate on the membrane (Liu et al., 2004; Vande Velde et al., 2008), or on the unfolded protein response in the endoplasmic reticulum, thought to be dysfunctional in ALS (Saxena et al., 2009).

Both the endoplasmic reticulum and mitochondria have been found to swell in ALS (Kong and Xu, 1998; Martin et al., 2007), though the triggering mechanism of these events is still unknown. This swelling, which starts in the dendrites and axons, has been shown to be so severe that it creates enormous vacuoles that take up large amounts of space in the soma of motor neurons (Dal Canto and Gurney, 1994). Later in the disease course however, the vacuoles in spinal motor neurons are believed to consist mostly of swollen mitochondria (Higgins et al., 2003; Vinsant et al., 2013). Due to the control exhibited by the mitochondria and endoplasmic reticulum over reactive oxygen species and mechanisms of programed cell death, the abnormalities seen in these two organelles is of particular interest as potential initiation points of pathogenesis. It has been proposed that aggregated protein moieties discussed earlier are disrupting normal function of the mitochondria and the endoplasmic reticulum. However, greater focus has been put on intracellular calcium abnormalities and excitotoxicity. The latter will be discussed in depth in section V of this chapter, but ultimately, these mechanisms are hinged upon the importance of mitochondrial regulation of intracellular calcium (Nicholls, 2002).

Multiple signaling cascades that converge on calcium imbalance have been proposed to contribute to ALS pathogenesis. Among these, increased electrophysiological activity associated with excessive calcium loading (Olney, 1969; Blizzard et al., 2015), emerged as a potential mechanism leading to excitotoxicity and motor neuron degeneration (van Zundert et al., 2012; Vucic et al., 2014). This model is corroborated by electrophysiological analyses of both FALS and SALS human patients that exhibited increases in motor neuron activity upon

transcranial magnetic stimulation (Vucic et al., 2013). Multiple pathways have been proposed to contribute to excitotoxicity in ALS models, such as increased intrinsic excitability (Kuo et al., 2004; Vucic et al., 2008; Bellingham, 2011; Quinlan et al., 2011), decreased glutamate transport (Rothstein et al., 1992; Foran et al., 2011; Wainger et al., 2014), increased extracellular glutamate levels (Rothstein et al., 1990; Sen et al., 2005), glutamate receptor alterations (Kawahara et al., 2004; Hideyama et al., 2010), mitochondrial dysfunction (Sasaki and Iwata, 1996; Ferri et al., 2006; Igoudjil et al., 2011), and reduced calcium buffering (Reiner et al., 1995; Vanselow and Keller, 2000; Beers et al., 2001; Sasaki et al., 2006; Jaiswal et al., 2009). Targeting these mechanisms, however, did not lead to a successful therapy for ALS. Riluzole, the only known drug to extend the survival of ALS patients, does target pathways that could contribute to excitotoxicity, such as presynaptic glutamate release (Gurney et al., 1994; Bellingham, 2011), but its effects are only modest and mechanism of its action is not well understood, warranting further investigation.

It has been demonstrated that by increasing the buffering capacity of mitochondria in the motor neurons of ALS mice, motor neuron death can be rescued. However, survival in these ALS-model mice is not increased, due to continued neuromuscular junction (NMJ) retraction (Parone et al., 2013), a hallmark of ALS disease progression (Kiernan et al., 2011). This evidence supports the hypothesis that increased activity triggers ALS pathogenesis, where increased calcium buffering capabilities prevent excitotoxic death in motor neurons, yet, activity-induced distal axonopathy still occurs (King et al., 2007; Vucic et al., 2014; Blizzard et al., 2015). Furthermore, ALS-vulnerable motor neurons in the brainstem of P4-P10 $SOD1^{G93A}$ mice displayed increased spontaneous synaptic activity mediated by excitatory glutamatergic transmission (van Zundert et al., 2008), occurring months before symptom onset. The results of another study suggest that there are augmented networks that drive ALS motor neurons, leading to heightened and disordered bursting activity (Jiang et al., 2009). Though the authors postulate that decreases in inhibitory interneurons could account for their findings, an equally

plausible explanation could be an increase in excitatory input. While several studies have reported deficiencies in inhibitory input in ALS models (Lorenzo et al., 2006; Chang and Martin, 2009; 2011; Nieto-Gonzalez et al., 2011; Chang and Martin, 2014), the question still remains whether there is also an increase in glutamatergic input and if these alterations in the spinal circuitry are brought on by cell autonomous or non-autonomous mechanisms.

III. Spinal motor neuron subtypes in ALS

An intriguing area of investigation in ALS has been the non-uniformity of pathogenesis between all motor neurons; moreover, some motor neurons demonstrate seemingly complete resistance to the disease. In the spinal cord, motor neurons are divided into three subtypes, fast α-motor neurons, slow α-motor neurons and γ-motor neurons. These subtypes can be identified by the muscle fibers they innervate as well as by their electrophysiological profiles (Figure 1.3). As detailed in this section, there are large differences between α-motor neurons and γ-motor neurons and likely these subtypes of motor neurons are fated early during the differentiation process, long before axonal outgrowth and target innervation (Stifani, 2014). That distinction is less clear between the slow and fast α-motor neurons. It may simply be the muscle fiber connections themselves that push the physiological differences between these two subtypes, arguing there may be a subtler shift in their expression profiles. To that point, after sectioning and reanastomosis of the medial gastrocnemius nerve, electrical properties of motor neurons were indistinguishable prior to reinnervation (Foehring et al., 1986). After reinnervation of the muscle fibers, they regained the normal electrical differences that exist between these two subtypes, arguing that these neurons dedifferentiated then redifferentiated. This will become relevant later as differential susceptibility in ALS is discussed.

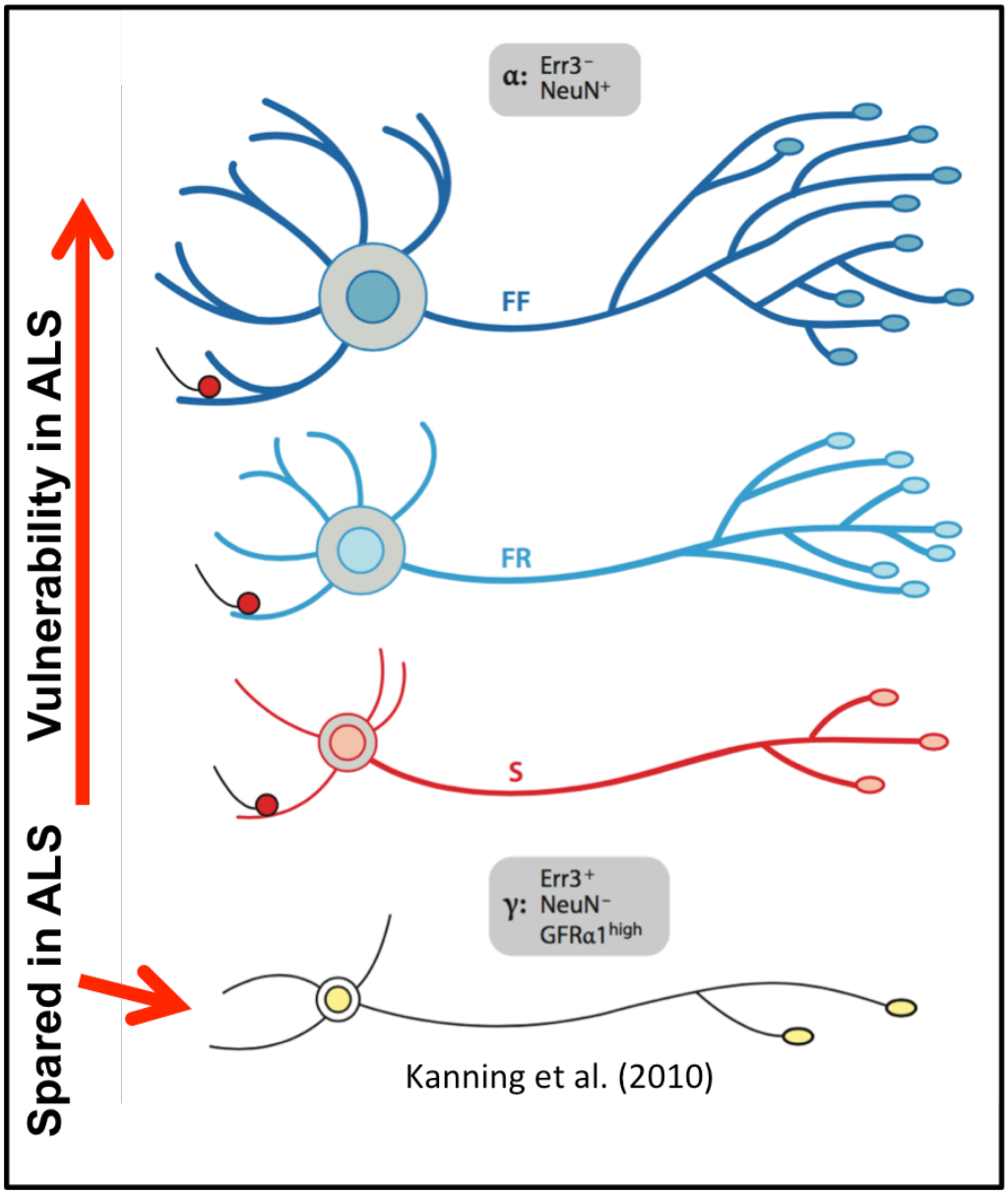

Figure 1-3: Spinal motor neuron subtypes and their sensitivity to ALS

α-Motor neurons that innervate fast-twitch fatigable (FF) type IIb muscle fibers typically degenerate first in ALS. Followed by α-motor neurons that innervate fast-twitch fatigue-resistant (FR) type IIa muscle fibers. The last to degenerate in ALS are the α-motor neurons that innervate slow-twitch fatigue-resistant (S) type I muscle fibers. γ-Motor neurons, innervating the intrafusal fibers of the muscle spindle, do not degenerate in ALS (Lalancette-Hebert et al., 2016). Adapted from (Kanning et al., 2010).

Fast α-motor neurons innervate the medium to low oxidative type IIa and IIb muscle fibers respectively, and fire action potentials in high frequency bursts. They exhibit higher rheobase (current activation threshold) and shorter afterhyperpolorizations (Kanning et al., 2010; Müller et al., 2014), a post-action potential event mediated by potassium current that drives the membrane potential 5-15mV below resting potential, effectively suppressing a subsequent action potential until its dissipation (Carp and Wolpaw, 2010). Fast α-motor neurons display the largest somal size and most complex dendritic arbor. In ALS, these are also the neurons that degenerate first, meaning they are the most vulnerable in the disease. Slow α-motor neurons, smaller and harboring a less complex dendritic arbor than the fast α-motor neurons, innervate the highly oxidative type I muscle fibers, and fire long trains of low frequency action potentials. In contrast to fast α-motor neurons, the slow α-motor neurons exhibit low rheobase and long afterhyperpolorizations (Kanning et al., 2010; Müller et al., 2014). Due to the relatively low current demands to fire a slow α-motor neuron, as well as a large persistent inward current, slow α-motor neurons exhibit bistability where a short burst of excitatory input can trigger a self-sustaining train of action potentials (Heckman et al., 2008). This self-sustaining tonic firing event requires inhibitory input to shut it down. In ALS, these motor neurons tend to degenerate later than their fast α-motor neurons counterparts, though they are still ultimately vulnerable in the disease.

Most unique of the spinal subtypes is the γ-motor neuron, much smaller compared to fast α-motor neurons and carry the least complex dendritic arbor. Unlike the extrafusal fiber innervation of the α-motor neurons, γ-motor neurons innervate the intrafusal fibers of the muscle spindle and regulate the output of the fusimotor system (Ellaway et al., 2015). The fusimotor system provides an electrical gain system for motor neurons, regulating motor neuron output dynamically throughout locomotion (Figure 1.4). To accomplish this, an intricate and complicated system of circuitry has evolved to send proprioceptive input, through the type Ia sensory fibers, back onto α-motor neurons. The Ia proprioceptive signal originates at the

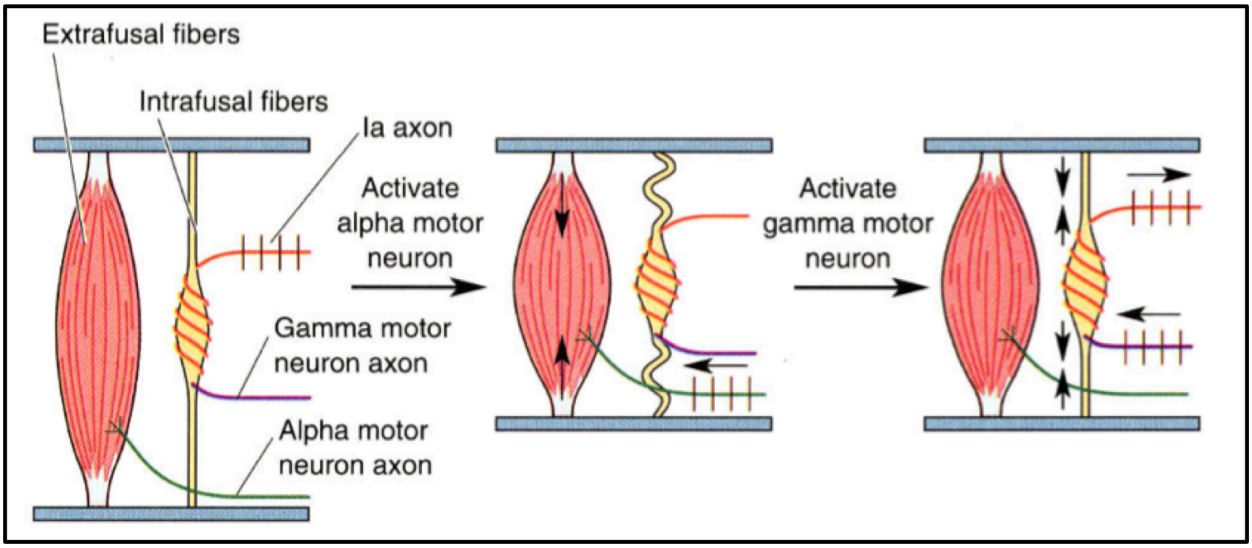

Figure 1-4: The fusimotor system

Without a mechanism to control it, as extrafusal muscle fibers are activated by α-motor neurons, the muscle spindle would lose tension and proprioceptive feedback to the motor system through the Ia circuit would be lost. However, γ-motor neurons precisely maintain tension on the spindle through contraction of intrafusal fibers. Additionally, the direct input of Ia afferent signaling onto α-motor neurons, allows γ-motor neurons to elicit a gain-like function, where they modulate the strength of afferent excitatory input (Ellaway et al., 2015). Figure adapted from (Widmaier et al., 2013).

muscle spindle, a sensory organ found in large numbers throughout skeletal muscles in mammals, that produces afferent information about stretch force. Through fast-conducting myelinated nerve fibers, these organs are capable of sending information back to the CNS about passive and active states of the skeletal muscles. Amazingly, in human leg and hand muscles, spindle-mediated Ia input onto the motor system accounts for 30-40% of the isometric contraction (Gandevia et al., 1990; Macefield et al., 1993). This function is carried out by the presence of two types of sensory nerve endings as well as motor innervation to regulate tension of the muscle spindles (Ellaway et al., 2015). As the skeletal muscle changes from either passive or standard locomotion to irregular or new movements, fusimotor drive is switched from a tonic static discharge, to a dynamic discharge that sends back more detailed information about the skeletal muscle movement to the CNS (Prochazka et al., 1985). The CNS is then able to tune the excitability of the α-motor neurons to suit the requirements of complex locomotor demands.

γ-Motor neurons also carry diversity amongst their subtype. Two known subtypes of γ-motor neurons exist, static and dynamic γ-motor neurons, and both possess distinct firing properties, though their conduction velocity cannot distinguish them as with other motor neuron subtypes. Both static and dynamic γ-motor neurons carry out distinct functions, innervating different muscle fibers within the muscle spindle, as well as operating the afferents originating at the muscle spindle in different ways (Hulliger, 2005). Most γ-motor neurons undergo a resting discharge of action potentials, where α-motor neurons are essentially shut down at rest so as to not elicit muscle contraction. Distinct tonic and phasic firing patterns have been found between static and dynamic γ-motor neurons, though it seems to be muscle dependent (Murphy and Martin, 1993). It has been difficult to directly record from and therefore their actually firing rates are unknown, though they are suspected to be similar to that of α-motor neurons (Hulliger, 2005; Ellaway et al., 2015). In ALS, γ-motor neurons are seemingly completely resistant to degeneration (Lalancette-Hebert et al., 2016), making them an interesting subtype by

comparison to their vulnerable α-motor neuron counterparts. That said, previous uncertainty as to the fate of γ-motor neurons (Kanning et al., 2010) was, at least in part, due to the observation of γ-motor neuron denervation of the muscle spindles from postmortem human ALS patients (Swash and Fox, 1974; Saito et al., 1978). It is unclear from those reports, however, the extent of influence that the atrophied extrafusal fibers and degenerated α-motor neurons has on the fusimotor system. It would be expected that significant rearrangement of this system might occur. Indeed, in these analyses, the intrafusal fibers were relatively resistant and only became atrophic in severely wasted muscles. As postulated in one study (Lalancette-Hebert et al., 2016), it is an interesting possible mechanism of pathology to consider the influence of compensatory behavior of the fusimotor system on the degeneration of α-motor neurons. It also posses the question whether the electrophysiological phenotypes discussed in the following sections can be found in populations of motor neurons spared in ALS, or if opposite or antagonistic phenotypes may be seen? Throughout this thesis, I will attempt to address this question as I investigate multiple vulnerable and resistant populations of motor neurons.

Importantly, potential contributions from interneurons should not be overlooked when considering subtype-specific vulnerability in ALS. While ALS may primarily effects motor neurons, interneuron loss could contribute to motor neuron degeneration or abnormal action potential firing patterns in interneurons could also have a down stream influence on motor neurons. Though most of the reports of interneuron loss have found degeneration of these neurons after motor neuron degeneration and may be a product of widespread effects downstream of that event (Nihei et al., 1993; Hossaini et al., 2011). However, some studies have pointed to early events that should not be discounted, such as a loss in inhibitory interneurons early in the disease (Brockington et al., 2013; McGown et al., 2013). As for firing patterns, the local spinal circuitry that produces rhythmic movement of limbs, complemented firing and inhibition of antagonistic muscle pairs, and coordinates alternating movements such as left-right stepping is called a central pattern generator (Carp and Wolpaw, 2010). This is a

delicately balanced network of multiple interneuronal subtypes elicits movements through the integration of input from descending, sensory and motor feedback circuits. Though it would seem that small perturbations could upset this balanced network, central pattern generator circuits are amazingly plastic (Molinari, 2009). However, some of the plasticity in the circuitry depends on the motor neuron's capability of adjusting to changes in input and providing feedback to the system (Lawton et al., 2017). Therefore, when discussing aberrant motor neuron activity, potential interneuronal dysfunction should be considered as well.

IV. Vulnerable and resistant populations of cranial motor neurons in ALS

Presentation of ALS in patients arises in multiple phenotypic patterns but most often occurs in the distal muscles (Kanning et al., 2010). However, a fifth of the patients present with bulbar symptoms that lead to dysphagia, dysarthria (Urban et al., 1998) and ultimately a worse prognosis (Swinnen and Robberecht, 2014). That said, after widespread paralysis and at the time of death in humans, postmortem tissue reveals pervasive loss of motor neurons in all regions of the anterior spinal cord and vulnerable cranial motor nuclei (Kanning et al., 2010). This puzzling heterogeneity in ALS first presenting in either distally projecting spinal motor neurons or vulnerable cranial motor neurons has not been investigated and may point to underlying differences in the pathogenesis of ALS.

From clinical analyses, ALS vulnerability in the cranial motor nuclei can be assumed to exist in cranial motor nuclei V (trigeminal), VII (facial) and IX-XII (glossopharyngeal, vagus, accessory, and hypoglossal) (Watts and Vanryckeghem, 2001; Kiernan et al., 2011; Vucic et al., 2014; Nijssen et al., 2017). In the SOD1 mouse models, reports consistently find approximately 40 – 60% motor neuron loss in the trigeminal and facial nuclei, similar to the loss seen in the spinal cord (Chiu et al., 1995; Nimchinsky et al., 2000; Haenggeli and Kato, 2002; Zang et al.,

2004; Ferrucci et al., 2010; Wootz et al., 2010). Little investigative effort in the mouse models has been focused on the dorsal motor nucleus of the vagus nerve. However, nucleus ambiguus contains a cluster of motor neurons projecting axons to the vagus and glossopharyngeal nerves and has also been shown to reflect similar motor neuron losses to facial and trigeminal. These studies provide mixed results about the hypoglossal nucleus, where some see severe degeneration and others show no significant difference compared to control. Most of these studies used the high-expresser $SOD1^{G93A}$ mice, however, different quantification measures ranged from magnetic nuclear resonance imaging methods to direct counting of neurons per section. It is possible that the disparities seen for degeneration of the hypoglossal nucleus are due to experimental error, or that heterogeneity exists in its vulnerability to ALS.

Though a predominant loss of motor neurons is seen throughout the spinal cord and brainstem, a remarkable divergence from this pattern is seen in the motor neurons that innervate the extraocular muscles. Cranial nuclei III (oculomotor), IV (trochlear), and VI (abducens) house these motor neurons where preservation is nearly complete (Nimchinsky et al., 2000; Haenggeli and Kato, 2002; Ferrucci et al., 2010; Kaplan et al., 2014; Nijssen et al., 2017). The preservation of these motor neurons allows full control over eye movement, providing one of the only means of communication for ALS patents (Nijssen et al., 2017). Though the motor neurons are spared in these nuclei, there is marked astrogliosis in the neuropil surrounding the oculomotor nucleus at end-stage (An et al., 2014). ALS resistance in these nuclei have fuelled many studies in the field and, as discussed throughout this chapter, have yielded a number of potential physiological mechanisms that provide protection. However, these motor neurons are perhaps even more unlike α-motor neurons than γ-motor neurons, meaning it has been difficult to tease out meaningful differences between the two that may confer ALS resistance.

Notably, oculomotor neurons are small compared to α-motor neurons and are almost the size of γ-motor neurons, including in their relatively simple level of complexity in their dendritic

structure (Figure 1.5). The extraocular muscles themselves harbor greater complexity as compared to most skeletal myosins, and oculomotor neurons innervate multiple fiber types (Nijssen et al., 2017). These motor neurons are also highly active relative to other cranial and somatic motor neurons. Rheobase measurements decrease in oculomotor neurons as they mature, opposite to what is shown to occur in many other types of neurons including spinal and hypoglossal motor neurons (Miles et al., 2004; Venugopal et al., 2015b). Oculomotor neurons fire action potentials most of the day and night as opposed to less than 2% of the day for some fast spinal α-motor neurons (Monster et al., 1978). Steady gaze firing frequency in oculomotor neurons is around 100Hz and saccadic eye movements produce up to 600Hz bursts (Robinson, 1970). This is far greater to spinal motor neuron firing that tops out around 100Hz in the mouse. Relevant to the excitotoxicity hypothesis, it would be expected that the increased activity in the oculomotor neurons would place an excessive load of calcium influx, however, these specialized motor neurons contain relatively high levels of calcium buffering proteins (Vanselow and Keller, 2000). One of which, parvalbumin, has been reported to increase, specifically in oculomotor neurons but not in ALS-vulnerable motor neurons, after large calcium influxes from axotomy. This pronounced buffering capability has been proposed to confer resistance to oculomotor neurons, moreover, overexpression of parvalbumin in ALS-vulnerable motor neurons delays onset and increases survival in SOD1 mice, though both of these effects are modest.

There are notable premotor circuitry differences for cranial motor neurons as well. The origin neurotransmitter composition of synaptic boutons found on cranial and spinal motor neurons vary significantly (Rekling et al., 2000), where disease relevant categorization is not clear. However, one large difference is the lack of Ia proprioceptive input from the fusimotor system as discussed previously. At least in mice, there are no muscle spindles in the extraocular muscles and therefore no Ia feedback (Lalancette-Hebert et al., 2016). Instead, there appear to be alternative pathways through which proprioceptive feedback is modulated in

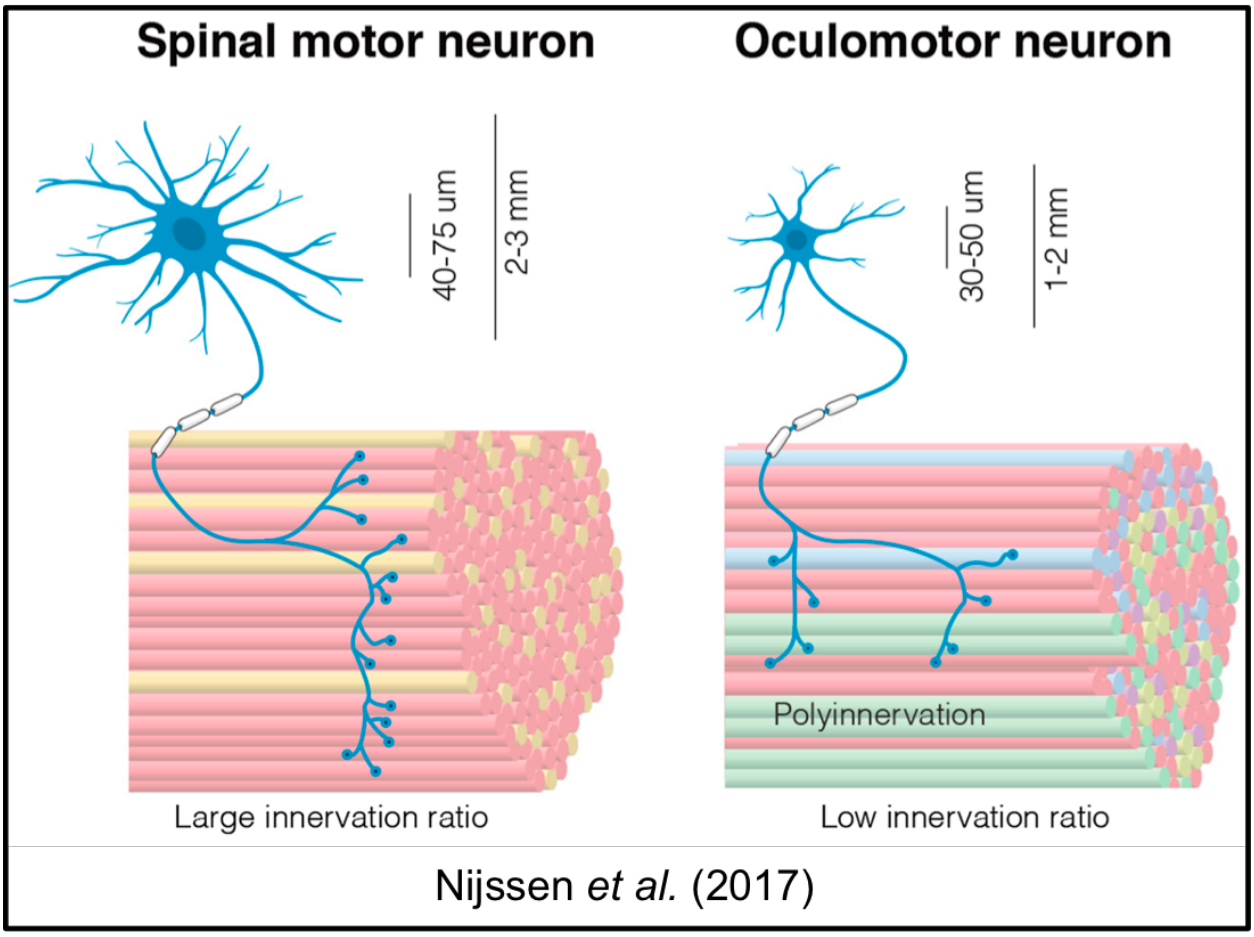

Figure 1-5: Spinal motor and oculomotor units

The much larger and dendritically more complex spinal motor neuron, and innervates 300 to 2000 muscle fibers. Additionally, spinal motor neurons are typically limited to the innervation of a single type of muscle fiber. Conversely, the relatively small and dendritically simple oculomotor neuron only innervates as few as 5 muscle fibers. Extraocular muscles contain greater diversity in their types of muscle fibers, and oculomotor neurons innervate multiple types in a single unit. Adapted from (Nijssen et al., 2017).

these muscles (Niechwiej-Szwedo et al., 2006). Trigeminal motor neurons, however, seem much more similar to spinal motor neurons in that there is a typical Ia sensory feedback system modulated by γ-motor neurons (Nishimura et al., 2018). Hypoglossal proprioception in rodents is still under investigation and some evidence points to the presence of muscle spindles in the tongue muscles of rats, but fusimotor systems are believed to be present in primate muscles innervated by hypoglossal motor neurons (O'Reilly and FitzGerald, 1990). At first glance, the lack of Ia input to the oculomotor, trochlear and abducens nuclei seems to be an intriguing difference from spinal motor neurons and might underlie a possible mechanism that imparts resistance in ALS. However, facial motor neurons in the mouse also lack Ia inputs, and the muscles they innervate are devoid of spindles, yet, they still degenerate in ALS (Whitehead et al., 2005). Likewise, though debated, extraocular muscles in humans and other mammals may have spindles, thus potentially using a proprioceptive system containing Ia circuitry (Maier et al., 1974). It is possible that Ia sensory feedback and the fusimotor system plays a role in spinal motor neuron pathology in ALS, but it seems less likely to underlie pathophysiology in all vulnerable motor neurons.

V. Electrophysiological Battlefield in ALS

Defining excitability

A recurring focus and a subject of controversy in ALS research, centers on whether observed changes in motor neuron excitability drive the pathophysiology of the disease.

I will cover this in some depth, however, it is first important to define excitability in the context of this thesis. Though a seemingly trivial point, “excitability” has been a catchall term in the ALS field that is often poorly explained when presented as a defining term for experimental findings. In simpler times, 1948 to be exact, Hodgkin recorded evoked firing patterns using current

injections to the axons of crustaceans (Hodgkin, 1948). He classified the firing responses into three groups known later as the Hodgkin excitability states (Prescott et al., 2008). These excitability states pertain to the spiking responses of neurons, rather than the exact voltages or currents that are required to induce an action potential. In the field of ALS, excitability has been used to describe both of these or even a mixture of these two very different measurements.

For the hypothesis of excitotoxicity, most arguments are trying to make a connection between the data they present and an increase in calcium influx expected to come from increased action potential firing. One of the issues with this position, however, is that there are no behavioral indications of aberrant action potential firing in patients or mouse models of ALS prior to symptom onset, which succeeds significant motor neuron death (Figure 1.1). This is problematic in that subtle shifts in motor neuron firing that occur below the threshold of behavioral effects will be difficult to observe experimentally.

It might be that Hodgkin's simple states of excitability, where neurons fall into these defined three categories, do not fairly represent the complexity and subtleties of firing patterns that may have significant consequences on the disease. It is known that spinal motor neurons do not maintain an abundance of calcium buffering proteins (opposite to oculomotor neurons) and, therefore, they rely mostly on their mitochondria, endoplasmic reticulum, and somal membrane calcium transporters to sequester transient calcium influx (Vanselow and Keller, 2000; Beers et al., 2001). It has also been reported that spinal motor neurons are selectively susceptible to over-activation (Hugon et al., 1989; Carriedo et al., 1996; Ikonomidou et al., 1996; Sugiyama and Tanaka, 2018), likely due to their inability to buffer calcium. It could be, then, that even a small shift in action potential kinetics and/or firing pattern could have long-term consequences due to increased stress from calcium overload. Further yet, if the balance and/or number of synaptic inputs are shifted to slightly increase excitation, stress induced through increased action potential firing, or even through subthreshold activation of voltage-gated calcium channels (Magee et al., 1995) in the dendrites may be relevant to ALS pathology. This

is an interesting possibility when considering the effects of Riluzole (discussed later) and that potential compensation in the dendritic calcium currents have been reported (Quinlan et al., 2015).

Now, considering the term excitability, what is most relevant here are changes in intrinsic properties that would lead to over-activation of calcium channels in ALS motor neurons. For this thesis, I will use "intrinsic excitability" to define properties that make a motor neuron more susceptible to reaching threshold, such as passive membrane properties and rheobase measurements. I will refer to the firing of action potentials as "activity", and the summation of synaptic input as "net excitation". Further consideration of the consequences of intrinsic excitability, however, should be discussed. After all, intrinsic excitability may not be a good indicator of neuronal output, as these two properties are not necessarily positively correlated. In fact, recent reports investigating the functional properties of fast α-motor neurons (Müller et al., 2014), the most vulnerable pool of neurons in ALS (Kaplan et al., 2014), find the fast α-motor neurons to be intrinsically hypoexcitable, relative to slow α-motor neurons (based on rheobase and input resistance). This is despite their propensity to fire high frequency trains of action potentials. Taking this into account, reports of intrinsic hypoexcitability do not refute the evidence of hyperactivity in ALS, and may in fact be exposing homeostatic mechanisms attempting to compensate for the increased action potential firing or increased net excitation.

As discussed previously, the hypothesis of excitotoxicity remains highly contested in the field of ALS. This degenerative pathway is supported by the beneficial effect of Riluzole within both human and mouse models (Bensimon et al., 1994; Miller et al., 1996; Gurney et al., 1998), where at clinically relevant concentrations, riluzole reduces glutamatergic synaptic activity and intrinsic excitability of motor neurons, likely leading to a reduction in action potential firing (King et al., 2007; Bellingham, 2011; Vucic et al., 2014; Blizzard et al., 2015). However, there have been a number of reports that draw contradictory conclusions arguing against this hypothesis. Certainly, at least some of the verbal disagreements in the ALS field surround a

misunderstanding of the term “excitability” as discussed above. Nevertheless, there are many studies published that, at face value, directly contradict one another. Here, I will try and compare and contrast some of these studies and perhaps offer some reasoning for the disparities.

Input Resistance

First, I will discuss intrinsic excitability, or better put, changes in electrical properties intrinsic to motor neurons. Input resistance is perhaps the best measure of the passive membrane properties in neurons. It is quantified by a reasonably consistent protocol across the literature where neurons are subjected to hyperpolarizing current steps and the voltage is recorded for each step. Per Ohm’s law ($Voltage = Current \times Resistance$), the slope of the current/voltage relationship is the passive membrane resistance measurement for that neuron (note care must be taken to avoid inaccuracies in the measurements caused by capacitance and the voltage-gated cation channels that underlie H-current (Lüthi and McCormick, 1998)). Despite the uniformity of the protocol, there have been inconsistent changes relative to controls seen within ALS transgenic models, with some studies reporting decreases (Bories et al., 2007; Quinlan et al., 2011) and others showing no change (Pieri et al., 2003; Kuo et al., 2004; 2005; van Zundert et al., 2008; Pambo-Pambo et al., 2009; Pieri et al., 2009; Meehan et al., 2010; Leroy et al., 2014). Conflicting evidence regarding action potential kinetics are also riddled throughout these studies, where opposite but still significant differences were reported. Some of this variation may be due to the differences between the models being used. Though most of these studies used mice carrying a mutant SOD1 transgene, differences still exist in the type of mutation as well as in the expression levels of the transgene across these models. For instance, even between the $SOD1^{G93A}$ mutants, a high expresser line carrying ~25 copies of the human SOD1 transgene was used in several studies (Pieri et al., 2003; Kuo et al., 2004; 2005;

van Zundert et al., 2008; Pieri et al., 2009; Quinlan et al., 2011) where the low expresser line carrying ~8 copies was used for another (Pambo-Pambo et al., 2009).

Interestingly, the reports that do show changes in input resistance perform their recordings on whole-cord preparations, where the dendrites remain intact. This is significant in this case as morphological abnormalities, typically reflecting an increased dendritic branching nodes, total length and surface area, have been reported in both transgenic models of ALS (Amendola et al., 2007; Amendola and Durand, 2008; Elbasiouny et al., 2012; Filipchuk and Durand, 2012) as well as in postmortem tissue from human ALS patients (Sasaki and Maruyama, 1992). However, as with many of the studies in the field, at least one account shows the exact opposite phenotype, where embryonic spinal motor neurons in the high expresser $SOD1^{G93A}$ mouse have a reduction in dendritic arbor size (Martin et al., 2013). Regardless, alterations in membrane surface area would likely result in decreased input resistance, but might not be present in primary cultures or slice recordings where the size of the dendritic arbor is severely truncated by sample preparation. This preparatory difference may also affect the action potential kinetics discussed above.

Action potential kinetics

Action potential kinetics include the firing characteristics of neurons such as action potential rate of rise, fall rate, duration, overshoot and afterhyperpolarization. All of these measures can effect maximal firing rate of the neuron, as well as the action potential waveform (Bean, 2007). Of the reports that show an action potential characteristic difference, the ones in the high expressing line see an decrease action potential duration where the low expressing line shows an increase in duration. Interestingly however, these two ALS models have largely different timelines of the disease course, where the disease onset in the low expresser line is 6-8 months compared to the 3 months to onset in the high expresser line (Turner and Talbot, 2008). As action potential kinetics are highly responsive to homeostatic mechanisms, the

differences between these two lines may reflect the differences in the pathogenic timeline, rather than true pathophysiological differences between the models.

In addition to heterogeneity between mouse models and populations of motor neurons analyzed (it has only been assumed that cranial and spinal motor neurons degenerate through similar pathogenic pathways), there were notable variations in experimental parameters including the usage of voltage clamp or current clamp, extracellular calcium concentrations and the time course of current injections. All of these will certainly add variation to the electrophysiological characteristics being quantified, and even perhaps underlie some of the contradictory data. Nonetheless, even when comparing motor neurons differentiated from human induced pluripotent stem cells under similar conditions, opposite results in firing frequencies were observed between a SOD1 mutant model (Wainger et al., 2014) and a C9ORF72 mutant model (Sareen et al., 2013). Again, the time in culture was different along with several other conditions that could explain the discrepancy, but regardless the inconsistencies continue to lead to confusion in the ALS and the hypothesis of excitotoxicity unproven.

Rheobase

More recently, Leroy *et al.* (2014) show in their preparation of neonatal spinal motor neurons in the high expresser $SOD1^{G93A}$ mouse, fast α-motor neurons (first motor neurons to degenerate in ALS) do not demonstrate differences in their intrinsic excitability (Leroy et al., 2014). Surprisingly, they also show that slow α-motor neurons (last motor neurons to degenerate in ALS) are intrinsically hyperexcitable. Leroy and Zytnicki claim that this is evidence that early intrinsic excitability is not part of the pathophysiology of ALS (Leroy and Zytnicki, 2015). There are some protocol differences, however, that exist between this study and previous analyses, one of which is their measurement of rheobase. Rheobase is simply the minimum current required to elicit an action potential and it is tested using whole-cell path clamp

in a current clamp configuration, and incrementally increasing the current injections until an action potential fires. In its standard definition, this current can be held for an infinite duration, however, neurons may encounter activation or inactivation of some voltage-gated ion channels during this time. Typically, current step durations are held for between 200 ms and 1 s. Yet for the recordings in Leroy *et al.* (2014), a 5 s current step is used. During this time, a clear depolarizing creep of the voltage can be seen in neurons that they call delayed firing neurons, indicative of the activation of voltage-gated sodium channels. Though this phenotype may suggest the presence of very relevant physiological differences, it may not be the most accurate way to measure rheobase or the subsequent measure of threshold voltage. Nevertheless, the differences described in this report insinuate that neonatal hyperexcitability does not drive pathogenesis in ALS.

Excitatory input

What, then, can be concluded about excitotoxicity from the studies reported thus far? Unfortunately, the field still seems left with little definitive evidence to suggest whether this hypothesis is correct or not. And yet, the effects of Riluzole still seem to drive these analyses forward. There are many disparities in recoding and tissue preparation methods in these reports, as well as within the mouse models used. Of additional concern is that the vast majority of these studies are carried out on embryonic and neonatal motor neurons, long before any of the descending corticospinal circuitry innervates the spinal cord (Gianino et al., 1999; Arlotta et al., 2005) and before the maturation of spinal circuitry (Gianino et al., 1999; Clarke and Still, 2001; Personius and Balice-Gordon, 2001; Arber, 2012). Any early changes in activity or intrinsic excitability then, may not reflect abnormalities in mature physiology that drives the pathogenesis of ALS. Furthermore, aberrations in spinal and corticospinal circuitry may also be influencing pathology in ALS. Activity output of a neuron can be measured as a kind of summation of net excitatory input and intrinsic excitability (Figure 1.7). Low intrinsic excitability

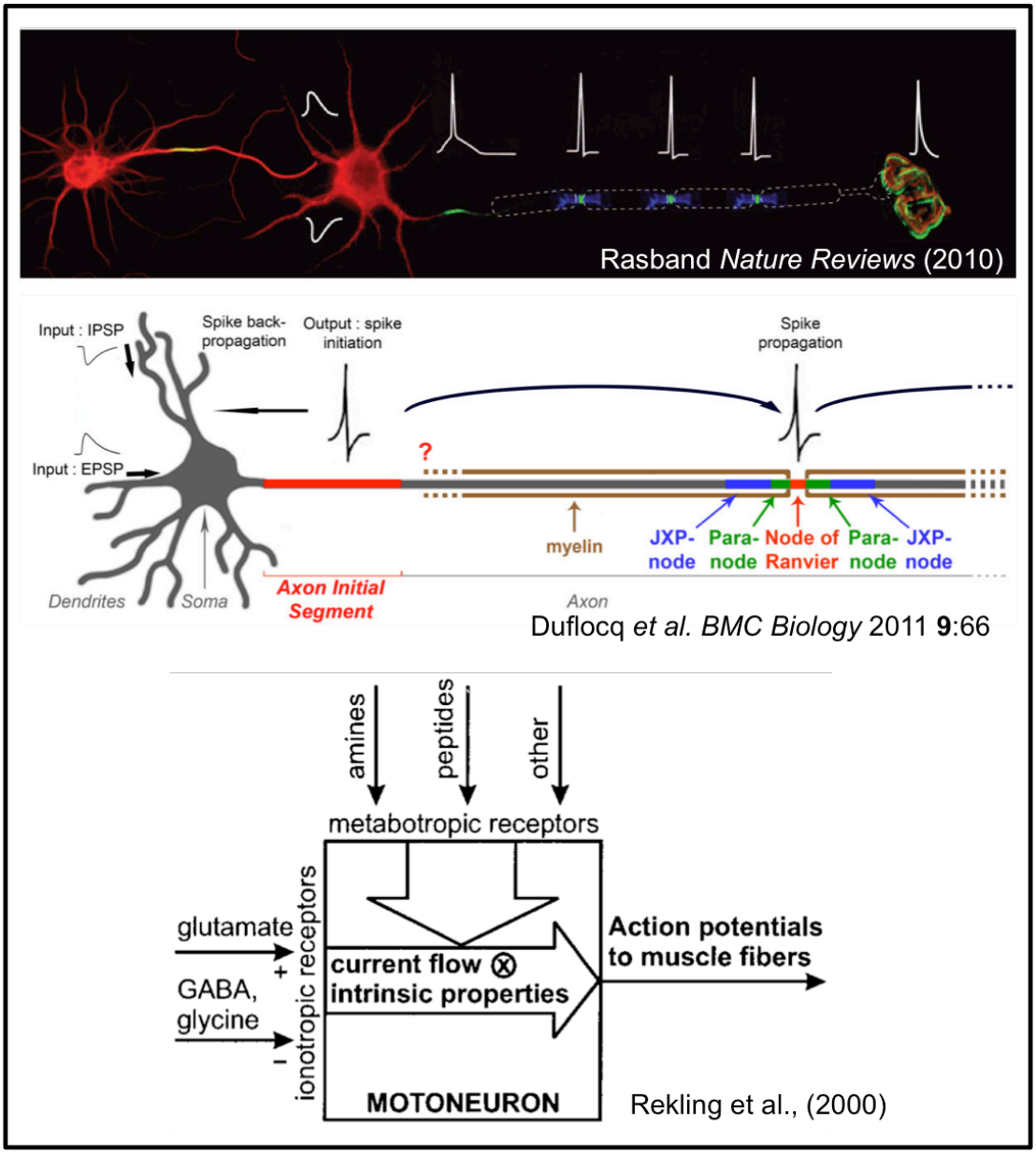

Figure 1-6: The axon initial segment and neuronal excitability

Top: immunostaining for pan-neuronal markers and Ankyrin G (green; visualization of the axon initial segment and the nodes of Ranvier) showing the progression of the action potential, initiating at the axon initial segment, and terminating at the neuromuscular junction. (Rasband, 2010)

Middle: Artistic rendition of the axon initial segment location in the proximal axon. Structural and molecular properties of the axon initial segment and the nodes of Ranvier are very similar, however, unlike the nodes of Ranvier, myelin formation is not required for assembly and function of the axon initial segment. (Duflocq et al., 2011)

Bottom: A simple representation of neuronal excitability, as defined by Hodgkin. Output, action potential firing, is controlled by two variable factors, intrinsic properties of the neuron, and ionotropic input. Metabotropic input can modify intrinsic properties along with homeostatic mechanisms. This thesis will define intrinsic properties as “intrinsic excitability” and output as “activity”. (Rekling et al., 2000)

with high excitation may still yield a highly active neuron. It could in fact be that the intrinsic excitability is reacting in a compensatory manor to excitatory input. To that point, it has been consistently reported in ALS mouse models, as well as in human ALS patients, that corticospinal neurons are hyperactive (Vucic et al., 2008; Saba et al., 2016; Kim et al., 2017). This would likely increase net excitation of spinal motor neurons and induce homeostatic changes in local circuitry and in intrinsic excitability.

There has been some evidence in spinal motor neurons that may suggest that circuitry changes do in fact occur. C-boutons, modulatory inputs to spinal motor neurons, are enlarged in ALS, where increased C-bouton input would increase intrinsic excitability (Witts et al., 2014). Evidence from ALS-model mice shows that early abnormalities in spinal circuitry may exist, where in response to polysynaptic activation by high stimulus intensity dorsal root stimulation, ventral root amplitudes were reduced (Bories et al., 2007). Furthermore, inhibitory glycinergic inputs onto spinal motor neurons in ALS may be reduced (Martin and Chang, 2012; Wootz et al., 2013). Though it is possible to quantify Ia input onto motor neurons, it has not been possible to quantify the entirety of the excitatory synaptic profile of motor neurons, due to their size, as well as the issues with electrophysiological recording discussed in this section. Problematically, electrophysiological analyses in adult spinal motor neurons are also quite difficult. For example, with spinal sections, the neurons often die from the ischemic conditions and severing their massive dendritic arbor induces severe stress (Mitra and Brownstone, 2012; Bucchia et al., 2018). Though some recent progress has demonstrated our improved ability to record from adult motor neurons in spinal sections (Martinez-Silva et al., 2018), our insight into the physiological activity and excitatory inputs of motor neurons in ALS remains opaque, and the ability to record from adult spinal sections does not mitigate all of the experimental variation discussed in this section. Additionally, parsing out the differences between homeostatic compensation within motor neurons due to synaptic input and other extrinsic influences, and what is intrinsically driving potential changes in motor neuron activity defines the heart of the

argument about excitotoxicity. I hope to address this issue throughout this thesis and provide evidence that adult motor neurons may be harboring electrophysiological abnormalities in ALS.

VI. The Axon Initial Segment

In 1957, several years after Eccles first recorded action potentials in motor neurons, Mary Becker and John Eccles proposed in separate works that the action potential must originate in the axon hillock due to a hyperpolarization of the threshold voltage (by about 15mV) in the hillock as compared to the soma. This was based in part on earlier observations of differences between orthodromic and antidromic stimulation, and that there was an inflection in the action potential that changed the rise rate from the initial rate and the post inflection rate (COOMBS et al., 1957; FUORTES et al., 1957). In these studies, the calculations that hypothesized the hyperpolarization in the hillock were mostly based on a local reduction in capacitance. Maintained by the small surface area of the axon hillock relative to the soma, the summation of excitatory input that occurs simultaneously in the soma and proximal axon would reach threshold more quickly in the low capacitance environment of the hillock. Later in the 1970s and 80s, theoretical modeling found the voltage threshold is likely much lower than what could be accounted for by capacitance alone. They proposed that the sodium channel density in the axon initial segment must be much higher as well (Dodge and Cooley, 1973; MOORE et al., 1983), thus sufficiently lowering the threshold to account for the anomalies seen in empirical data. It took over 50 years for empirical evidence to prove they were correct, at least with part of them mechanism.

Though immunostaining for sodium channels agreed with these models, the first empirical testing in the late 1990s and early 2000s determined there was an alternative mechanism at play. Using cell-attached and outside-out patch clamp analyses, it was reported

that densities of sodium channels in the axon initial segment were comparable to those of the soma (Colbert and Johnston, 1996; Colbert and Pan, 2002). Given that empirical whole-cell recordings still showed a hyperpolarized voltage threshold in the hillock as compared to the soma, these groups posited that a unique subtype of sodium channel must be present and responsible. However, in a very elegant series of experiments, definitive evidence proved that the sodium channel densities in the axon initial segment were close to 50-fold higher than in the somatodendritic compartment (Kole et al., 2007; Kole and Stuart, 2008; Kole et al., 2008). It is now understood that the sodium channels in the axon initial segment are bound to the cytoskeletal scaffolding (Huang and Rasband, 2016) in the proximal axon and in the previous studies that used outside-out patches from the hillock, the sodium channels likely were pulled from the membrane patches that were removed by the patch pipette.

Further studies of the axon initial segment uncovered additional properties that highlight a more complex function of this highly specialized sub-cellular structure. It is not just that the action potential initiates at the axon initial segment, it does so heterogeneously across the proximo-distal axis (Figure 1.7). Studies established that the action potential initiates in the distal part of the axon initial segment (Colbert and Pan, 2002; Kole et al., 2008; Lorincz and Nusser, 2008), and that this is likely due in some cases (including motor neurons) to the distal localization of a particular voltage-gated sodium channel subtype, $Na_V1.6$ (Hu et al., 2009; Duflocq et al., 2011). $Na_v1.6$, harboring a relatively hyperpolarized gating threshold, sits distally in the axon initial segment to $Na_v1.1$ or $Na_v1.2$, both of which carry depolarized gating thresholds relative to $Na_v1.6$. This compartmentalization of sodium channel subtypes in the axon initial segment creates a system of backpropagation of the action potential in neurons that travels in both directions from the distal initial segment. This perhaps contrasts the original doctrine of the “Law of Dynamic Polarization of the Neuron” by Ramon y Cajal, whose assertion was that information flows along a neuron in one direction. However, the backpropagation is vital for homeostatic feedback for the neuron (Hu et al., 2009) and provides information that

travels back to the somatodendritic compartment in the opposite direction of Cajal's information flow.

In addition to being the epicenter for the summation of synaptic input and initiation of the action potential, the axon initial segment is also vital to the maintenance of neuronal polarity. Polarity of the neuron is established early in development through positive and negative intracellular signaling pathways (Arimura and Kaibuchi, 2007), however, maintaining polarity through these mechanisms would place a large metabolic demand on the neuron over the duration of its life (Rasband, 2010). Therefore, the neuron establishes a gateway using the axon initial segment to preform this duty. AnkyrinG is the first protein to cluster in the proximal axon after polarity is established and recruits and interacts with most of the other membrane and submembrane components of the axon initial segment (Jones and Svitkina, 2016). AnkyrinG is indispensable, not just for establishment of the axon initial segment, but also in its structural retention. Selective loss of the scaffolding protein ankyrinG, master organizer of the axon initial segment (Kapfhamer et al., 1995; Yoshimura and Rasband, 2014), results in the disruption of neuronal polarity (Hedstrom et al., 2008). Furthermore, deficiencies in ankyrinG in neurons have been shown to play a role in the pathology of multiple neurological diseases including epilepsy, schizophrenia, angleman syndrome, bipolar disorder, autism spectrum disorder and Alzheimer's disease (Kaphzan et al., 2011; Sun et al., 2014b; Huang and Rasband, 2018; Yue et al., 2018).

Adding to the already immense load of utility that axon initial segment provides to a neuron, it is not simply a static structure that forms and takes root to preform its functions. Instead, it has been shown to have dynamic structural plasticity and it important for physiological homeostasis in the neuron. The dynamic nature of the axon initial segment was postulated in the 1980s, when literature emerged reporting on electrophysiological recordings that were carried out in the spinal cords of cats. The range of input resistance seen in these motor neurons did not account for the large range observed in the rheobase measurement, a

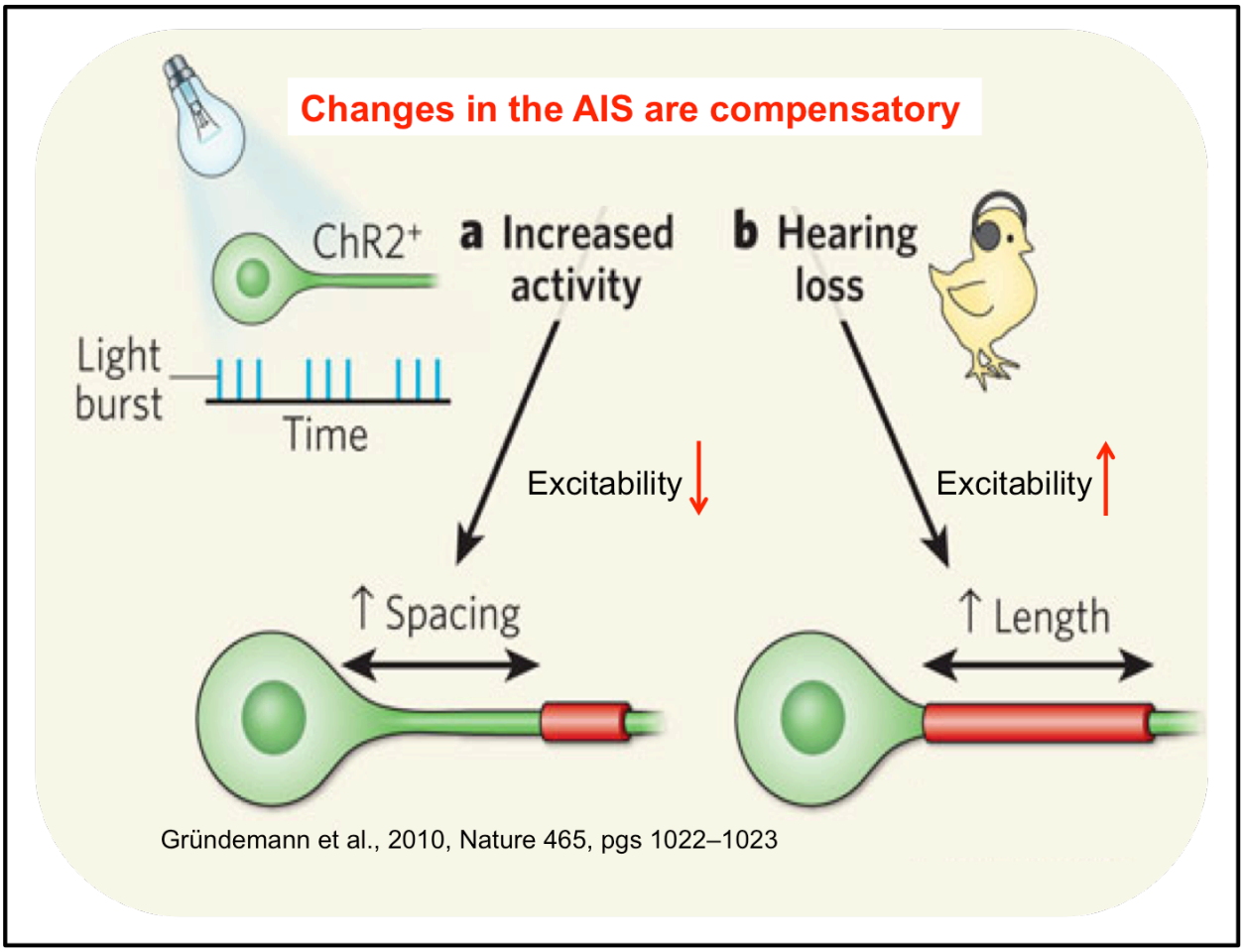

Figure 1-7: Plasticity in the axon initial segment

Changes in net excitatory input can provoke structural rearrangement in the axon initial segment. As the initiation point of the action potential, structural rearrangement in the axon initial segment can affect the action potential threshold. As distal shift of the axon initial segment will depolarize the threshold due to signal attenuation, as it must travel further down the axon. A lengthening of the axon initial segment will increase the voltage-gated sodium channel numbers, effectively hyperpolarizing the action potential threshold. In excitatory neurons, structural rearrangement in the axon initial segment is always coupled to a compensatory response in intrinsic excitability. Adapted from (Gründemann and Häusser, 2010).

relationship that, according to Ohm's law, should be linear (Fleshman et al., 1981; Pinter et al., 1983; Gustafsson and Pinter, 1984). They reasoned that the most likely cause was a shift in threshold and since the axon initial segment set the threshold, there must be dynamic properties in that region. Indeed, this was the case. Seminal studies showed that the axon initial segment underwent compensatory structural changes when the level of net synaptic excitation was modified (Grubb and Burrone, 2010; Kuba et al., 2010) (Figure 1.8). Grubb and Burrone (2010) showed that by stimulating cultured hippocampal neurons they were able to induce a shift of the axon initial segment away from the soma. This distal shift was accompanied by a reduction in intrinsic excitability and these neurons fired action potentials at lower frequencies. All of the reported changes to intrinsic excitability in these neurons matched the shift in excitability caused directly by the axon initial segment, and thus, were all compensatory. Similarly, but this time in an *in vivo* preparation, Kuba *et al.* (2010) reported a lengthening in the axon initial segment in the neurons of the nucleus magnocellularis, a critical relay center in the auditory system, after losing synaptic input following the removal of the cochlea. Fitting with the previous reports of high sodium channel density at the axon initial segment, the lengthening also marked a significant increase in sodium current. Using an elegant paired-patch recording experiment, a cell-attached pipette was added to the patched cell in the whole-cell patch configuration. With this, the authors were able to show that the increased current was not due to increased sodium channel densities on the somal membrane, and therefore most likely mediated by the axon initial segment lengthening. Like the Grubb and Burrone (2010) findings, the activity-induced structural changes in the axon initial segment were coupled to additional changes in intrinsic excitability where all reported parameters followed a compensatory response to try and make the neurons hyperactive and hyperexcitable. Likewise, all excitatory neurons tested to date exhibited a compensatory response in the axon initial segment and other measures of intrinsic excitability (Grubb and Burrone, 2010; Kuba et al., 2010; Kaphzan et al.,

2011; Evans et al., 2013; Kaphzan et al., 2013; Kuba et al., 2014; Muir and Kittler, 2014; Chand et al., 2015; Wefelmeyer et al., 2015).

Though the development (Le Bras et al., 2013), structure and channel subtype composition (Duflocq et al., 2011) of the axon initial segment in motor neurons have been reported, to date, no studies have investigated axon initial segment plasticity in these neurons. Additionally, as noted above in this section, axon initial segment deficiencies have been implicated in disease pathology. In epilepsy, a well-known disease caused by hyperactivity in various subtypes of neurons, the axon initial segment was shown to exhibit structural plasticity as a compensatory response to over-activation in these neurons (Harty et al., 2013; Yue et al., 2018). Axon initial segment structural plasticity would, therefore, serve as a useful visual indicator of anomalous synaptic circuitry within disease-state neuron populations compared to their healthy control counterparts. This would carry the distinct advantage of providing a true physiological snapshot of intrinsic excitability in ALS motor neurons, circumventing the electrophysiological limitations discussed in this introduction. As such, this thesis will attempt to address three questions regarding the axon initial segment: 1) Do motor neurons exhibit activity-dependent structural plasticity in the axon initial segment and 2) Do motor neurons in a mouse model of ALS display structural changes in the axon initial segment 3) Do structural changes in the axon initial segment correlate with motor neuron degeneration? If these questions are found to be true, it may provide insight not only into motor neuron biology, but also physiological evidence of pathophysiology in ALS motor neurons.

Chapter 2: Length changes in the axon initial segment is induced prior to p62 pathology and mitochondrial swelling in a mouse model of Amyotrophic Lateral Sclerosis

Summary

In amyotrophic lateral sclerosis (ALS) α-motor neurons of the spinal cord progressively degenerate throughout the course of the disease. A well-known hypothesis describing ALS pathogenesis proposes that excitotoxicity induced by increased excitatory activity in these motor neurons contributes to the pathophysiology of the disease. However, testing this mechanism has been complicated and limited by difficulties in electrophysiological analysis of adult motor neurons. Here, I report that spinal motor neurons exhibit plasticity in their axon initial segment and, similar to other excitatory neurons, their axon initial segment responds to increased excitation in a compensatory manner, resulting in a reduction in length. In a critical analysis of adult spinal motor neurons in the SOD1G93A mouse model of ALS, I analyzed axon initial segment length as a visual proxy for net excitation in adult spinal motor neurons, where a shorter axon initial segment would indicate increased neuronal excitation. Reduced axon initial segment length of alpha, but not ALS-resistant gamma spinal motor neurons was found very early in presymptomatic ALS mice, but only after circuit maturation. Axon initial segment length reduction is persistent and progressive at ages when neuronal degeneration and neuromuscular junction denervation occurs. Shortening of the axon initial segment was found to precede other phenotypes of cellular stress, specifically p62 aggregation and gross swelling of the mitochondria; furthermore, only those motor neurons that later emerge with these phenotypes undergo axon initial segment shortening. As degeneration begins, the axon initial segment length changes observed in all motor neurons may reflect broad circuitry abnormalities as the motor system compensates for functional motor unit loss. These findings indicate an early

modification in motor neuron activity in ALS mice that may contribute to the subtype-specific pathophysiology of the disease.

Introduction

Excitotoxic stress, thought to be facilitated by increased electrophysiological activity (Vucic et al., 2014) has been fiercely debated in the literature, which has provided conflicting evidence describing both hypo and hyperexcitability in ALS motor neurons (Elbasiouny et al., 2012; van Zundert et al., 2012; Leroy and Zytnicki, 2015). However, most of the studies testing the excitotoxicity hypothesis focus on intrinsic measures of excitability (Elbasiouny et al., 2012) and infer that motor neuron action potential firing (activity) will be proportional to these measures. It has also been proposed that motor circuitry may be abnormal in ALS (Leroy and Zytnicki, 2015), meaning that some of the electrophysiological changes observed could be reflecting homeostatic responses to irregular synaptic inputs, another possible source of stress for motor neurons due to long-term demands on compensatory mechanisms.

The majority of these studies have been carried out in neonatal motor neurons or in primary motor neuron cultures (Elbasiouny et al., 2012), resulting in an opaque sense of the true nature of adult motor neuron physiology. Historically, it has proven very difficult to perform electrophysiological recordings in adult mouse motor neurons, limiting our understanding of pathophysiological changes in ALS. For example, with spinal sections, the neurons often die from the ischemic conditions and severing their massive dendritic arbor induces severe stress (Mitra and Brownstone, 2012; Bucchia et al., 2018). Though some recent progress has demonstrated our improved ability to record from adult motor neurons in spinal sections (Martinez-Silva et al., 2018), our insight into the physiological activity and excitatory inputs of

motor neurons in ALS remains obscure, leading to much debate surrounding excitability in ALS motor neurons.

Axon initial segment plasticity has gained attention recently after a score of reports have shown structural changes to occur in response to modifications in excitatory input. Due to a relatively high density of voltage-gated sodium channels, and low relative capacitance as compared to the somatodendritic compartment, the action potential initiates at the axon initial segment, imbuing this structure with key regulatory power over threshold voltage (COOMBS et al., 1957; Kole et al., 2008; Kole and Stuart, 2012). In neurons (e.g. hippocampal neurons (Grubb and Burrone, 2010; Wefelmeyer et al., 2015), olfactory bulb neurons (Chand et al., 2015) and auditory neurons (Kuba et al., 2010)), excitation-driven changes are seen in either the length of the axon initial segment, or its distance from the soma, both of which impact intrinsic excitability. The plastic response of the axon initial segment to net excitatory input in these neurons is compensatory, where an increase in neuronal excitation leads to a decrease in intrinsic excitability that was mediated, at least in part, by the structural rearrangement of the axon initial segment. Consistently, these changes in axon initial segment structure were coupled with additional adjustments to excitability, including passive membrane properties and voltage-gated K+ conductance (Grubb and Burrone, 2010; Kuba et al., 2010). Therefore, the axon initial segment presents as a potential molecular marker to visualize relative excitability in a population of neurons that reflects the level of compensatory input. To this point, changes in the axon initial segment have been observed in effected neurons in several different diseases, thought to be mediated by changes in activity (Kaphzan et al., 2011; Baalman et al., 2013; Harty et al., 2013; Hamada and Kole, 2015).

Here, I have utilized axon initial segment plasticity to assess motor neuron excitability in ALS mice as a way to circumvent issues with recording from adult motor neurons and to get a physiological snapshot of motor neuron excitation. I compared motor neurons in the same lumbar segments in ALS model mice to their non-transgenic (Nt) littermates, where

hyperexcitation (increased net excitatory input) may result in a shorter axon initial segment length indicating a shift toward reduced intrinsic excitability. Using mouse embryonic stem cell-derived motor neurons (ESC-MNs), I demonstrate that like other excitatory neurons, motor neurons respond to activity changes by altering the structure of their axon initial segment and intrinsic excitability in a compensatory manner. With that in mind, I compared the axon initial segment length in lumbar motor neurons at multiple time points in pre-symptomatic SOD1G93A mice. I find the axon initial segment to be significantly shorter starting in young adult mice at postnatal day 25, marking a very early phenotype in the disease, and this shift persists through at least postnatal day 70. Confirming that the shift in the axon initial segment marks motor neurons that are likely to be the first to degenerate, I found those with the shortest axon initial segments possess other phenotypic markers of stress, namely p62 aggregation and vacuolar degeneration. Taken together, I've identified one of the earliest markers of pathophysiology in mature motor neurons in ALS mice, one that may suggest vulnerable spinal motor neurons are intrinsically hypoexcitable early in the disease course.

Results

Activity modifications in motor neurons induce plastic changes in axon initial segment length

Though the development and channel composition of the axon initial segment in motor neurons has been reported (Duflocq et al., 2011; Le Bras et al., 2013; Jacko et al., 2018), activity-driven plasticity of the motor neuron axon initial segment has not been conclusively demonstrated. To test the link between motor neuron activity and axon initial segment plasticity,

I took advantage of a well-established *in vitro* preparation of ventral spinal neurons derived from mouse embryonic stem cells (mESC) (Wichterle et al., 2002; Wichterle and Peljto, 2008).

Stem cell differentiation yields a complex mixture of ventral spinal neurons, primarily composed of motor neurons, V3, V2a and V2b interneurons (Wichterle et al., 2002; Alaynick et al., 2011; Sternfeld et al., 2017). Motor neurons are identified in this milieu of spinal neurons by their expression of green fluorescent protein (GFP) driven off the motor neuron-specific promoter for the homeodomain protein Hb9 (Figure 2.1A). After a week in culture, motor neurons elaborate complex processes, establish axon initial segments, and exhibit robust synaptic activity. Glutamatergic synapses, positive for VGluT2, were observed apposed to motor neuron cell bodies and proximal dendrites (Figure 2.1A). Whole-cell patch clamp recording of individual motor neurons revealed EPSPs and spontaneous action potentials, both of which were effectively inhibited by AMPA channel blocker CNQX (Honoré et al., 1988) (Figure 2.1B). Though I have yet to identify the specific glutamatergic presynaptic neurons, it is likely to be either the V2a or V3 interneurons as they are generated alongside motor neurons and both were characterized as premotor glutamatergic interneurons *in vivo* (Wichterle et al., 2002; Xu and Sakiyama-Elbert, 2015; Sternfeld et al., 2017).

To elicit maximal activity-dependent structural changes in the axon initial segment, I cultured mESC-derived motor neurons in for 17 days *in vitro* (DIV17) in a control condition, or in the presence of tetrodotoxin (TTX) (Figure 2.1C), a potent voltage-gated sodium channel blocker (NARAHASHI et al., 1964). Furthermore, it was unclear if the full formation of the axon initial segment would take place devoid of any neuronal activity. Then, to determine if the axon initial segment is indeed plastic in motor neurons, I cultured motor neurons under control conditions and inhibited activity only for the final two days. I then utilized whole-cell patch electrophysiology in the current clamp configuration to analyze the intrinsic excitability of the motor neurons within these conditions. Patch pipettes contained biocytin that allowed for identification of neurons post recording. Interestingly, I find that motor neurons increase the

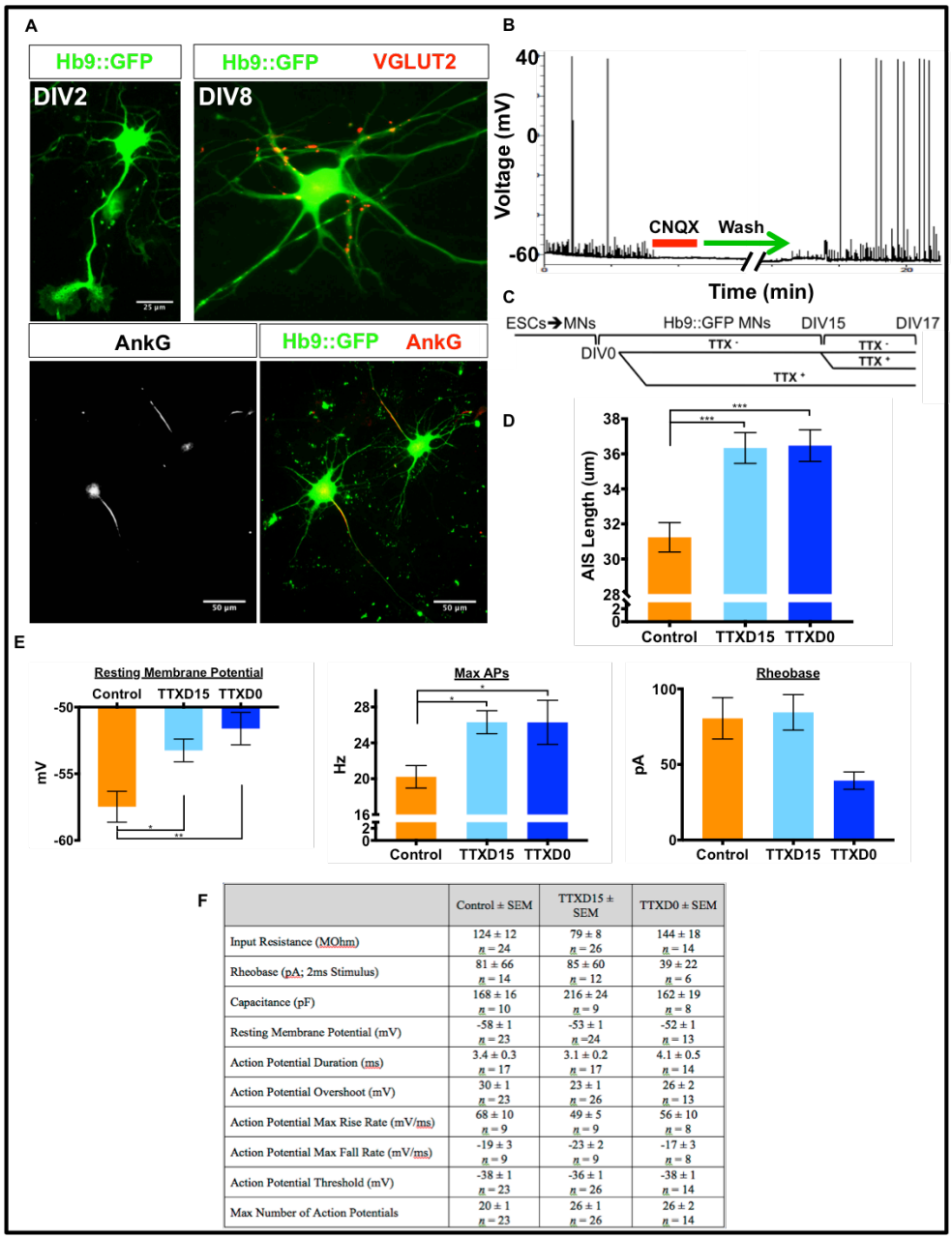

F

	Control ± SEM	TTXD15 ± SEM	TTXD0 ± SEM
Input Resistance (MOhm)	124 ± 12 n = 24	79 ± 8 n = 26	144 ± 18 n = 14
Rheobase (pA; 2ms Stimulus)	81 ± 66 n = 14	85 ± 60 n = 12	39 ± 22 n = 6
Capacitance (pF)	168 ± 16 n = 10	216 ± 24 n = 9	162 ± 19 n = 8
Resting Membrane Potential (mV)	-58 ± 1 n = 23	-53 ± 1 n =24	-52 ± 1 n = 13
Action Potential Duration (ms)	3.4 ± 0.3 n = 17	3.1 ± 0.2 n = 17	4.1 ± 0.5 n = 14
Action Potential Overshoot (mV)	30 ± 1 n = 23	23 ± 1 n = 26	26 ± 2 n = 13
Action Potential Max Rise Rate (mV/ms)	68 ± 10 n = 9	49 ± 5 n = 9	56 ± 10 n = 8
Action Potential Max Fall Rate (mV/ms)	-19 ± 3 n = 9	-23 ± 2 n = 9	-17 ± 3 n = 8
Action Potential Threshold (mV)	-38 ± 1 n = 23	-36 ± 1 n = 26	-38 ± 1 n = 14
Max Number of Action Potentials	20 ± 1 n = 23	26 ± 1 n = 26	26 ± 2 n = 14

Figure 2-1: Activity-induced changes in motor neuron axon initial segments reflect adaptation of intrinsic excitability.

A) Representative images of maturing ESC-derived motor neurons. Emergence of VGLUT2 staining indicates the presence of *in vitro* synaptic networks. Axon initial segments can be visualized in ESC-derived motor neurons using the scaffolding protein, ankyrinG. B) Current clamp trace of EPSPs and spontaneous action potential formation. EPSPs are completely blocked by bath-applied CNQX and recover after a wash. C) Experimental design to assess axon initial segment plasticity in motor neurons. Control ESC-derived motor neurons are cultured normally until DIV17. Manipulation of the axon initial segment will be accomplished using TTX to abolish action potential firing either from DIV0 or DIV15. All conditions will undergo electrophysiological analysis at DIV17. D) Axon initial segment length increases with the length of time activity is removed. E) Lengthening of the axon initial segment reflects an increase in intrinsic excitability. Significance by one-way ANOVA and Bonferroni post hoc analysis. F) Data table for measured electrophysiological analyses. Statistics not preformed on all parameters as data reflects preliminary results.

length of their axon initial segment in response to a loss of activity (Figure 2.1D). The axon initial segment length in the TTX at DIV15 condition (36.33μm ± 0.88; n=123) became equal that of the axon initial segment in the motor neurons cultured in TTX from DIV0 (36.47μm ± 0.90; n=105). Both differed significantly from the axon initial segment length in the control condition (31.24μm ± 0.84; n=95). Consistent with a compensatory shift in axon initial segment length, intrinsic excitability also was increased in the motor neurons cultured in TTX. The maximum frequency of firing reached by current step was significantly increased in both TTX conditions and resting membrane potential decreased (Figure 2.1E). Interestingly, rheobase was only affected in the motor neurons cultured with TTX from DIV0, indicating intrinsic excitability may be elevated to a greater extent in these neurons. These data propose that like other excitatory neurons, motor neurons exhibit homeostatic plasticity in their axon initial segment that compensates for changes in activity.

The axon initial segment of vulnerable motor neurons shortens in presymptomatic ALS mice

Changes in neuronal physiology were reported in early postnatal ALS mice (Turner and Talbot, 2008; Elbasiouny et al., 2012; van Zundert et al., 2012; Vucic et al., 2014). Taking advantage of the observed axon initial segment plasticity in motor neurons, I opted to examine changes in the axon initial segment as a visual proxy of motor neuron excitability. I initially attempted to analyze both axon initial segment length and distance; however, in motor neurons, the axon does not always sprout directly from the soma, complicating the distance measurement, increasing variability, and reducing confidence in the accuracy of the quantification. Therefore, I focused on axon initial segment length for this study.

Using the SOD1^{G93A} mouse model of ALS, I first analyzed the axon initial segment in lumbar spinal cord segments 4 and 5 (L4-5) of young adult mice, at postnatal ages 23-26 (P23-26). I also restricted our analysis to the lateral motor column, providing a population of almost entirely fast fatigable α-motor neurons (Burkholder et al., 1994; Augusto et al., 2004; Bácskai et al., 2014) that display the highest vulnerability in ALS (Kanning et al., 2010). This age precedes the onset of endoplasmic reticulum (ER) stress (Saxena et al., 2009), cell death markers (Li et al., 2000) and axonal retraction from the neuromuscular junction (NMJ) (Frey et al., 2000). Thus, changes in the axon initial segment may represent a component of the pathogenesis of ALS, rather than the downstream consequence of other pathology that may be present in stressed motor neurons as the disease progresses. Furthermore, this age immediately follows motor circuit and neuromuscular maturation (Clarke and Still, 2001; Arber, 2012), removing variability that may be caused by differences in rates of circuitry development. Finally, to distinguish between the ALS-vulnerable alpha (Kanning et al., 2010) and resistant gamma (Lalancette-Hebert et al., 2016) motor neuron subtypes I stained spinal cord sections for NeuN (Rbfox3) that is selectively down-regulated in γ-motor neurons but persists in vulnerable α-motor neurons (Shneider et al., 2009).

100μm sections from L4-5 were taken from SOD1^{G93A} mice and compared to those from non-transgenic (Nt) littermates. Using immunohistochemistry (IHC), motor neurons were visualized by targeting choline acetyltransferase (ChAT) and their axon initial segments by the structural protein ankyrinG (AnkG or *Ank3*), master organizer of and densely clustered at the axon initial segment (Zhou et al., 1998; Yang et al., 2007; Song et al., 2009; Brachet et al., 2010; Kuba et al., 2014; Jacko et al., 2018). The axon initial segment length was then quantified through the Z-stack using the Simple Neurite Tracer plugin in ImageJ (Longair et al., 2011). Intriguingly, α-motor neurons of the L4-5 spinal cord in ALS mice display shorter axon initial segments (23.3μm ± 0.26; n=207) as compared to their Nt littermates (24.8μm ± 0.26; n=182), indicating that ALS motor neurons are intrinsically hypoexcitable (Figure 2.2). In

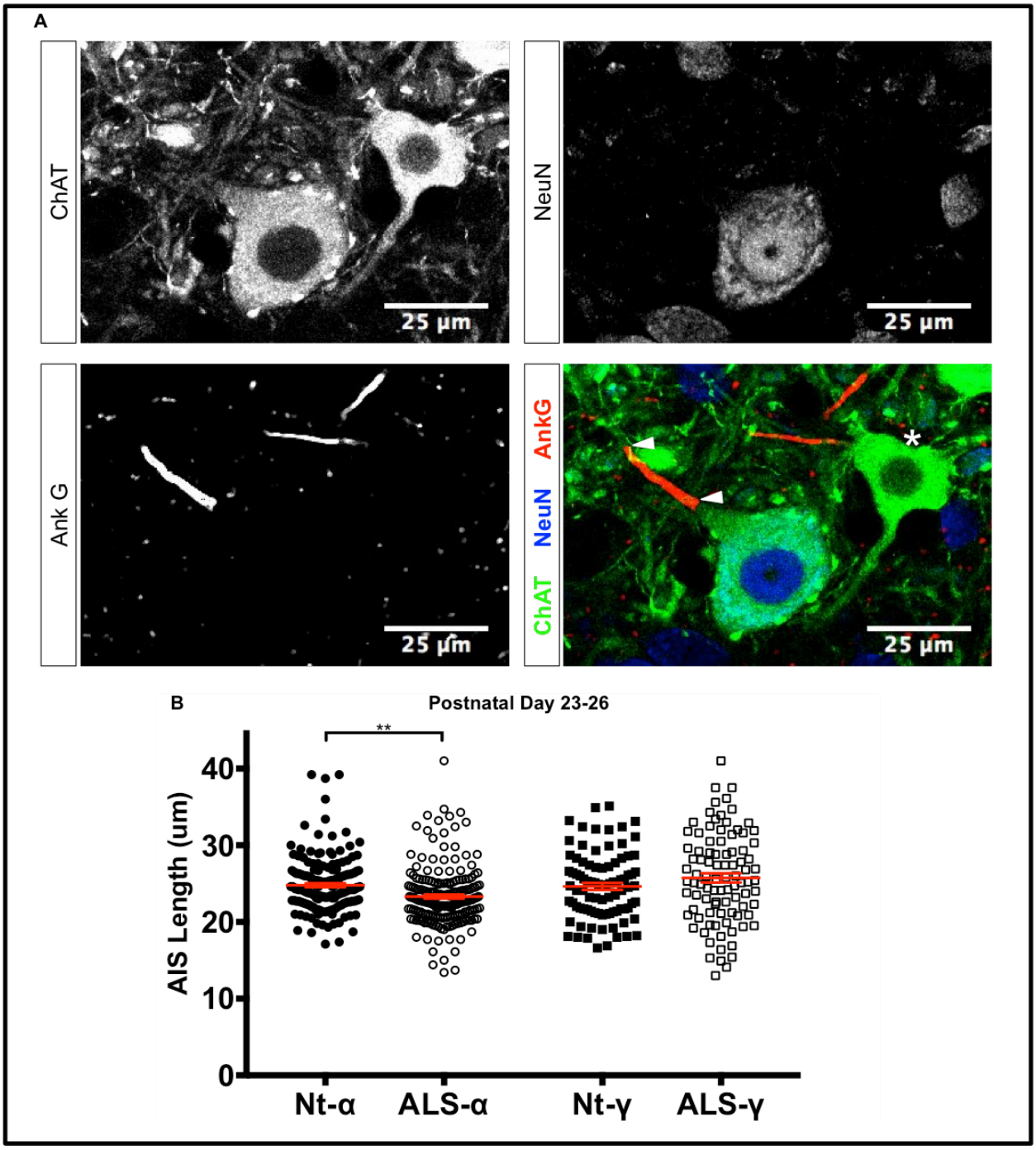

Figure 2-2: Axon initial segment length is reduced in α-motor neurons of young adult ALS mice.

A) Representative images of ChAT and NeuN positive α-motor neurons, ChAT positive and NeuN negative γ-motor neurons, and axon initial segments visualized by ankyrinG. White arrows denote the proximal and distal ends of the axon initial segment and asterisk marks a γ-motor neuron. B) Quantification of axon initial segment length. Each dot represents a single motor neuron and the red bar marks the mean. Significance by one-way ANOVA and Bonferroni post hoc analysis.

contrast, the γ-motor neurons did not display a significant change in axon initial segment length between ALS motor neurons (25.8μm ± 0.61; n=93) and their Nt littermates (24.6μm ± 0.46; n=89) (Figure 2.2).

Axon initial segment shortening succeeds spinal circuit maturation

To determine if axon initial segment shortening is present prior to circuit maturation, I examined neonatal mice in their first week of age, before descending fiber innervation (Clarke and Still, 2001; Arber, 2012). I find no difference in axon initial segment length in the P4-6 lumbar spinal cord (Figure 2.3), suggesting a necessity of circuitry maturation before axon initial segment changes in the SOD^{G93A} mice are detectable. Interestingly, the length of the axon initial segment in these neonatal mice [(Nt-alpha 31.9μm ± 0.36; n=177) ($SOD1^{G93A}$-alpha 33.0μm ± 0.42; n=128) (Nt-gamma 43.2μm ± 0.92; n=82) ($SOD1^{G93A}$-gamma 42.8μm ± 1.01; n=66)] is notably longer as compared to the P23-26 mice, consistent with the relatively low levels of activity that have been reported in immature motor neurons of this age (Personius and Balice-Gordon, 2001). This same shift in axon initial segment length between neonatal and young adult (~P25) mice is seen in both the alpha and γ-motor neuron subtypes, suggesting that these neurons both undergo structural changes in the axon initial segment in response to circuit maturation.

Axon initial segment shortening is persistent and progressive

To assess whether the change in axon initial segment length in young adult ALS mice simply reflects a transient alteration of this structure, I looked at the same region of the spinal cord (L4-5) at later, but still presymptomatic time points. Choosing points approximately every

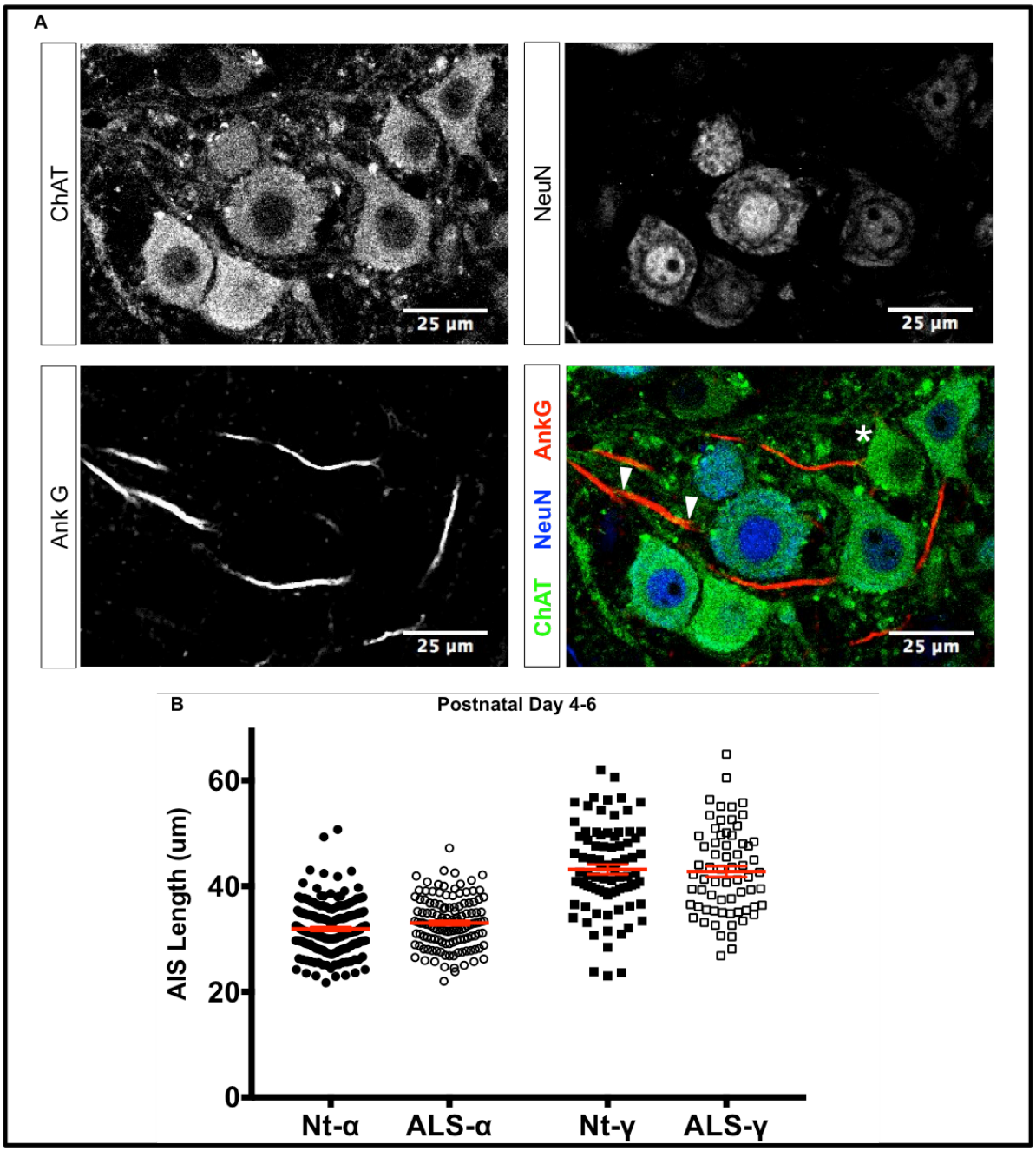

Figure 2-3: Axon initial segment length is unchanged in α and γ-motor neurons of neonatal ALS mice, though markedly longer than their adult equivalents.

A) Representative images of ChAT and NeuN positive α-motor neurons, ChAT positive and NeuN negative γ-motor neurons, and axon initial segments visualized by AnkyrinG. White arrows denote the proximal and distal ends of the axon initial segment and asterisk marks a γ-motor neuron. B) Quantification of axon initial segment length. Each dot represents a single motor neuron and the red bar marks the mean. Significance by one-way ANOVA and Bonferroni post hoc analysis.

20 days, I reexamined the axon initial segment length in aging ALS mice. At postnatal days 44-46, I observed a persistent phenotype, where ALS α-motor neurons display shorter axon initial segments (21.9μm ± 0.18; n=139) compared to their Nt littermates (22.7μm ± 0.21; n=86) (Figure 2.4A,B). And γ-motor neurons did not display a significant change in axon initial segment length between ALS motor neurons (22.6μm ± 0.70; n=32) and their Nt littermates (22.5μm ± 0.56; n=40) (Figure 2.4A,B).

The axon initial segment progressively shortened in α-motor neurons as the $SOD1^{G93A}$ mice aged to P63-70, an age near the beginning of degeneration in this mouse model (Turner and Talbot, 2008). A-motor neurons in the $SOD1^{G93A}$ mice contained significantly shorter axon initial segments (19.8μm ± 0.36; n=136) than their Nt littermates (22.2μm ± 0.18; n=142) (Figure 2.4C). Remarkable, I observe opposite axon initial segment length changes in the $SOD1^{G93A}$ mice γ-motor neurons (25.7μm ± 0.54; n=48) at this age, compared to Nt gammas (22.9μm ± 0.46; n=64) (Figure 2.4C).

p62 pathology marks vulnerable α-motor neurons and precedes vacuole invasion of the soma

Later stages of ALS are marked by retraction of the neuromuscular junction and motor neuron degeneration (Fischer et al., 2004; Pun et al., 2006). Prior to these phases of the disease, early pathological markers in the $SOD1^{G93A}$ mouse model includes the formation of large p62 immunoreactive structures (Rudnick et al., 2017), as well as the formation of large vacuoles that likely result from mitochondrial swelling (Dal Canto and Gurney, 1994; Higgins et al., 2003). Given the presence of p62 aggregates in several other neurodegenerative diseases (Liu et al., 2017), and that not all motor neurons in ALS present with this phenotype, I regarded is as an appropriate marker of neuronal stress to identify motor neurons that would likely be the

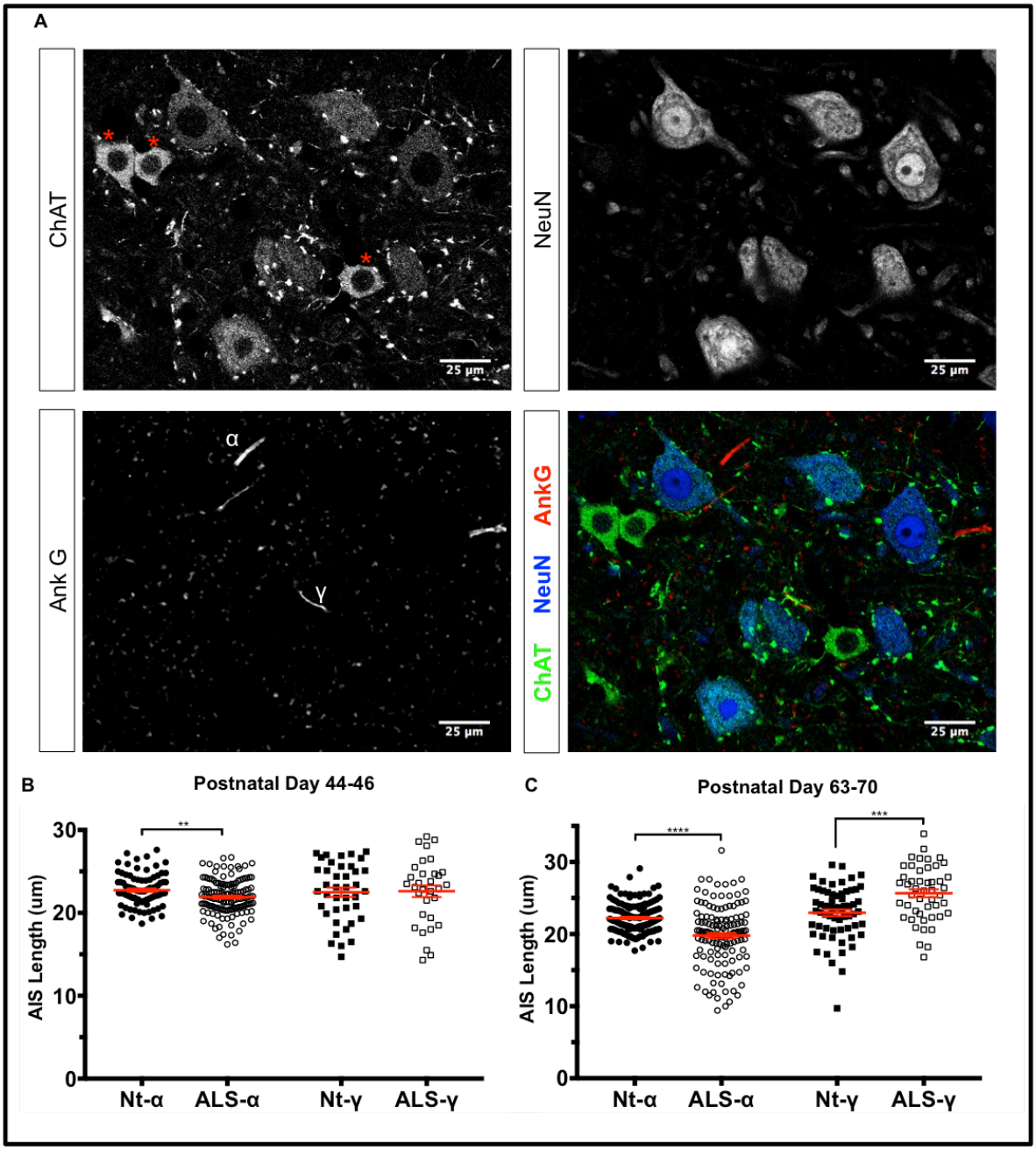

Figure 2-4: Axon initial segment length changes are persistent in α-motor neurons of adult ALS mice and present in γ-motor neurons as the disease progresses.

A) Representative images of ChAT and NeuN positive α-motor neurons, ChAT positive and NeuN negative γ-motor neurons, and axon initial segments visualized by AnkyrinG. Red asterisks mark γ-motor neurons. B) Quantification of axon initial segment length. Each dot represents a single motor neuron and the red bar marks the mean. Significance by one-way ANOVA and Bonferroni post hoc analysis.

first to degenerate. I aimed to identify a timeline of *in vivo* motor neurons that presented with markers of cellular stress in ALS prior to degeneration. I first analyzed the development of p62-possitive aggregates, important in binding a number of ubiquitinated products and aiding in their targeting for autophagic degradation (Komatsu et al., 2012). I next characterized the emergence of soma-invading vacuoles, presenting as an additional marker for progressive cellular stress (Wong et al., 1995). Though somal vacuoles were clearly recognizable with the ChAT antibody alone, I also visualized vacuoles by targeting the external mitochondrial membrane protein, TOMM20 (Pfanner et al., 1997).

At postnatal day 23-26, where I first see emergence of the axon initial segment phenotype, I see no evidence of p62 aggregation or vacuole formation (Figure 2.5). By postnatal day 45 a robust presence of p62 aggregation emerges, however, very few somal vacuoles were observed (Figure 2.5). Severe somal vacuolation accompanied by p62 aggregation occurs by postnatal days 63-70 (Figure 2.5), though, not all motor neurons containing p62 aggregates harbored vacuoles. Importantly, vacuole formation was seemingly only observed in α-motor neurons, though I based this only on size rather than NeuN staining. Nevertheless, is appears that γ-motor neurons are markedly spared of this cellular stress phenotype. Additionally, in another qualitative analysis, p62 aggregation was only observed in spinal motor neurons and was not observed elsewhere in the spinal sections at this stage (data not shown).

Increased excitation leads to early stress in ALS motor neurons

It is possible that the axon initial segment shortening observed in $SOD1^{G93A}$ α-motor neurons is random throughout the motor neuron population, rather than presenting as an early indicator of cells to become stressed. To address this possibility, I used our characterization of

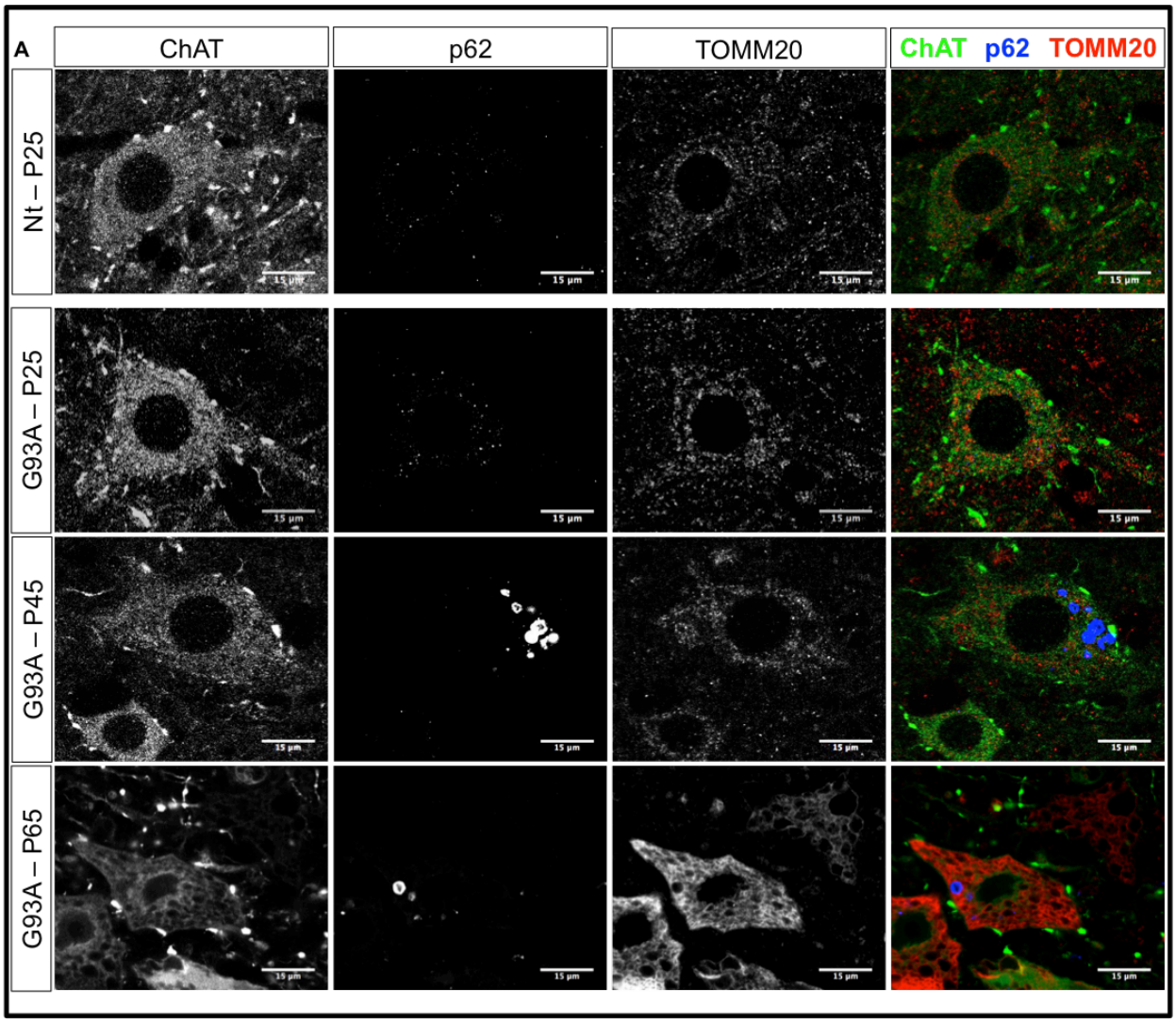

Figure 2-5: Axon initial segment shortening is an early phenotype in ALS, emerging prior to p62 aggregation and vacuolization

A) Representative images of ChAT positive motor neurons where abundant p62 aggregation is visualized in Postnatal Day 45 $SOD1^{G93A}$ mice. Though vacuoles emerge in a small number of motor neurons at Postnatal Day 45, they are not abundantly represented in motor neuron somas until Postnatal Day 65. Vacuoles are visualized by the outer mitochondrial membrane marker, TOMM20.

known pathological markers in ALS to identify motor neurons undergoing early cellular stress events. The axon of α-motor neurons is known to be much larger in diameter as compared to γ-motor neurons (Kanning et al., 2010), making their axon initial segment easily identifiable with the AnkG stain alone (Figure 2.2A). So, as a method of blinding, axon initial segment measurements were made on all α-motor neuron axon initial segments with just the AnkG staining in P44-46 L4-5 spinal cord sections. After measurement, the composite image was used to verify first whether the axon initial segment measured belonged to a ChAT-positive motor neuron, and second to divide into motor neurons that contain p62 aggregates and those that do not display any tested pathologies ("normal"). Intriguingly, the motor neurons that contain p62 aggregates display significantly shorter axon initial segments as compared with both Nt littermates and to "normal" $SOD1^{G93A}$ motor neurons (Figure 2.6A,B,D). The same blinding procedure was used to analyze motor neurons in postnatal day 63-66 L4-5 spinal cord sections. This time, however, motor neurons were split into three groups, "normal" motor neurons, those that contain only p62 aggregates, and those with vacuoles, identified using the ChAT staining. Similarly to the P45 mice, the shortest axon initial segments belonged to those with stress markers, yet the vacuole-containing motor neurons displayed the shortest, p62 aggregate-only motor neurons the second shortest, and the "normal" $SOD1^{G93A}$ motor neurons did not significantly differ from their Nt littermates.

Discussion

Here, I show that the axon initial segment exhibits early structural changes in ALS, suggestive of an early decrease in intrinsic excitability. The motor neurons displaying axon initial segments that are shortest, also, display early markers of neuronal stress and are likely the first neurons to undergo degeneration. I describe axon initial segment plasticity in motor

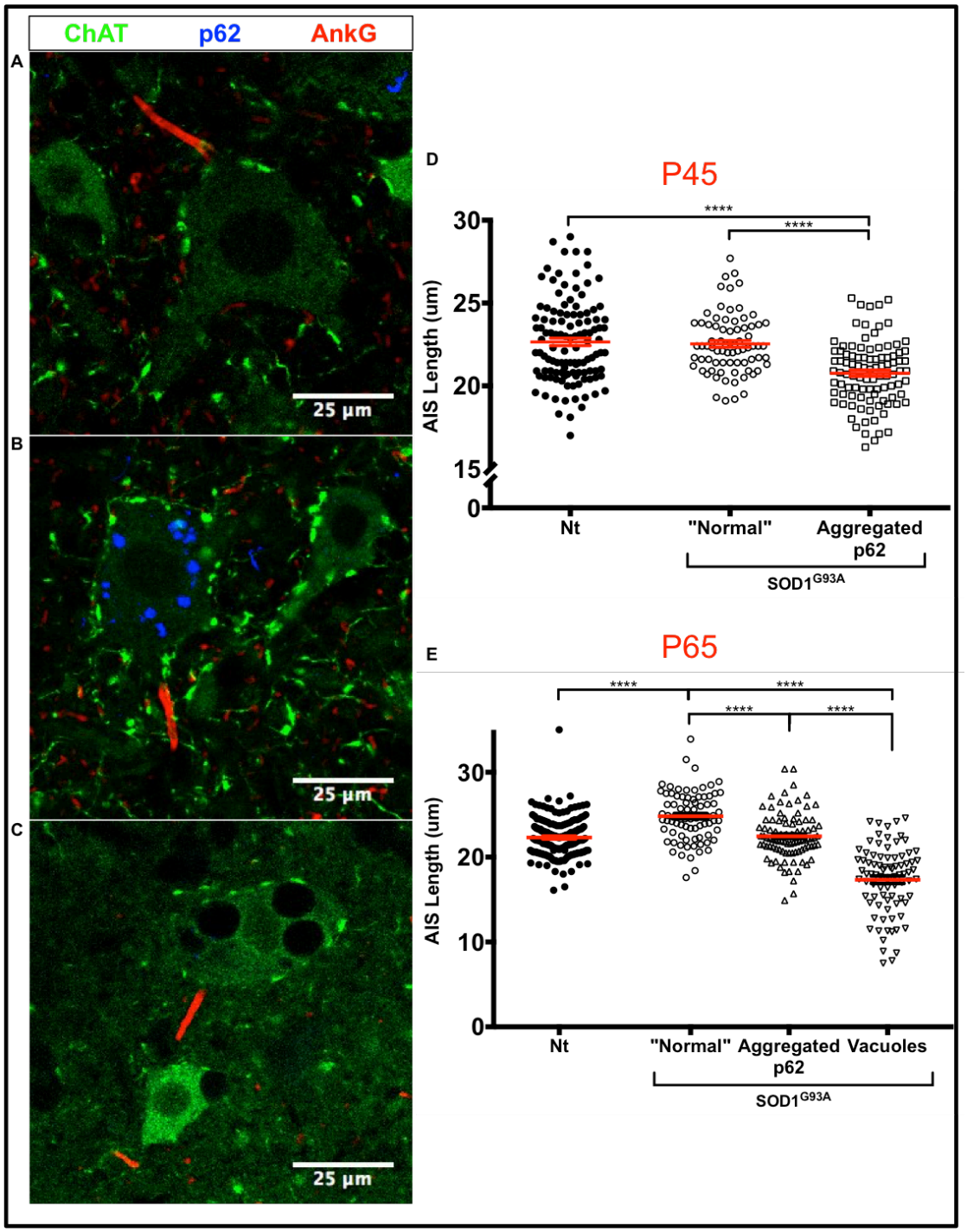

Figure 2-6: Axon initial segment shortening is restricted to motor neurons that display phenotypic markers of stress

A) Representative image of a "normal" ChAT positive motor neuron lacking p62 aggregates or vacuoles. B) Abundant p62 aggregation in a motor neuron lacking vacuoles. C) Vacuolized motor neuron. D) Quantification of axon initial segment length in P45 motor neurons. $SOD1^{G93A}$ motor neurons are divided into two groups, those with p62 aggregates and those without (denoted "Normal"). E) Quantification of axon initial segment length in P65 motor neurons. $SOD1^{G93A}$ motor neurons are divided into three groups, those with vacuoles, those with p62 aggregates and those without either (denoted "Normal"). Significance by one-way ANOVA and Bonferroni post hoc analysis.

neurons to function as homeostatic compensation for synaptic drive, as others have defined in various other excitatory neurons in the CNS (Grubb and Burrone, 2010; Kuba et al., 2010; Chand et al., 2015; Wefelmeyer et al., 2015). Our *in vitro* study of axon initial segment plasticity in motor neurons is reinforced by the observation that the axon initial segment shortens, even in the Nt mice, from the neonatal age to the young adult *in vivo* (Figures 2.2 and 2.3), a period where known increases in activity take place (Personius and Balice-Gordon, 2001). Taken together, these data suggest the emergence of intrinsic hypoexcitability early in ALS mice may hold a pathogenic influence that plays a role in degeneration.

Hyperexcitability vs hyperexcitation

Leroy and Zytnicki well define the conflicting evidence describing hyperexcitability in ALS motor neurons and further differentiating between excitability and excitation (Leroy and Zytnicki, 2015). Many studies of ALS motor neurons focus on intrinsic measures of excitability (Elbasiouny et al., 2012) and infer that motor neuron action potential firing (activity) will be proportional to these measures. Intrinsic electrophysiological properties, however, may not be a sufficient guide to uncover aberrant activity in motor neurons. Situations arise, such as with the fast and slow α-motor neuron subtypes, where the intrinsically hypoexcitable neuron ends up firing at significantly higher frequencies (Müller et al., 2014). Furthermore, our data suggest that motor neurons that are likely intrinsically hypoexcitable may be so as a result of hyperexcitation (Figure 2.1). Intrinsic excitability may reflect homeostatic shifts in response to excitation, rather than underlie the driving force, thus inversely proportional to their amplitude of excitation.

Interestingly, I see no significant changes in axon initial segment length in the neonatal mice. This result compares with findings in Leroy et al., who do not find significant electrophysiological differences in fast α-motor neuron in ALS (Leroy et al., 2014). Likewise, I do not see axon initial segment length changes that would reflect electrophysiological

abnormalities in SOD1^{G93A} mice. The shift in excitability of slow α-motor neurons in their report would likely not show up in our analysis, as there are limited numbers of type I muscle fibers in small mammals such as mice (Peters et al., 1999). Moreover, the vast majority of the muscles innervated by motor neurons that originate in L4-5 region are comprised almost entirely of type II fibers (Burkholder et al., 1994; Augusto et al., 2004; Bácskai et al., 2014). To that point, the soleus muscle, one of the crural muscles innervated by L4-5 and well known for its composition of ~50% type I fibers (Peters et al., 1999), likely represents only ~20 motor neurons total (Fladby and Jansen, 1987). Therefore, it is unlikely that significant contamination from slow α-motor neurons exist in the present analysis. This is supported by my observation that axon initial segment shortening occurs in the motor neurons that first display phenotypic markers of stress, where these early-affected motor neurons tend to be the fast alpha subtype. Furthermore, descending circuitry of the corticospinal tract does not connect with lumbar motor neurons until the end of postnatal week two (Gianino et al., 1999; Arlotta et al., 2005). Prior to the descending circuitry's innervation of lumbar motor neurons, they have also been found to have low levels of activity compared to their adult counterparts (Personius and Balice-Gordon, 2001), reflected here by their relatively long axon initial segments (Figure 2.3). So, it is likely that shifts in intrinsic excitability seen in neonatal fast α-motor neurons in the spinal cord have a small effect until after circuit maturation, when there may be larger homeostatic events such as seen here with axon initial segment plasticity.

Circuitry Defects and Compensation

The axon initial segment changes seen at P23-26 are possibly reflective of circuitry abnormalities. Yet, I cannot rule out the possibility of activity-independent mechanisms at play. For instance, one could posit that disruptions to calcium homeostasis could be involved. This could effect the calcium-dependent mechanism of axon initial segment plasticity (Yoshimura and Rasband, 2014). However, the calcineurin-mediated mechanism that underlies axon initial

segment plasticity seems more likely to be triggered through a calcium microdomain surrounding L-type calcium channels, than through global perturbations of calcium (Huang and Rasband, 2018). Additionally, if cytosolic calcium levels became too disrupted, one might expect to see calpain-mediated dissolution of the axon initial segment in motor neurons close to death (Schafer et al., 2009). I do not see a full loss of the axon initial segment even in extremely swollen and vacuolized cells. Thus, I deem it less likely that calcium disruption in ALS leads to the shortened axon initial segment, and that it is more likely a product of canonical excitation-driven changes.

Our data support this claim when considering the shift in axon initial segment length that occurs even in the Nt mice from the neonate to the young adult. Motor neurons display relatively low amounts of activity in the early postnatal period and do not gain adult activity levels until P14-15 (Personius and Balice-Gordon, 2001), after the descending circuitry matures (Gianino et al., 1999; Clarke and Still, 2001; Arber, 2012). This would suggest that the changes in axon initial segment length in ALS motor neurons require circuitry maturation and are indicative of abnormally high net excitation. The lack of neonatal phenotype also suggests that intrinsic activity-independent mechanisms that control axon initial segment assembly are not compromised.

In contrast to changes in axon initial segment in alpha motor neurons, I observed lengthening of the axon initial segment in gamma motor neurons in the P70 mice (Figure 2.4). The γ-motor neurons are resistant to degeneration, but their function is intimately linked to that of the α-motor neurons. The opposite change of axon initial segment length observed in alpha and gamma motor neurons is indicative of more complex, motor circuit level aberrations emerging at the time when first alpha motor neurons start to degenerate, perhaps revealing modulatory attempts to reduce alpha excitation. Evidence of such effects may be supported by the observation of longer axon initial segments in the “normal” motor neurons in the $SOD1^{G93A}$ mice. Additionally, as major behavioral changes aren’t observed in $SOD1^{G93A}$ mouse models until

~P90 (Turner and Talbot, 2008), it is likely that the axon initial segment and other intrinsic compensatory systems contribute to the outwardly normal functioning of the motor systems in early adult life, mimicking ALS in humans where few early functional abnormalities have been detected.

It will be interesting to address whether the homeostatic mechanisms, likely active here, underlie an increase in cellular stress that exacerbates the disease. Also of interest, neuronal polarity and axonal transport breakdown have been seen in ALS (De Vos and Hafezparast, 2017). Given the important role of the axon initial segment in maintaining polarity (Rasband, 2010), it is possible that chronic induction of plastic events in this subcellular structure degrades its ability to properly separate the axonal and somatodendritic compartments.

Methods

Animals

Staining in the lumbar spinal cord was performed on tissue from first generation crosses of C57BL/6J females and *SOD1*^{G93A} transgenic male mice [C57BL/6J, 000664; B6.Cg-Tg (SOD1*G93A)1Gur/J, 004435, Jackson Laboratory]. All experiments utilizing laboratory animals were performed in accordance with NIH guidelines for the care and use of laboratory animals, and with approval of the Institutional Animal Care and Use Committees of Columbia University.

Animal Tissue Collection, Immunofluorescence Staining and Imaging

SOD1^{G93A} mutant mice and their non-transgenic littermates (first generation cross only) at postnatal days 66 and 100 ± 3 were deeply anesthetized using Avertin (tribromoethanol, Sigma) and fixed by transcardial perfusion with 4% paraformaldehyde (from 32% stock, 15714, Electron Microscopy Sciences) in phosphate-buffered saline (PBS) pH 7.4 (70011,

ThermoFisher). The CNS was removed and fixed overnight in the same solution noted above. Whole brain and lumbar segments 4 and 5 were dissected, embedded in 4% (w/v) agar and sectioned on a vibratomb (Leica VT1000 S). 100 µm transverse spinal cord sections and sagittal whole brain sections were cut. Sections were blocked overnight in Tris-buffered saline (TBS) with 10% donkey serum (D9553, Sigma) and 0.4% Triton X-100 (T8787, Sigma). Sections then were incubated at room temperature for two days in the above blocking buffer with primary antibodies [goat polyclonal anti-ChAT (1:100; AB144P, Millipore); mouse monoclonal anti-NeuN, clone A60 (1:100; MAB377, Millipore); mouse monoclonal anti-SQSTM1 / p62 (1:500; ab56416, Abcam); mouse monoclonal anti-misfolded human SOD1 (1:250; MM-0072-02, MédiMabs); rabbit polyclonal anti-ankyrin G (Stock 0.2 µg/mL, 1:100; 386 003, Synaptic Systems)]. After the primary incubation, six washes (>30 minutes each) in TBS with 0.4% Triton were followed by a one-day incubation at room temperature in the above wash buffer with donkey anti-mouse and anti-goat secondary antibodies (1.5 µg/mL; Jackson ImmunoResearch). After six more washes (as stated above), sections were mounted on microscope slides in Fluoromount G (OB100, ThermoFisher) using 100 µm spacers and allowed to set for >12hrs. Staining was visualized by confocal microscopy (Zeiss LSM 800).

Cell Culture

Mouse embryonic stem cells (ESCs) were cultured in EmbryoMax DMEM (EMD Millipore) supplemented with 15% embryonic stem cell screened fetal bovine serum (HyClone), 2mM L-glutamine (Life Technologies), 1x non-essential amino acids EmbryoMax MEM (EMD Millipore), 1x EmbryoMax nucleosides (EMD Millipore), 0.1mM β-mercapthoethanol (Sigma-Aldrich), 1000U/ml ESGRO Leukemia inhibitory factor (EMD Millipore), 1.25µM GSK-3 inhibitor XVI (EMD Millipore) and 100nM FGF receptor antagonist PD173074 (Tocris). All cells were determined to be negative for mycoplasma using the Venor GeM Mycoplasma detection kit (Sigma-Aldrich).

Motor neuron differentiation, fixation and staining

ESCs were differentiated into spinal neurons in embryoid bodies following established protocols (Wichterle et al., 2002; Wichterle and Peljto, 2008; Sternfeld et al., 2017). During the differentiation process, primary cortical astrocytes were plated onto plasma-treated coverslips coated in polyornithine/laminin and incubated from 4-5 days in media [Advanced DMEM/F12 (Life Technologies), 2mM L-glutamine (Life Technologies), 10% fetal bovine serum]. After 6 days of differentiation, embryoid bodies were dissociated and neurons were plated on astrocyte monolayer in maturation media [Neurobasal medium (Life Technologies), 500μM L-glutamine (Life Technologies), 1x B-27 Supplement (serum free) (Life Technologies), 1:1000 β-mercapto ethanol (Chemicon ES-007-E), 2% heat-inactivated horse serum, containing neurotrophic factors (10ng/mL BDNF (R&D Systems), 10ng/mL GDNF (R&D Systems), 10ng/mL CNTF (R&D Systems), 10ng/mL IGF-1 (R&D Systems), 10μM Forskolin (Sigma), and 100μM IBMX (R&D Systems)]. The media was replaced every 2-3 days starting from two days after plating. Motor neuron differentiations were consistently around 40% efficient.

In vitro motor neurons were fixed with 4% paraformaldehyde (from 16% stock, 15710, Electron Microscopy Sciences) in phosphate-buffered saline (PBS) pH 7.4 (70011, ThermoFisher). Equal volume paraformaldehyde was first added to the media of each well and incubated for 2 minutes. This ~2% paraformaldehyde solution was then aspirated and the 4% paraformaldehyde added and incubated at 4°C for 20 minutes. After the incubation, three washes (>5 minutes each) in PBS were performed. Cultures were blocked for >30 minutes in PBS with 10% donkey serum (D9553, Sigma) and 0.1% Triton X-100 (T8787, Sigma). *In vitro* motor neurons were then were incubated at 4°C overnight in the above blocking buffer with primary antibodies [mouse monoclonal anti-vesicular glutamate transporter 2 (1:100; MAB5504, EMD Millipore) or rabbit polyclonal anti-ankyrin G (Stock 0.2 μg/mL, 1:100; 386 003, Synaptic Systems)]. After the primary incubation, three washes (>5 minutes each) in PBS with 0.1%

Triton were followed by a 1.5hr incubation at room temperature in the above wash buffer with donkey anti-mouse or anti-rabbit secondary antibodies (1.5 µg/mL; Jackson ImmunoResearch). After three more washes (as stated above), coverslips were mounted on microscope slides in Fluoromount G (OB100, ThermoFisher) and allowed to set for >12hrs.

Axon initial segment analysis

Motor neurons plated on primary cortical astrocytes were imaged using a laser-scanning confocal microscope (LSM 800, Zeiss) using a 40x oil-immersion objective. The settings were adjusted to prevent signal saturation and the images were taken in z-stacks with 1 µm steps. Z-stack images were projected into a single plane using maximum intensity projections and intensity across the length of the axon initial segment was quantified using the image analysis software Fiji (Schindelin et al., 2012). Briefly, the cutoff intensity for axon initial segment start/end was 1/3 of the maximum intensity similar to methods used previously (Grubb and Burrone, 2010). AnkyrinG signal in the soma at times was quite high, therefore the axon initial segment starting point was manually determined.

For *in vivo* axon initial segment analysis, sections were imaged using a laser-scanning confocal microscope (LSM 800, Zeiss) and a 40x oil-immersion objective. The settings were adjusted to prevent signal saturation and the images were taken in z-stacks with 1 µm steps. The start and end of the *in vivo* initial segment is extremely distinct as seen in the reported images. Therefore, the start and end were manually chosen and Simple Neurite Tracer (Longair et al., 2011) software through the Fiji platform was used to automatically generate lengths of the axon initial segment.

Whole cell current clamp

Excitability was assessed using conventional whole cell current clamp technique. Briefly, astrocytes were prepared as previously described (Albuquerque et al., 2009) and plated on 15-mm diameter coverslips at a density of 100,000 cells per well in a 24-well plate. 4-6 days following astrocyte plating, non-sorted motor neurons added to the wells at a density of 50,000 total cells per well. Cultures were maintained for 17 days before recording, as per experimental design (Figure 2.1). Membrane potential recordings were performed using a Multiclamp 700B amplifier and a Digidata 1550 digital-to-analog converter. Signals were recorded at a 10-kHz sample rate using pClamp 10 software (all equipment from Molecular Devices). Patch pipettes were fabricated with a P-97 pipette puller (Sutter Instruments) using 1.5 mm outer diameter, 1.28 mm inner diameter filamented capillary glass (World Precision Instruments). Pipette resistance was 2-5 MΩ when filled with the pipette solution. The external recording solution contained 145 mM NaCl, 5 mM KCl, 10 mM HEPES, 10 mM glucose, 2 mM $CaCl_2$ and 2 mM $MgCl_2$. The pH was adjusted to 7.3 using NaOH and the osmolality adjusted to 325 mOsm with sucrose. The pipette solution contained 130 mM CH_3KO_3S, 10 mM CH_3NaO_3S, 1 mM $CaCl_2$, 10 mM EGTA, 10 mM HEPES, 5 mM MgATP and 0.5 mM Na_2GTP (pH 7.3, 305 mOsm). Experiments were performed at room temperature (21–23 °C). During recordings, current was injected to hold the cells at -60 mV. The liquid junction potential between pipette and external solutions was calculated empirically, and the correction applied before the experiment. Resting membrane potential was measured immediately following establishment of the whole-cell configuration. Membrane resistance and capacitance were calculated from the membrane potential changes in response to 1 s duration hyperpolarizing current steps that increased incrementally by 5 pA. Action potentials were evoked and rheobase obtained using 1 s duration depolarizing current steps that increased incrementally by 5 pA. For blocking EPSPs, bath perfusion containing CNQX was used, followed by a wash with bath solution.

An action potential was defined as a transient depolarization of the membrane which had a minimum rise rate > 10 mV/ms and reached a peak amplitude > 0 mV. Action potential characteristics were measured from the first action potential at rheobase. The threshold potential was measured at the point where the voltage increases at a rate greater than 10 ms/mV. The duration was calculated from the full width at the half maximum voltage. For this calculation, the amplitude was measured from the threshold potential to the maximum potential. The maximum number of action potentials was measured from a 1 s current step. The amplitude of the step was dependent on the individual cell. Quantification was carried out using custom written scripts for Igor Pro v. 6 (Wavemetrics, USA). Outliers within Rheobase, Input Resistance, and Capacitance, that would indicate a poor seal, were identified using the ROUT method (Q = 0.5%) in GraphPad Prism version 7.0a for Mac, GraphPad Software, La Jolla California USA (www.graphpad.com). For each outlier detected, data from the entire neuron was removed from the analysis. Statistical comparisons were made using unpaired Student's t-test in GraphPad Prism. P-values < 0.05 were considered significant.

Chapter 3: Heterogeneity of ALS phenotypes between cranial motor nuclei and spinal motor neurons

Summary

ALS is marked by progressive degeneration of motor neurons in the spinal cord, midbrain and cortex. Studies have investigated physiological differences between ALS-vulnerable and resistant populations; however, it is unclear whether populations of molecularly distinguishable ALS-vulnerable motor neurons encounter identical pathogenic pathways.

Marked shortening of the axon initial segment was observed in spinal motor neurons. This phenotype was most pronounced in motor neurons that displayed p62 aggregation and vacuole formation. Contrary to what was found in spinal motor neurons, ALS-vulnerable motor neurons of the brain stem exhibit lengthening of their axon initial segment. Additionally, p62 aggregation and somal vacuole formation present heterogeneously across ALS-vulnerable cranial motor neuron populations and are distinct from their phenotypic pattern in the spinal motor neurons. I further characterized mutant SOD1 aggregation in both spinal and cranial motor neurons. This phenotype maintained more consistency between the populations, however, was most prevalent at outer membranes of the vacuoles. Lastly, I quantified degeneration within cranial and spinal motor neuron populations, finding that though phenotypically distinct, the timeline of degeneration is consistent.

Introduction

As described in Chapter 1, across the cranial motor nuclei, motor neurons in nuclei that innervate the extraocular muscles (oculomotor, trochlear, and abducens) are spared in ALS while all others see significant degeneration at similar levels to what is seen in spinal motor neurons (Turner and Talbot, 2008; Nijssen et al., 2017). In ALS patients, those that first present with bulbar symptoms have a worse prognosis, possibly indicating some heterogeneity in the mechanisms of disease pathogenesis, though similar to other clinical presentations of ALS, studies show degeneration throughout the motor system in postmortem tissue in these patients (Nijssen et al., 2017). The vulnerable cranial motor neurons (trigeminal, facial, ambiguus, and hypoglossal) are thought to undergo similar pathophysiology as spinal motor neurons in ALS (Turner and Talbot, 2008), however, given that these mechanisms have not yet been identified, this insight remains unclear. Certainly, phenotypes observed in spinal motor neurons such as

SOD1 and p62 aggregation have been reported in ALS (An et al., 2014). However, there are far fewer studies carried out in cranial motor neuron pathogenesis in ALS as compared to spinal motor neurons. Furthermore, a detailed quantification of the penetrance of these phenotypes across multiple vulnerable and resistant populations in both spinal and cranial motor neurons has not been conducted.

In Chapter 1, studies that were discussed arrived at seemingly contradictory conclusions regarding motor neuron activity and excitotoxicity. However, much of the excitotoxic effects thgouht to be present in vulnerable motor neuron pathophysiology is based on evidence from spinal motor neurons and the over-activation of corticospinal circuitry. Only a few analyses have investigated this hypothesis in vulnerable cranial motor neurons. Furthermore, it is unclear whether corticobulbar circuitry harbors similar hyperactivity to the corticospinal circuits in ALS. The few studies that have addressed excitability and activity in cranial motor neurons, however, have found increases in intrinsic excitability and excitatory input (van Zundert et al., 2008; 2012; Venugopal et al., 2015b), albeit with comparable caveats to what was discussed in Chapter 1 regarding electrophysiological analyses. Specifically, the cranial motor neurons analyzed were all at neonatal ages, leaving the same questions addressed for spinal motor neurons, where the differences in intrinsic excitability and activity reported for young cranial motor neurons may not reflect disease-relevant adult physiology.

In this chapter I examined the axon initial segment in ALS-vulnerable and resistant cranial motor neurons in the $SOD1^{G93A}$ mouse model as a proxy for changes in motor neuron excitation. Additionally, using the other ALS phenotypes characterized in Chapter 2, I will assess the timeline, presentation and severity of p62 aggregation and vacuole formation in and resistant vulnerable cranial motor neurons coupled to axon initial segment plasticity. This will have the added benefit of finding any transient phenotypic presentation in these populations. As an added measure of stress in ALS, I will investigate SOD1 aggregation within spinal and

cranial motor neurons. As with γ-motor neurons in the spinal sections, I will use the ALS-resistant oculomotor and trochlear motor neurons as internal controls for these experiments.

Results

Dynamic and heterogeneous plasticity of the axon initial segment in cranial motor nuclei

I previously reported the early phenotype of axon initial segment shortening in the lumbar spinal cord of the $SOD1^{G93A}$ mouse model of ALS. Axon initial segment length changes are not observed in ALS-resistant γ-motor neurons until later in the disease course, where a lengthening in this structure is observed (Figures 2.2 and 2.4). To investigate an additional resistant motor neuron population, and whether this phenotype of axon initial segment shortening is consistent across all vulnerable motor neurons, even those that are molecularly distinct, I looked at cranial motor neurons. I quantified the lengths of axon initial segments within the ALS-vulnerable facial, hypoglossal, and trigeminal motor pools, and in the oculomotor and trochlear pools, both spared in ALS (Figure 3.1). Ambiguus motor nucleus, though clearly vulnerable in ALS (Figure 3.1), was not analyzed for axon initial segment length due to the very dense clustering of motor neurons that cause uncertainty when assigning the axon initial segment to a motor neuron. To reduce variability from perfusion and staining artifacts, I collected the entire CNS from the mice used in the analysis in Chapter 2, and analyzed cranial motor neurons from these same tissue samples. 100μm sagittal sections from the midbrain were taken from Neonatal, P25 and P65 $SOD1^{G93A}$ mice and compared to those from non-transgenic (Nt) littermates. Using immunohistochemistry (IHC), motor neurons were visualized by targeting choline acetyltransferase (ChAT) and their axon initial segments by the structural

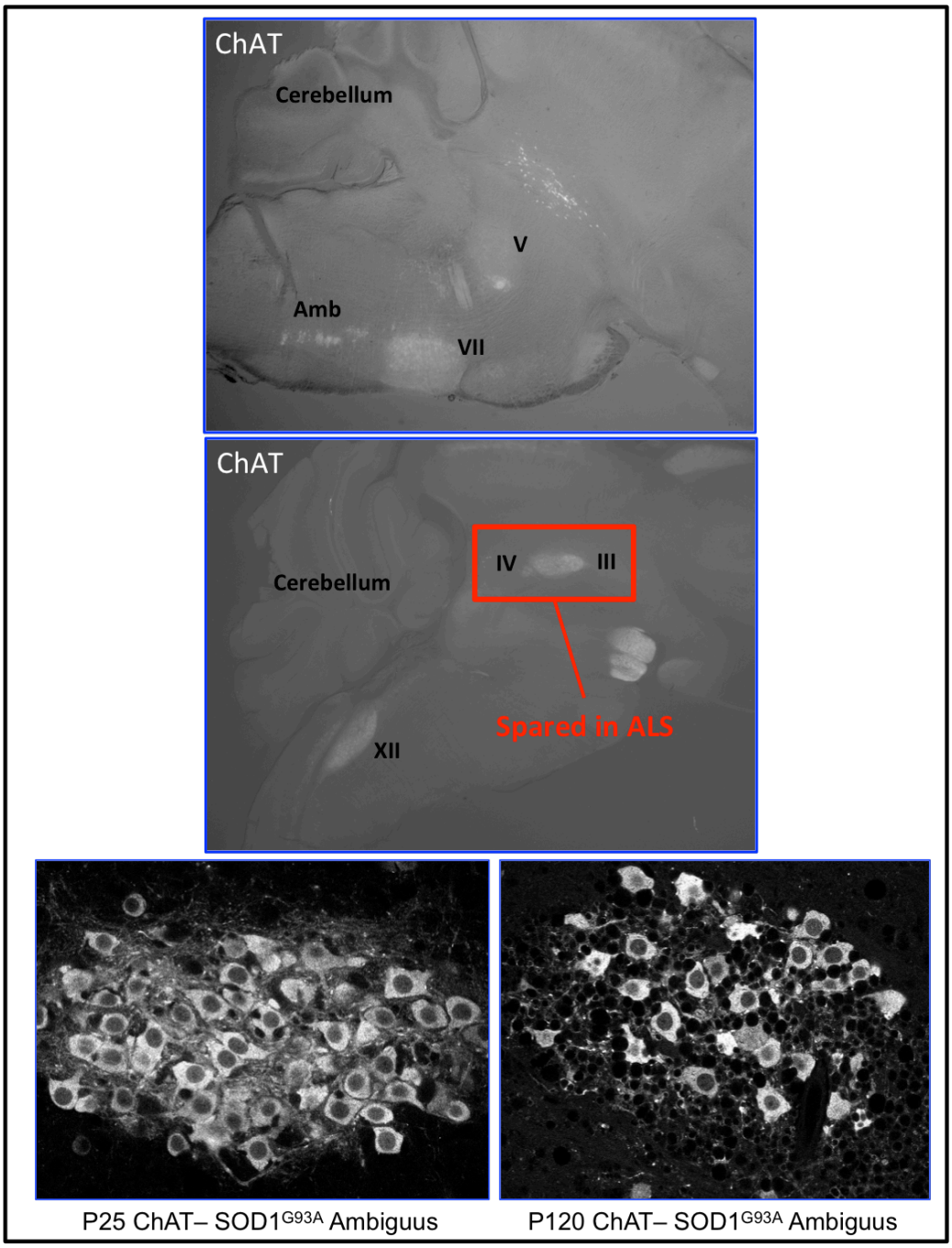

Figure 3-1: Visualizing cranial motor neurons in ALS

Top and Middle: Sagittal sections of whole brains from SOD1^{G93A} mice were immunostained for choline acetyl transferase (ChAT) and visualized by fluorescence microscopy. ALS-vulnerable cranial motor nuclei (V-trigeminal; VII-facial; XII-hypoglossal; Amb-ambiguus) and ALS-resistant cranial motor nuclei (III-oculomotor; IV-trochlear) were identified and analyzed for ALS phenotypes. Bottom: Nucleus ambiguus from young and post-symptomatic SOD1^{G93A} mice clearly demonstrate vulnerability to ALS in cranial motor neuron.

protein ankyrin G (AnkG or *Ank3*). The axon initial segment length was then quantified through the Z-stack using the Simple Neurite Tracer plugin in ImageJ (Longair et al., 2011).

Postnatal days 23-26

In SOD1^{G93A} mice at P25 I see evidence of axon initial segment plasticity in ALS-vulnerable motor neurons of the cranial nuclei. However, in contrast to the changes observed in spinal motor neurons, I detected an increase in axon initial segment length in ALS-vulnerable cranial motor neurons (Figure 3.2C). However, longer axon initial segments are seen only in trigeminal and hypoglossal MNs, but not in facial motor neurons, marking an additional level of heterogeneity in these vulnerable populations. Like the resistant γ-motor neurons of the spinal cord, the axon initial segment of motor neurons in the trochlear and oculomotor nuclei do not significantly change in the P25 SOD1^{G93A} mice.

Postnatal days 63-70

In the spinal cord, the axon initial segment of α-motor neurons became progressively shorter as the SOD1^{G93A} mice aged to P63-70 (Figure 2.4). To see if the phenotype in ALS-vulnerable cranial motor neurons persisted to later stages of the disease as well, I analyzed them at this age, again attaining tissue samples from the same mice that were used for the spinal motor neuron analysis. In the P63-70 cranial motor neurons, I find some ALS-vulnerable motor neurons to retain significant changes in the axon initial segment as compared to their Nt littermates. Again, however, I observe heterogeneity between populations of different cranial motor nuclei. Lengthening of the axon initial segment is observed again in the trigeminal motor neurons, as well as the facial motor neurons where a significant change is now apparent (Figure 3.2D). Conversely, the hypoglossal motor neurons are not found to be significantly longer, though a trend of longer axon initial segment length is seen. Dynamic changes are also observed in the ALS-resistant motor neurons, where, the P63-70 motor neurons in the

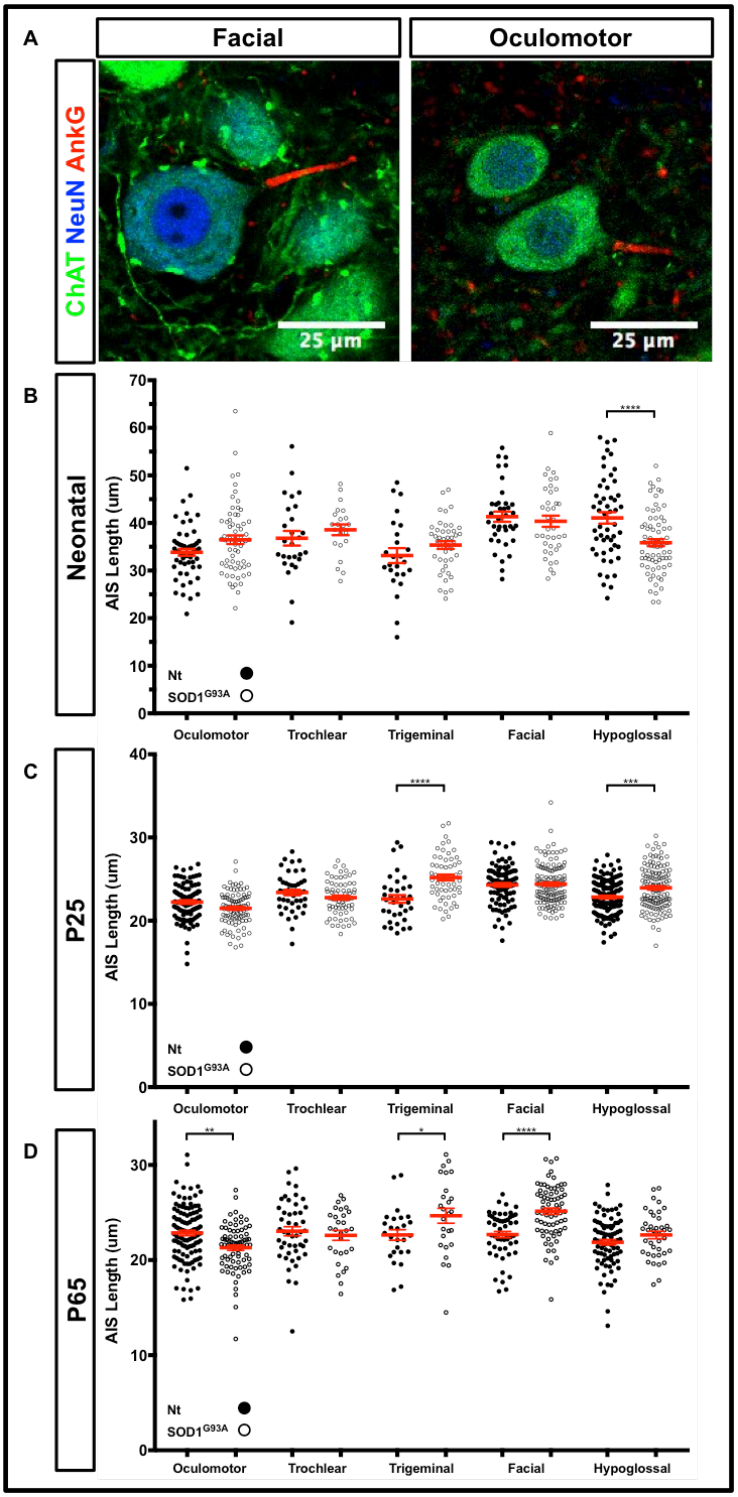

Figure 3-2: Changes in the axon initial segment in cranial motor neurons

A) Representative images of ChAT and NeuN positive motor neurons in the facial and oculomotor nuclei where axon initial segments can be visualized by AnkyrinG. B, C, and D) Quantification of axon initial segment length across cranial motor nuclei at the respective ages. Each dot represents a single motor neuron and the red bar marks the mean. Significance by one-way ANOVA and Bonferroni post hoc analysis.

oculomotor nucleus become significantly shorter. This reflects the opposite shift seen the spinal cord between alpha and γ-motor neurons. Nevertheless, this shift is not observed in the trochlear motor neurons (Figure 3.2D).

Postnatal days 4-6

Lastly, I analyzed neonatal mice to compare the axon initial segment of cranial motor neurons. As with motor neurons in the lumbar spinal cord (Figure 2.3), the axon initial segment in all of the cranial motor nuclei were noticeably longer in the neonates as compared to the adult mice (Figure 3.2B). Moreover, the axon initial segment in most of the $SOD1^{G93A}$ cranial motor neurons in the neonates were not significantly different from their Nt littermates. With one unexpected exception, the axon initial segment of the $SOD1^{G93A}$ hypoglossal motor neurons were significantly shorter than those in the Nt control (Figure 3.2B).

p62 aggregation is heterogeneous across vulnerable cranial motor nuclei

Given that the axon initial segment phenotype was vastly different in the cranial motor neurons than what was observed in the spinal motor neurons, I questioned whether other phenotypes showed similar heterogeneity. I started this analysis with p62 aggregation, abundant in spinal motor neurons and previously reported to present in ALS-vulnerable cranial motor neurons as well (An et al., 2014). Unlike the prolific presence of p62 aggregation in the P45 spinal α-motor neurons, I was unable to find any p62 aggregation in the cranial motor neurons. Finally by P65, I observed p62 aggregation in some ALS-vulnerable cranial motor neurons (Figure 3.3). However, I observed almost no evidence of p62 aggregation in the hypoglossal motor neurons (out of all sections analyzed, one neuron displayed aggregates and one skein-like inclusions). Furthermore, though not quantified, the dorsal motor nucleus of the

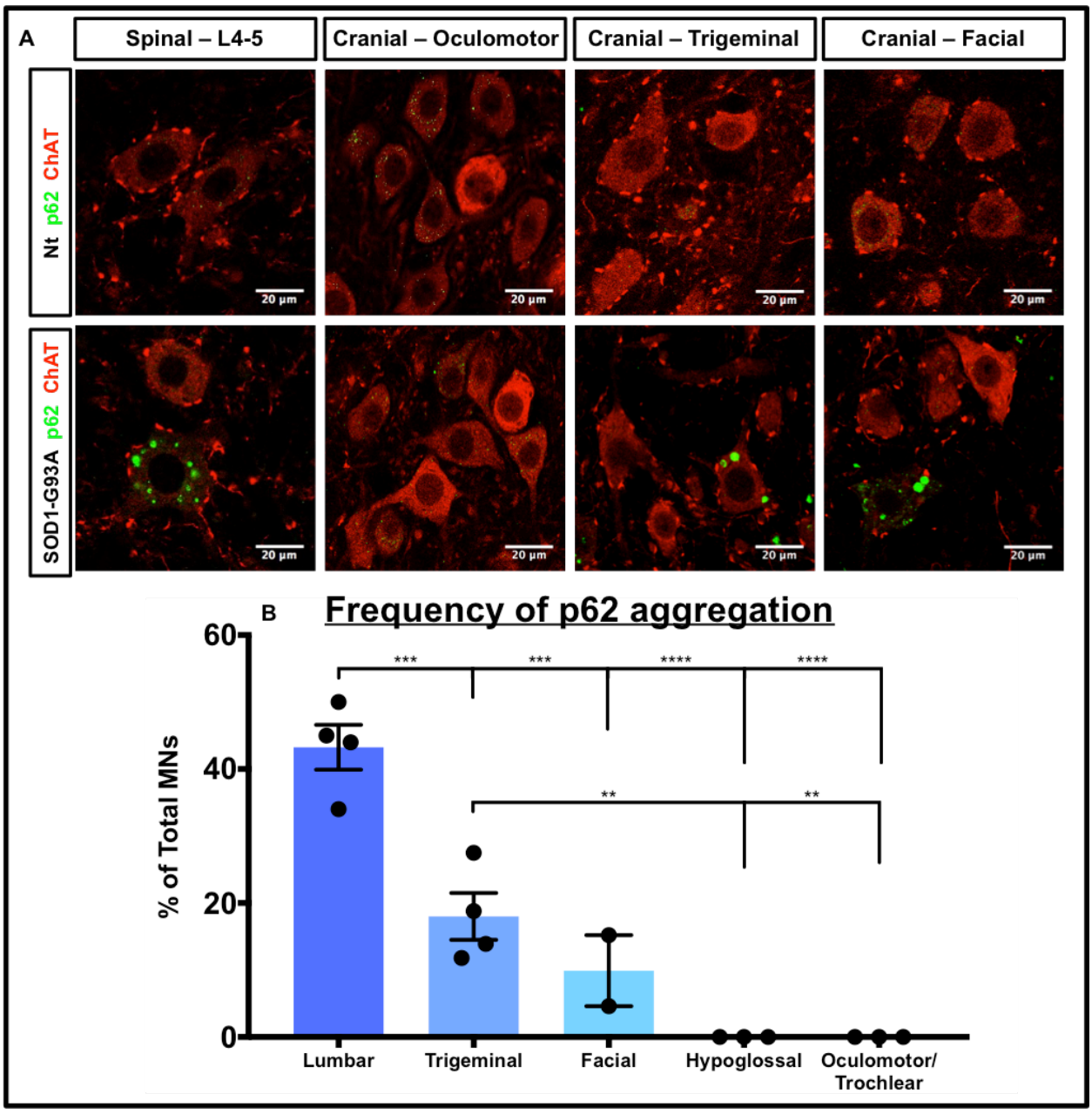

Figure 3-3: p62 aggregation is less abundant in ALS-vulnerable cranial motor neurons as compared to spinal motor neurons

Representative images of oculomotor neurons, trigeminal and facial motor neurons, and lumber 4-5 spinal motor neurons from littermates of P66-P97 non-transgenic (NT) and $SOD1^{G93A}$ mice. ChAT antibody stained motor neurons in red. p62 antibody stained p62-containing inclusions in green. (E) Quantification of percentage of cells containing p62 inclusions in cranial motor neurons and spinal motor neurons from $SOD1^{G93A}$ mice [n = 4 animals for lumbar and trigeminal, 3 for hypoglossal and oculomotor/trochlear, and 2 for facial, mean ± SEM).

vagus nerve that sits directly dorsal to the hypoglossal, displayed marked p62 aggregation in stark contrast to hypoglossal motor neurons. Lastly, in all of the ages tested (P5, P25, P45, P65, and P95) and in end-stage SOD1^{G93A} mice, I never observed p62 aggregates in the ALS-resistant cranial motor neurons within the oculomotor and trochlear nuclei.

Though I did observe some p62 aggregation in the trigeminal and facial motor neurons at P65, qualitatively it was clear that the number of neurons with aggregates were far fewer than the number in the spinal cord. I next quantified this in P65 SOD1^{G93A} motor neurons by counting the number of neurons with p62 aggregates as a percentage of the total number of motor neurons. A third of the spinal motor neurons had aggregates at P65, whereas only ~18% of trigeminal motor neurons presented with p62 aggregates. Fewer yet were seen in the facial motor neurons (though not enough sections were quantified for this figure to run a statistical analysis), highlighting further heterogeneity in ALS phenotypes between spinal and cranial motor neurons.

In Chapter 2, I reported that progressive shortening of the axon initial segment structural occurs in spinal motor neurons that display phenotypic markers of stress (p62 aggregation and vacuole formation). I performed the same analysis here for trigeminal motor neurons and found no significant differences between motor neurons with p62 aggregates and those without (data not shown). However, due to the heterogeneity across ALS-vulnerable cranial nuclei, and the low number of motor neurons that contained p62 aggregates, I abandoned that analysis.

ALS-vulnerable cranial motor neurons exhibit minimal somal invasion of vacuoles

Large vacuoles, believed to arise from swelling and the subsequent degradation of mitochondria (Higgins et al., 2003), have been reported in mouse models of ALS (Dal Canto and Gurney, 1994). In the previous chapter, I presented a timeline in spinal motor neurons

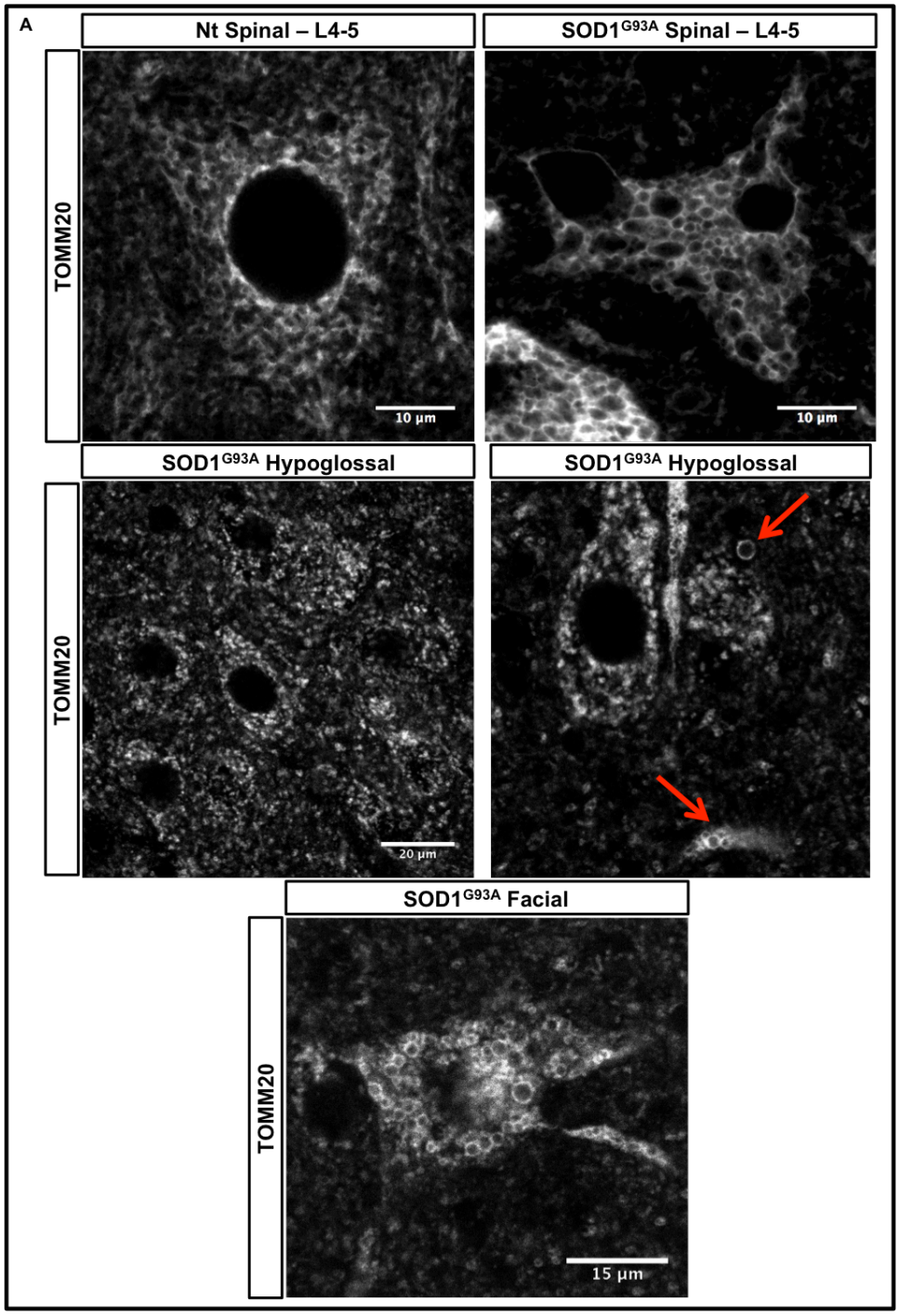

Figure 3-4: Vacuole localization in cranial motor neurons differs from localization in spinal motor neurons

Top: Representative images of vacuoles in SOD1^{G93A} spinal motor neurons, visualized by immunostaining of TOMM20, as compared to normal TOMM20 staining in Nt spinal motor neurons. Middle: Representative images of TOMM20-lined vacuoles in the neuropil of SOD1^{G93A} hypoglossal motor neurons. Bottom: Rarely, somal invasion by small vacuoles cans be seen as represented here by a facial motor neuron.

(Figure 2.5), where vacuole emergence occurs in a small number of motor neurons at P45 and is abundantly present by P65. To continue the phenotypic comparison of spinal and cranial motor neurons, I looked in the ALS-vulnerable and resistant populations of motor neurons in the midbrain using an antibody targeting the outer-mitochondrial membrane, TOMM20. Like the spinal motor neurons, abundant vacuoles within the ALS-vulnerable cranial motor neurons are not seen until P65 and were never observed through end-stage in the ALS-resistant oculomotor and trochlear motor nuclei. However, vacuoles in the cranial motor neurons did not present like those in the spinal motor neurons (Figure 3.4). Interestingly, where large vacuoles clearly invade the soma of spinal motor neurons, most of the vacuoles in the cranial motor neurons are found in the neuropil. As seen in Figure 3.4, the motor neurons of the hypoglossal nucleus do not show somal vacuoles. In this same figure, I included an example of one of the few motor neurons of the facial nucleus that had somal vacuoles. It is notable that the vacuoles that do form in the somas of the cranial motor neurons are not nearly as large as what is seen in the spinal motor neurons. Qualitatively, it does not appear that there is a reduction in the abundance of vacuoles, only that they do not invade the soma (Figure 3.5).

Aggregation of misfolded SOD1 succeeds p62 pathology and accompanies somal vacuole invasion in spinal motor neurons

Using the three phenotypes that were highlighted in spinal motor neurons in Chapter 2 (axon initial segment length, p62 aggregation, somal vacuole formation), I was unable to identify tight phenotypic parallels between spinal and cranial motor neurons. So I looked at a fourth phenotype, misfolded SOD1 aggregation, and first characterized its time line in the spinal motor neurons. SOD1 has been reported to aggregate in ALS and accumulate on outer mitochondrial

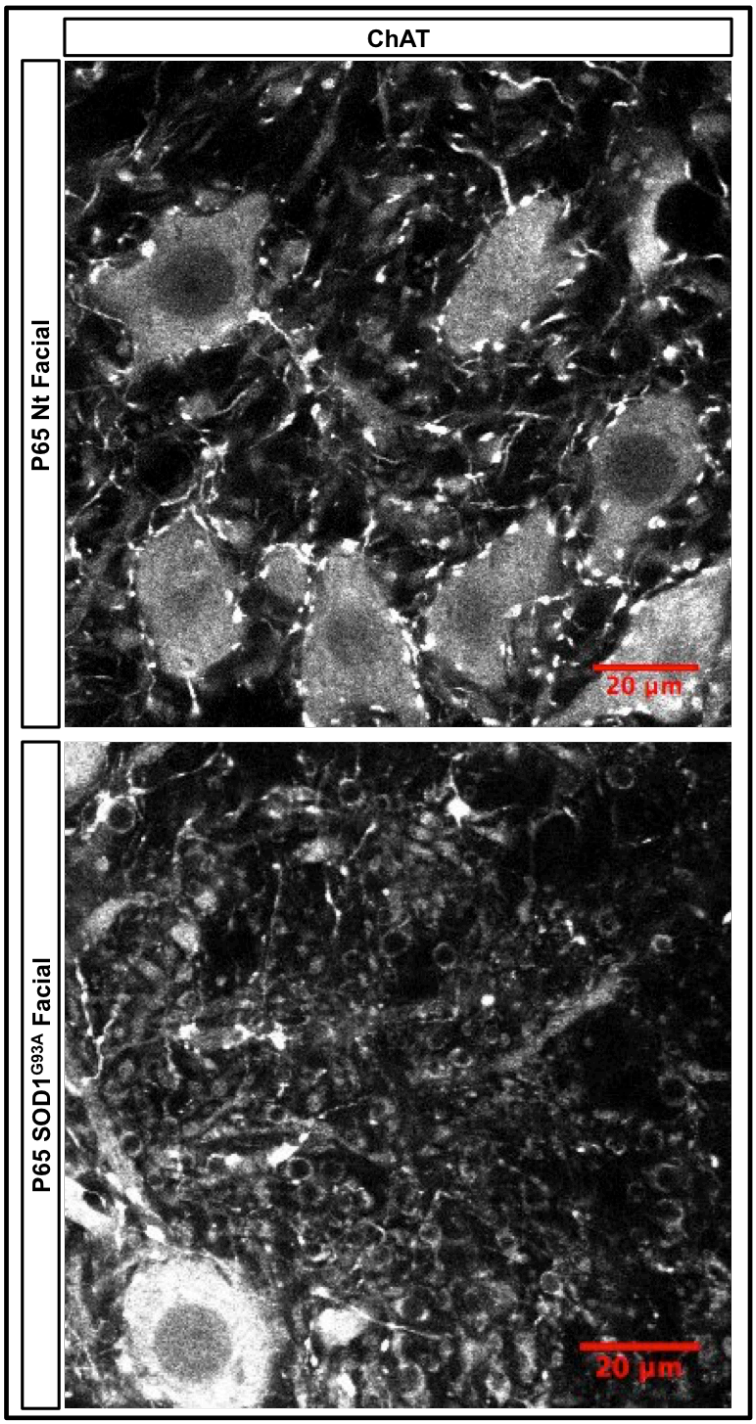

Figure 3-5: Abundant vacuole formation in the neuropil of cranial motor neurons in SOD1^{G93A} mice

Top: Nt facial motor neurons stained with ChAT with no abnormalities seen in the neuropil. Bottom: Vacuoles are found throughout the neuropil of ALS-vulnerable cranial motor neurons and can be seen in ChAT-positive neurites.

membranes in ALS (Mattiazzi et al., 2002; Liu et al., 2004; Vijayvergiya et al., 2005; Bergemalm et al., 2006; Deng et al., 2006; Vande Velde et al., 2008). SOD1 aggregation has also been shown in both sporadic and familial forms of ALS (Paré et al., 2018), highlighting its potential importance to effect many ALS patients and serve as a robust marker for pathological stress in neurons. Though it has recently been shown that the small soluble trimeric aggregates of SOD1 are in fact the toxic moieties (Zhu et al., 2018), the large aggregates are a visual downstream event that should mark neurons undergoing pathogenic events.

I stained lumbar sections from the preparations performed in Chapter 2. Sections were immunostained with an antibody that specifically recognizes human misfolded SOD1 protein (C4F6) (PMID: 17277077, 20953194) and an antibody against choline acetyltransferase (ChAT) to identify motor neurons. By P65, abundant misfolded SOD1 aggregation is observed in motor neurons and their projections throughout Lumbar spinal cord segments 4-5 (Figure 3.6). The ubiquitous, non-aggregated misfolded SOD1 signal is noticeably higher in ventral spinal motor neurons as compared other areas in the dorsal and ventral segments. Though a careful analysis with a pan-neuronal marker was not carried out, the motor neurons clearly stood out in the spinal cord segments, where other neurons had relatively low signals. This same observation was true within the motor neuron pool, where small motor neurons likely to be γ-motor neurons, had relatively low signals of misfolded SOD1. To verify the specificity of the misfolded SOD1 antibody and to ensure the signal was not reflecting endogenously expressed SOD1, I also stained sections from the Nt littermates. No signal was observed in these sections (data not shown). Within the motor neurons, aggregates were found both within and outside vacuoles (Figure 3.6). Of note, these small motor neurons with bright ChAT signals, likely to be γ-motor neurons do not possess misfolded SOD1 aggregates, though their ubiquitous, non-aggregated misfolded SOD1 signal was still elevated relative to the background throughout the spinal cord sections. I have also stained for p62 and misfolded SOD1 in the same sections and surprisingly, the aggregates of each of these proteins do not seem to co-localize.

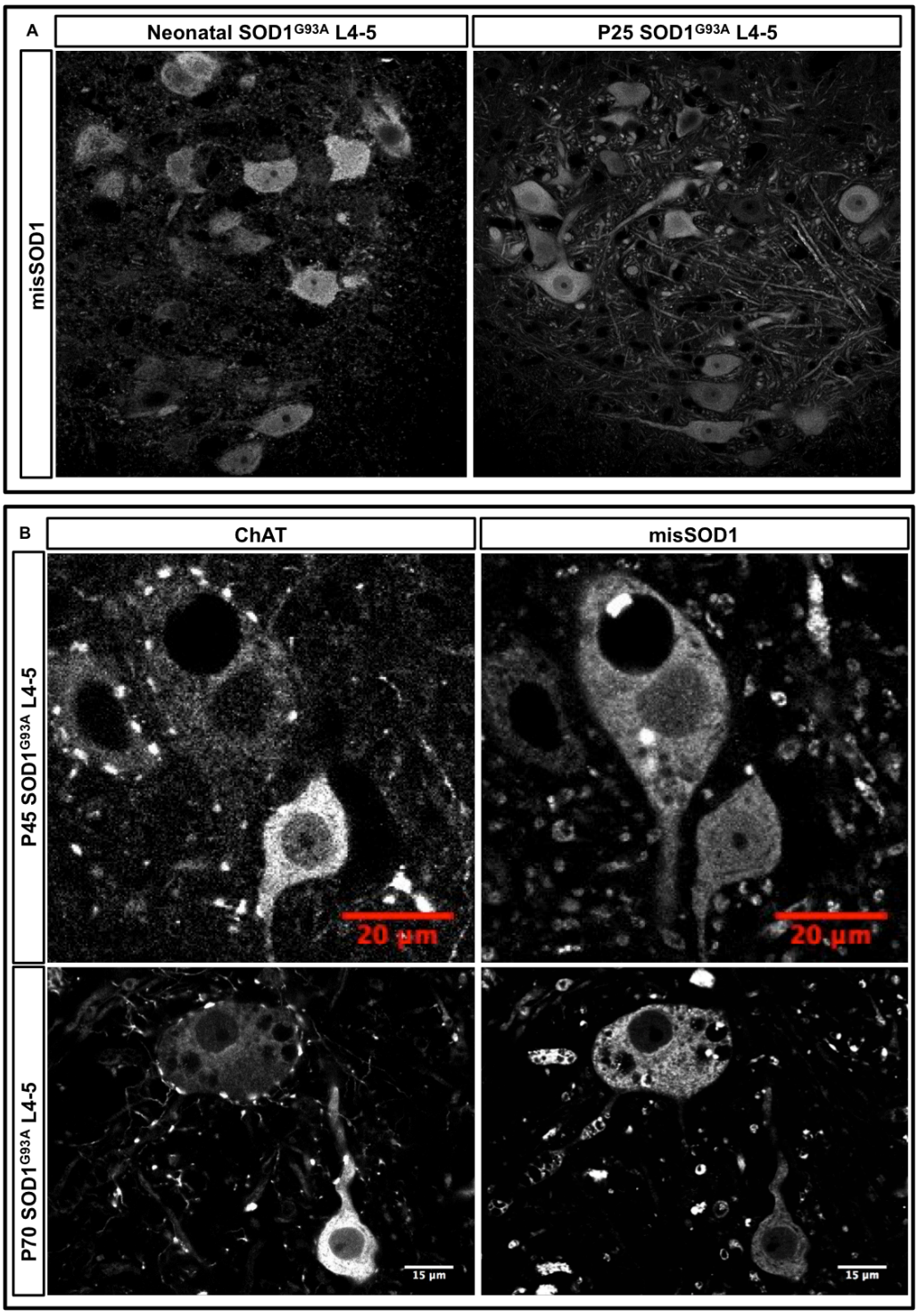

Figure 3-6: A timeline of misfolded human SOD1 aggregation in spinal motor neurons of SOD1^{G93A} mice

A) Misfolded human SOD1 is visualized in neonatal and P25 spinal motor neurons from SOD1^{G93A} mice using immunostaining. Though high ubiquitous signal arises from these neurons, aggregation is absent at these ages. B) By P45, a small number of motor neurons display misfolded human SOD1 aggregates, and only those neurons with somal vacuoles. By P70, abundant misfolded human SOD1 aggregates are found in SOD1^{G93A} spinal motor neurons.

I proceeded to analyze Lumbar spinal motor neurons from SOD1^{G93A} mice ages P4-6, P23-26, and P44-46. Even in the neonates, the ubiquitous, non-aggregated misfolded SOD1 signal was elevated as compared to the rest of the spinal cord sections. This phenotype persisted to P23-26, but no aggregates were observed through this young adult age (Figure 3.6). Intriguingly, in P44-46 mice, where copious p62 aggregation is observed, very few motor neurons contained misfolded SOD1 aggregates. Furthermore, misfolded SOD1 aggregates thatwere present at this age were only found in the few spinal motor neurons that contained somal vacuoles (Figure 3.6).

Oculomotor neurons maintain reduced SOD1 signal and resist aggregation

To begin to compare the spinal motor neuron misfolded SOD1 aggregation phenotype to cranial motor neurons, I began by looking at the ALS-resistant oculomotor neurons. 100μm sagittal sections from the midbrain and transverse sections from Lumbar segments 4-5 were taken from postnatal day 100 (P100) SOD1^{G93A} mice. Sections were immunostained with an antibody that specifically recognizes human misfolded SOD1 protein (C4F6) (PMID: 17277077, 20953194) and an antibody against choline acetyltransferase (ChAT) to identify motor neurons. I aimed to quantitatively investigate SOD1 aggregation in spinal motor neurons and compare it to the ALS-resistant oculomotor and trochlear motor neurons.

Interestingly, I found a third of all spinal motor neurons [34% ± 4.2 (SEM); 195 motor neurons from 3 mice] contain aggregates of misfolded hSOD1, however, we were unable to detect any aggregation within oculomotor or trochlear motor neurons (328 motor neurons from 3 mice) (Figure 3.7). Additionally, oculomotor and trochlear motor neurons exhibited strikingly lower overall levels of misfolded hSOD1 compared to spinal motor neurons, necessitating

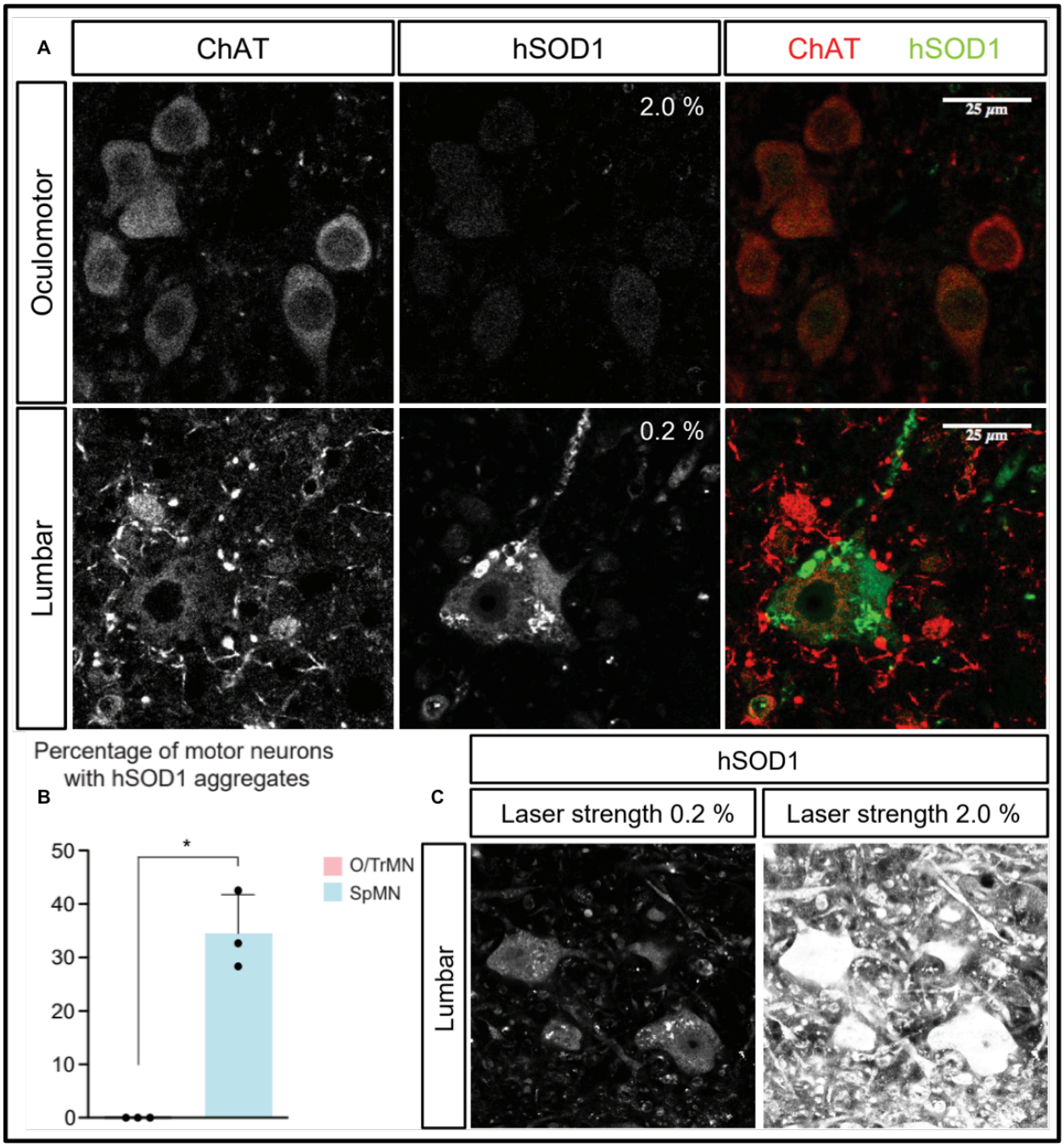

Figure 3-7 Misfolded human SOD1 aggregates are not present in ALS-resistant oculomotor neurons of SOD1^{G93A} mice

A) Representative images of oculomotor neurons and lumber 4-5 spinal motor neurons from P100 SOD1^{G93A} mice. Motor neurons were stained by ChAT antibody in red. Misfolded human SOD1 aggregates were present in spinal motor neurons and stained by misfolded human SOD1 antibody in green. Confocal laser intensity used for imaging misfolded human SOD1 was 2% in oculomotor neurons and 0.2% in lumber spinal motor neurons (laser intensity for ChAT imaging was same for both motor neuron types). B) Quantification of percentage of cells containing hSOD1 aggregates in oculomotor neurons and spinal motor neurons from SOD1^{G93A} mice (n= 3 animals, spinal motor neurons counted - 195, cranial motor neurons counted - 328, significance by Welch's t-test). C) Spinal motor neurons from P100 SOD1^{G93A} mice, immunostained by misfolded human SOD1 antibody and imaged with confocal laser strengths reflecting the 0.2% laser intensity used to image spinal motor neurons and the same field at the 2.0% laser intensity used to image oculomotor neurons. hSOD1 staining of spinal motor neurons imaged with 2% laser strength was highly saturated.

imaging under 5-10 times higher confocal laser intensity. Imaging the spinal motor neurons at the same intensity produced an image with fully saturated motor neurons (Figure 3.7).

Misfolded SOD1 aggregation lines vacuoles of the neuropil in vulnerable cranial motor neurons

I found previously that misfolded SOD1 aggregates emerge in spinal motor neurons concomitantly with somal invasion of vacuoles. As it was also previously described that somal vacuoles are scarce in ALS-vulnerable cranial motor neurons, it was unclear whether misfolded SOD1 aggregates would be detected. To address this question, I created 100μm sagittal sections from the midbrain of postnatal day 100 (P100) and P120 $SOD1^{G93A}$ mice. Sections were immunostained with an antibody that specifically recognizes human misfolded SOD1 protein (C4F6) (PMID: 17277077, 20953194) and an antibody against choline acetyltransferase (ChAT) to identify motor neurons. Through a qualitative analysis, motor neuron degeneration was readily noticeable in the vulnerable cranial motor nuclei, however, somal aggregates of misfolded SOD1 were relatively rare (Figure 3.8). Comparable to the spinal data, only the neurons that possessed somal vacuoles harbored misfolded SOD1 aggregates (Figure 3.8). However, interestingly there were still misfolded SOD1 aggregates in the neuropil. Furthermore, many of the vacuoles in the neuropil were visualized by the misfolded SOD1 staining (Figure 3.8), where the outer membrane appeared to be lined with misfolded SOD1.

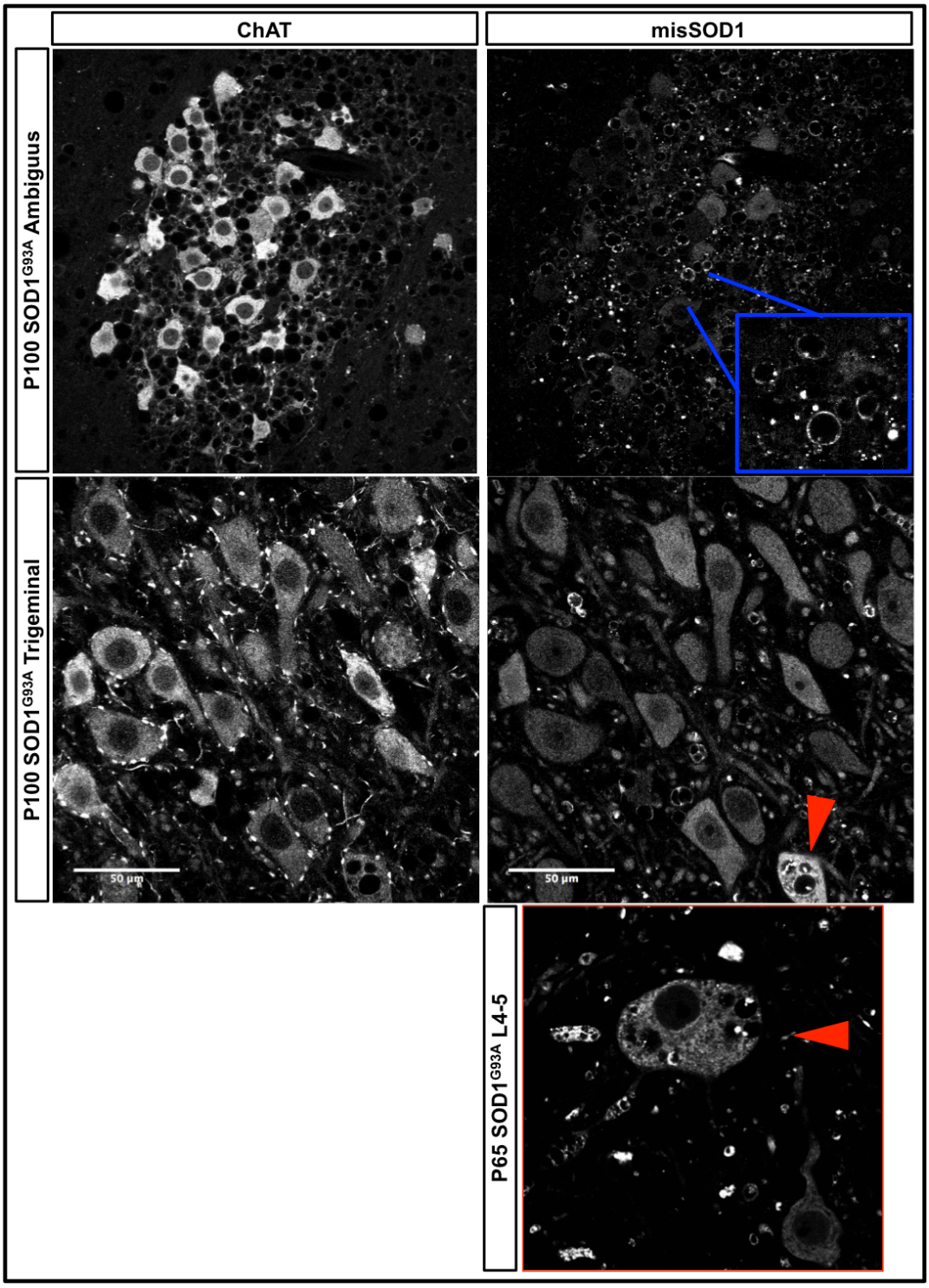

Figure 3-8: Misfolded human SOD1 aggregation follows the pattern of vacuole formation found in cranial motor neurons

Top: ChAT and misfolded human SOD1 immunostained SOD1^{G93A} ambiguus motor neurons that display aggregation of misfolded human SOD1 in the neuropil and an accumulation on the outer membranes of vacuoles. Middle and Bottom: Representative image of misfolded human SOD1 aggregate accumulation in the rare somal vacuoles in trigeminal motor neurons from SOD1^{G93A} mice, and their similarity to those seen in abundance in spinal motor neurons.

Discussion

Here, in the SOD1^{G93A} mouse model of ALS, I have analyzed multiple phenotypes in cranial motor neurons at multiple ages. Like spinal motor neurons, I observe significant structural plasticity in the axon initial segment of ALS-vulnerable cranial motor neurons. Surprisingly, the axon initial segment structural changes indicate a dynamic and oppositeelectrophysiological landscape in ALS-vulnerable cranial motor neurons as compared to spinal motor neurons. For the ALS-vulnerable cranial motor nuclei, the axon initial segment undergoes a lengthening event in adult ages, where spinal motor neurons display axon initial segment shortening. As with γ-motor neurons in the Lumbar spinal cord, I find structural plasticity in the axon initial segment of oculomotor neurons in later stages of the disease. Interestingly, prior to the axon initial segment lengthening I observed in the adult, neonatal hypoglossal motor neurons display a shortening in this subcellular structure. Furthermore, the other reported ALS phenotypes, p62 aggregation, vacuole formation, and SOD1 aggregation all present heterogeneously across vulnerable cranial motor neuron populations and differently than spinal motor neurons. Noted similarities between spinal and cranial motor neurons were the absence of phenotypic markers early in ALS-resistant motor neurons.

Axon initial segment plasticity

Perhaps the greatest surprise when collecting this data was the opposite phenotype found in cranial motor neurons as compared to spinal motor neurons. The lengthening seen here would indicate that there is a reduction in net excitation onto cranial motor neurons. Though notable circuitry differences between spinal and cranial motor neurons have been reported (Rekling et al., 2000) and are expected considering the functional differences of cranial musculature, if the excitotoxicity phenotype is considered, then this result is counter to what would be anticipated. These results would suggest that by P25, net excitation is reduced in

ALS-vulnerable cranial motor neurons. Interestingly at later stages in the disease resistant oculomotor neurons display shortening in the axon initial segment, further supporting the conclusion increased motor neuron activity is unlikely the key driver of motor neuron degeneration in the mouse model of ALS. While it is not clear what causes circuit changes leading to the shortening of axon initial segment in ALS oculomotor neuron, astrogliosis and microgliosis surrounds the oculomotor nucleus at end-stage (An et al., 2014) and could be affecting oculomotor circuitry.

So, if excitotoxicity plays a role in ALS pathology in spinal motor neurons, it may not underlie pathophysiology in cranial motor neurons. These data do not support the hyperactivity or hyperexcitation that would be expected to be driving an excitotoxic effect. It is possible that these two populations undergo different pathogenic events and later converge in similar downstream events, or alternatively, the early pathogenic events between the two are similar and the downstream events diverge. It is also possible that abnormalities found in motor neuron activity and excitability are simply compensatory events that do not contribute to ALS pathophysiology. If that were true, however, the same would have to be considered for at least p62 aggregation and possibly vacuole invasion of the soma.

Phenotypic heterogeneity in ALS-vulnerable motor neurons

Like the differences in axon initial segment plasticity, all other phenotypes investigated here showed heterogeneous presentation throughout the ALS-vulnerable cranial pools, as well as when compared to spinal motor neurons. p62 aggregation has been reported as an indicator of ALS pathogenesis (Rudnick et al., 2017). However, here I show that p62 aggregation is significantly less abundant in some ALS-vulnerable cranial motor neurons, and almost completely devoid in others. Considering that all of these nuclei have been reported to undergo similar degeneration as compared to spinal motor neurons, then a large number of cranial motor neurons undergo degeneration without containing p62 aggregates.

The same holds true for somal vacuoles, where the vast majority of cranial motor neurons do not display somal vacuoles. Since they do, however, have an abundance of vacuoles in their neuropil, as do the spinal motor neurons, it is possible that the vacuoles in projections of motor neurons confer toxic effects if they do at all. The true nature, mechanism, and roles in ALS that vacuoles play are still highly contested. Perhaps the heterogeneous localization of vacuoles in cranial and spinal motor neurons will provide some insight into physiological differences between these to populations of neurons.

SOD1 aggregation follows a similar profile to the vacuoles, where somal aggregates are rare in cranial motor neurons. SOD1 aggregates, as shown in spinal motor neurons, co-emerge with vacuoles and also occupy on their outer membrane. Considering that the small, trimeric aggregates are seemingly the toxic entities in ALS motor neurons (Zhu et al., 2018), perhaps more important to disease pathology is the increased SOD1 signal in spinal motor neurons as compared to oculomotor neurons. In future studies, this will be an important phenotype to investigate, as a resistance to building up misfolded SOD1 might spare oculomotor neurons from degeneration.

Methods

Animals

Staining in the lumbar spinal cord was performed on tissue from first generation crosses of C57BL/6J females and *SOD1*^{G93A} transgenic male mice [C57BL/6J, 000664; B6.Cg-Tg (SOD1*G93A)1Gur/J, 004435, Jackson Laboratory]. All experiments utilizing laboratory animals were performed in accordance with NIH guidelines for the care and use of laboratory animals, and with approval of the Institutional Animal Care and Use Committees of Columbia University.

Animal Tissue Collection, Immunofluorescence Staining and Imaging

SOD1^{G93A} mutant mice and their non-transgenic littermates (first generation cross only) at postnatal days 66 and 100 ± 3 were deeply anesthetized using Avertin (tribromoethanol, Sigma) and fixed by transcardial perfusion with 4% paraformaldehyde (from 32% stock, 15714, Electron Microscopy Sciences) in phosphate-buffered saline (PBS) pH 7.4 (70011, ThermoFisher). The CNS was removed and fixed overnight in the same solution noted above. Whole brain and lumbar segments 4 and 5 were dissected, embedded in 4% (w/v) agar and sectioned on a vibratomb (Leica VT1000 S). 100 µm transverse spinal cord sections and sagittal whole brain sections were cut. Sections were blocked overnight in PBS with 10% donkey serum (D9553, Sigma) and 0.4% Triton X-100 (T8787, Sigma). Sections then were incubated at room temperature for two days in the above blocking buffer with primary antibodies [goat polyclonal anti-ChAT (1:100; AB144P, Millipore); mouse monoclonal anti-NeuN, clone A60 (1:100; MAB377, Millipore); mouse monoclonal anti-SQSTM1 / p62 (1:500; ab56416, Abcam); mouse monoclonal anti-misfolded human SOD1 (1:250; MM-0072-02, MédiMabs); rabbit polyclonal anti-ankyrin G (Stock 0.2 µg/mL, 1:100; 386 003, Synaptic Systems)]. After the primary incubation, six washes (>30 minutes each) in PBS with 0.4% Triton were followed by a one-day incubation at room temperature in the above wash buffer with donkey anti-mouse and anti-goat secondary antibodies (1.5 µg/mL; Jackson ImmunoResearch). After six more washes (as stated above), sections were mounted on microscope slides in Fluoromount G (OB100, ThermoFisher) using 100 µm spacers and allowed to set for >12hrs. Staining was visualized by confocal microscopy (Zeiss LSM 800).

Axon initial segment analysis

For *in vivo* axon initial segment analysis, sections were imaged using a laser-scanning confocal microscope (LSM 800, Zeiss) and a 40x oil-immersion objective. The settings were adjusted to prevent signal saturation and the images were taken in z-stacks with 1 µm steps.

The start and end of the *in vivo* initial segment is extremely distinct as seen in the reported images. Therefore, the start and end were manually chosen and Simple Neurite Tracer (Longair et al., 2011) software through the Fiji platform was used to automatically generate lengths of the axon initial segment.

Chapter 4: Aberrant synaptic input drives axon initial segment plasticity in an *in vitro* model of ALS

Summary

In vitro motor neuron studies in ALS have also reported the effects of excitotoxic mechanisms in these models (Wainger et al., 2014). These reductionist models are great tools for parsing out cell-autonomous pathology in diseases. However, it is unclear whether the circuitry level changes that are supported by the data I have presented in the previous chapters would manifest in such a model. Nevertheless, *in vitro* analyses may mitigate difficulties surrounding the investigation into excitotoxicity in spinal motor neurons that arise when trying to distinguish between cell-autonomous and non-autonomous effects. Moreover, electrophysiological analysis in adult spinal motor neurons is not yet possible. Here, I use a reductionist model of ALS to try and address whether circuit dysfunction may present *in vitro,* and whether this arises from cell-autonomous mechanisms. I find that ALS-model motor neurons *in vitro* undergo significant axon initial plasticity, and correspondingly, become intrinsically hypoexcitable. These changes are a compensatory response to increased synaptic drive and marked increases in action potential firing. Furthermore, the increased synaptic drive may originate with a subtype of spinal interneuron, but mediated by a cell-autonomous

mechanism in the motor neurons themselves that increase synaptic recruitment. These findings suggest that ALS-model spinal motor neurons may receive increased excitatory synaptic input early in development and may intrinsically compensate for the increased activity.

Introduction

From Chapter 2, it appears that aberrant spinal circuitry may affect spinal motor neurons in ALS and precedes other phenotypic markers of stress. Though it is still unclear whether the compensatory response seen in spinal motor neurons contributes to ALS pathophysiology, the potential increase in excitatory synaptic drive supports the excitotoxicity hypothesis. In Chapter 1, I discussed in depth the problems involved in electrophysiological recordings from adult spinal motor neurons in ALS. These issues also pertain to being able to test the possibility of increased net excitation in motor neurons. Therefore, I aimed to find a reductionist model of ALS and utilized an *in vitro* culture system to test whether phenotypes would present that paralleled my *in vivo* findings in spinal motor neurons.

In vitro cultures can provide a powerful system with which to model disease and examine excitability and synaptic phenotypes. The differentiation technique used in our lab (Wichterle and Peljto, 2008) produces not only motor neurons, but also inhibitory and excitatory interneurons. Glutamatergic V3 and V2a interneurons identified by the transcription factors Sim1 and Chx10 respectively, are found in different efficiencies depending on the concentration of spinal cord ventralizing signal, smoothened agonist, during motor stem cell differentiation (Wichterle et al., 2002; Alaynick et al., 2011; Sternfeld et al., 2017). This culturing method provides the multiple neuronal constituents found in *in vivo* spinal motor networks to form robust *in vitro* synaptic networks that may mimic preferential synaptic connections found i*n vivo* (Sternfeld et al., 2017; Hoang et al., 2018). Another advantage to this system, especially for

electrophysiological recording, is the identification of neuronal subtypes by fluorescent reporters: motor neurons by endogenous expression of fluorescent proteins driven off of the promoter for the motor neuron-specific homeobox protein Hb9 (Wichterle et al., 2002), and V2a and V3 interneurons by expression of fluorescent reporters controlled by Chx10-Cre and Sim1-Cre (Sternfeld et al., 2017).

Carrying out this analysis in the mouse embryonic stem cell-derived model rather than using motor neurons generated from human induced pluripotent stem cells, is advantageous in that the more aggressive onset and progression in the $SOD1^{G93A}$ mouse model of ALS is more likely to reveal disease relevant phenotypes. Furthermore, the mouse embryonic stem cell-derived motor neurons mature more quickly in culture (Miles et al., 2004; Boulting et al., 2011; Turner et al., 2013). To that point, we do not see synaptic innervation of human induced pluripotent stem cell-derived motor neurons until 2-3 months of culture, while mouse stem cell-derived motor neurons become synaptically active by day 10 in culture. Therefore, using mouse embryonic stem cell-derived motor neurons allows for a rapid analysis and removes the technical difficulties of long-term culture. Moreover, while for analyzing a novel phenotype, the mouse models are better established, thus allowing for comparison and interpretations using published literature.

Here, I utilized previously established embryonic stem cell lines derived from the same high-expressing human $SOD1^{G93A}$ mouse line used for my in vivo analysis, as well as high-expressing human $SOD1^{WT}$ mice as a control (Thams et al., 2018). I first further investigated the effects of axon initial segment manipulation in motor neurons. I then asked if plasticity in this subcellular region would be present in the $SOD1^{G93A}$ embryonic stem cell-derived motor neurons. In turn, were circuitry abnormalities responsible for any observed differences. Finally, I attempted to uncover any cell-autonomous mechanisms that might be altered in this *in vitro* motor neuron preparation.

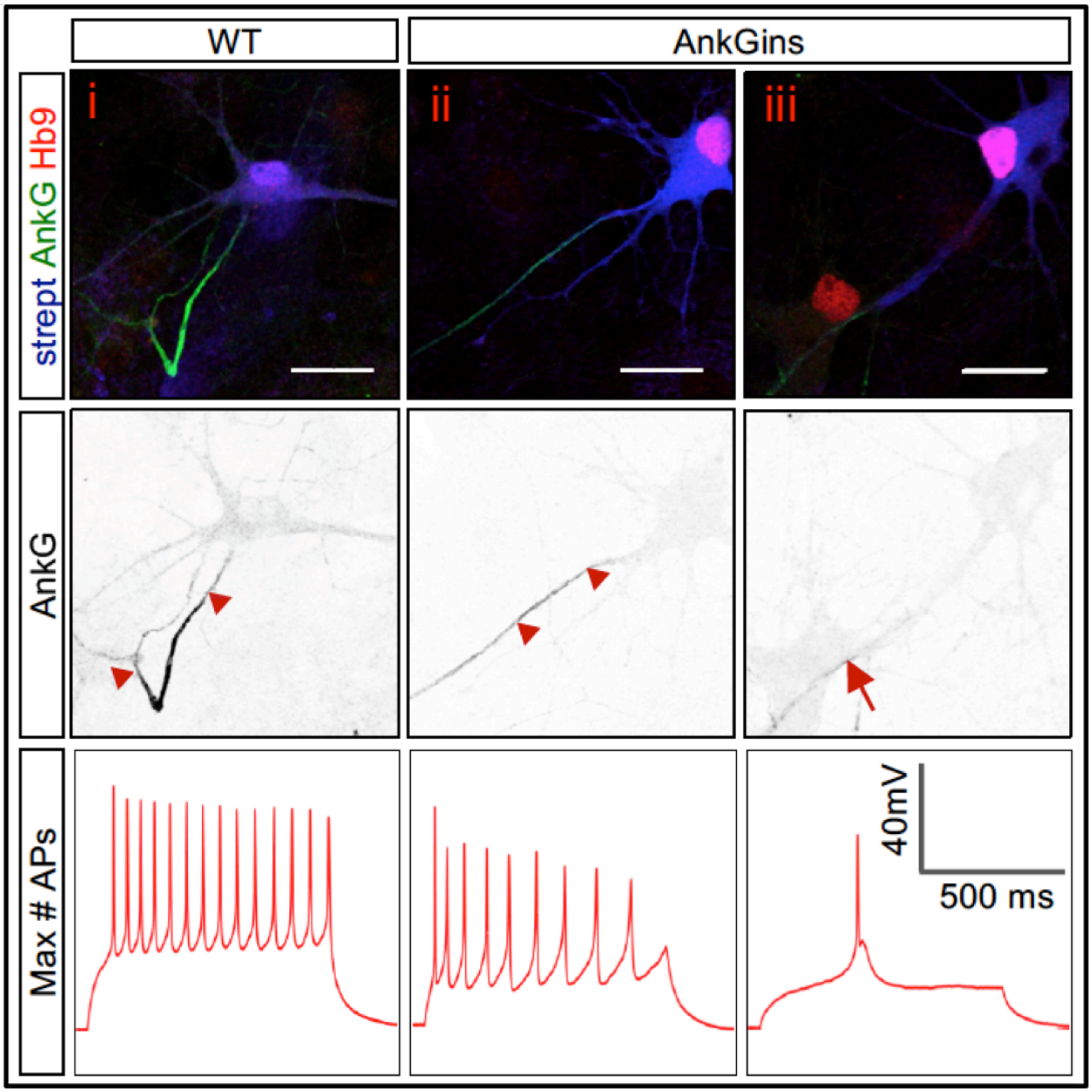

Figure 4-1: Disruption of the axon initial segment alters action potential firing in motor neurons

Immunostaining and whole-cell patch clamp recordings showing the maximum number of fired action potentials after current injection for representative motor neurons

Results

Reduction of the axon initial segment integrity *in vitro* disrupts normal action potential properties

From Chapter 2, motor neurons possess the ability to structurally change their axon initial segment in response to a reduction in action potential firing (Figure 2.1). This plasticity is coupled to what is likely a myriad of homeostatic physiological changes that affect firing properties of these neurons. However, it is unclear what direct effects the axon initial segment itself may have on intrinsic firing properties. To address this, I utilized an embryonic stem cell (ESC) line created in Wichterle lab that forced expression of an embryonic isoform of AnkG (denoted AnkGins) that results in the impairment of axon initial segment establishment (Jacko et al., 2018). Motor neurons derived from the AnkGins ESC line heterogeneously developed fully formed axon initial segments, partially formed axon initial segments, or no axon initial segments (Figure 4.1).

To determine whether defects in the axon initial segment alone disrupt firing properties of maturing neurons, I performed whole-cell patch-clamp recordings of AnkGins motor neurons followed by *post hoc* immunostaining analysis of AnkG, to visualize the axon initial segment, and Hb9, to identify motor neurons. Overall, AnkGins neurons fired fewer action potentials, the action potential overshoot was reduced, and the duration was increased as a result of reduction in both the action potential rise and fall rates (Figures 4.1 and 4.2), indicative of a reduction in voltage-gated sodium channel densities. Interestingly, the input resistance and rheobase were unchanged in these conditions. The level of the axon initial segment perturbation, as measured by axon initial segment length, correlated well with the degree of the firing reduction

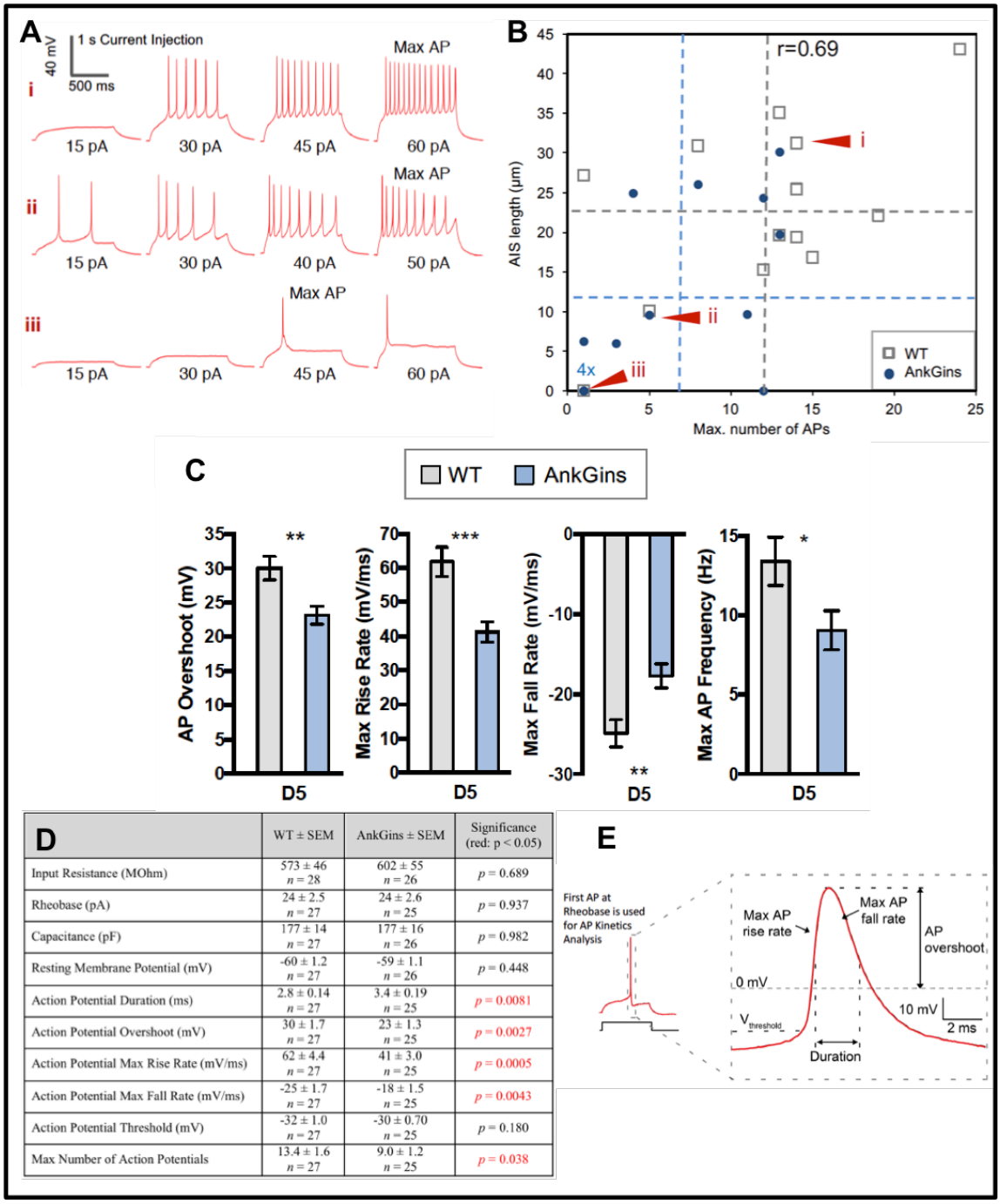

D	WT ± SEM	AnkGins ± SEM	Significance (red: p < 0.05)
Input Resistance (MOhm)	573 ± 46 n = 28	602 ± 55 n = 26	p = 0.689
Rheobase (pA)	24 ± 2.5 n = 27	24 ± 2.6 n = 25	p = 0.937
Capacitance (pF)	177 ± 14 n = 27	177 ± 16 n = 26	p = 0.982
Resting Membrane Potential (mV)	-60 ± 1.2 n = 27	-59 ± 1.1 n = 26	p = 0.448
Action Potential Duration (ms)	2.8 ± 0.14 n = 27	3.4 ± 0.19 n = 25	p = 0.0081
Action Potential Overshoot (mV)	30 ± 1.7 n = 27	23 ± 1.3 n = 25	p = 0.0027
Action Potential Max Rise Rate (mV/ms)	62 ± 4.4 n = 27	41 ± 3.0 n = 25	p = 0.0005
Action Potential Max Fall Rate (mV/ms)	-25 ± 1.7 n = 27	-18 ± 1.5 n = 25	p = 0.0043
Action Potential Threshold (mV)	-32 ± 1.0 n = 27	-30 ± 0.70 n = 25	p = 0.180
Max Number of Action Potentials	13.4 ± 1.6 n = 27	9.0 ± 1.2 n = 25	p = 0.038

Figure 4-2: Action potential firing properties effected by axon initial segment disruption

A) Full panel of current step output related to the representative motor neurons shown in figure 4.1. B) Correlation of action potential firing and AIS length in WT and AnkGins motor neurons. Post hoc quantification of AIS was performed in motor neurons based on AnkG staining after whole-cell patch-clamp recording. The gray and the blue data points represent individual WT and AnkGins motor neurons, respectively with the dotted lines indicating the average values. C) Quantification of significantly changed electrophysiological characteristics from whole-cell patch-clamp measurements of WT and AnkGins motor neurons on day 5. Significance by student t-test. Error bars represent S.E.M. D) Summary of quantitative analysis of electrophysiological recordings for WT and AnkGins neurons on day 5. E) Illustration showing representative analysis of action potential kinetics.

($r=0.69$, $p<3.8\times10^{-5}$, Pearson correlation test; Figure 4.2). These data demonstrate that full formation of the axon initial segment is required for the establishment of mature neuronal firing properties.

Axon initial segment length correlates with action potential firing frequency in *in vitro* motor neurons

To begin to examine axon initial segment plasticity in $SOD1^{G93A}$ ESC-derived motor neurons, I cultured them for 6 days on polyornithine, laminin, and fibronectin coated coverslips. I first asked whether the plasticity in axon initial segment observed in Chapter 2 (Figure 2.1) correlates with changes in motor neuron spontaneous activity. I quantified activity in individual motor neurons after loading them with the calcium indicator Fluo-4 and imaging the fluorescence intensity at a frequency of 5 Hz. It was determined that the calcium transients observed resulted from action potential firing as they were completely abolished by the presence of tetrodotoxin (TTX) (data not shown). Following calcium imaging, the motor neurons were post-fixed and immunostained to visualize the axon initial segment. Calcium transient frequency was quantified and the length of the axon initial segment was measured in each observed motor neuron. The axon initial segmetn length was plotted versus the frequency of spontaneous activity (Figure 4.3). Using a Pearson correlation analysis, we found a significant correlation between the length of the axon initial segment and the frequency of activity where the shorter axon initial segments were found in the motor neurons with the higher frequency of calcium transients. This observation supports the function of axon initial segment plasticity as a compensatory mechanism in motor neurons and is secondary to increased spontaneous activity.

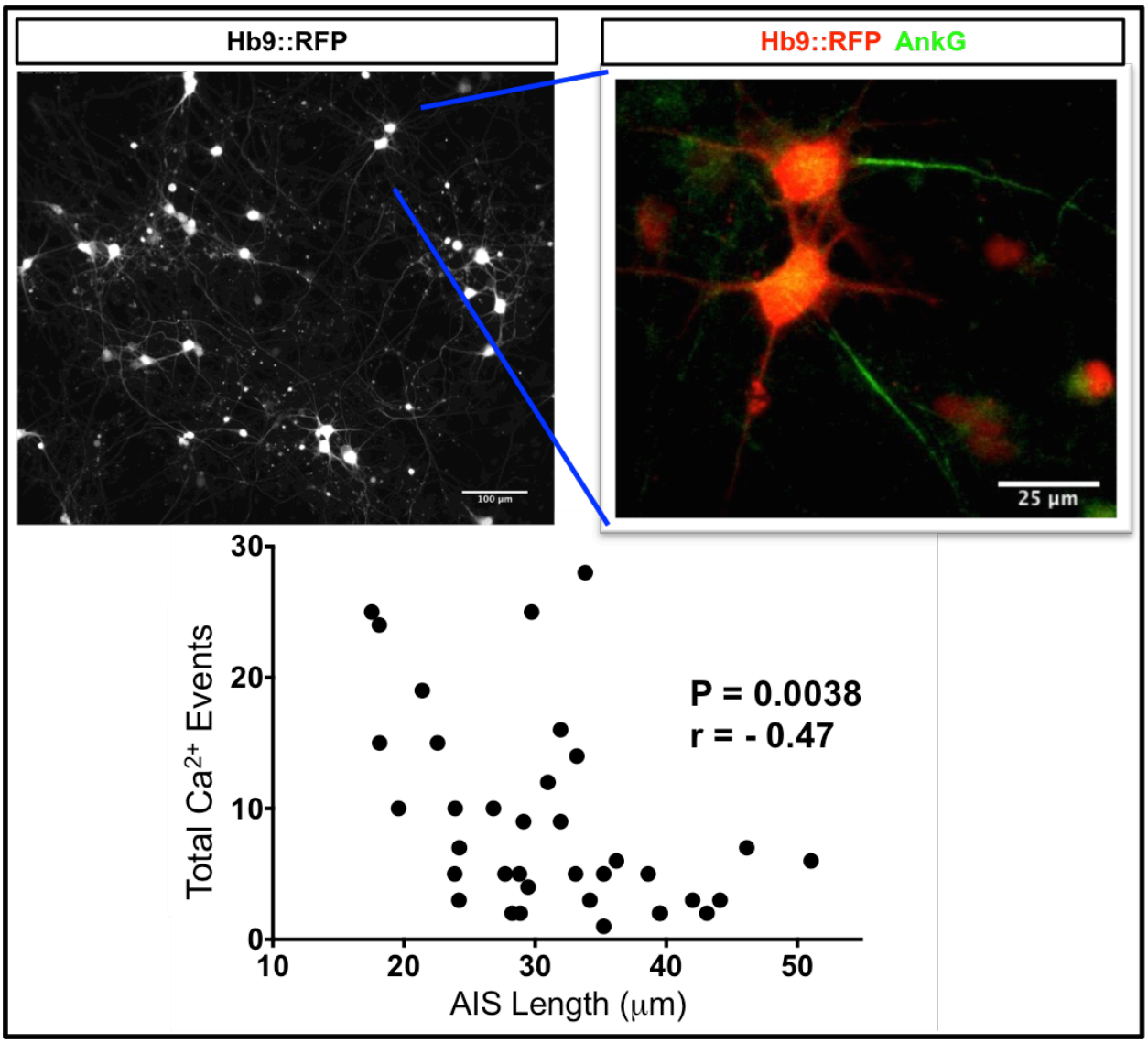

Figure 4-3: Axon initial segment length correlates with frequency of activity

Top: Representative image of a field used for calcium imaging where motor neurons are visualized by endogenous expression of RFP. Blown up is a region from this field after post-fixation and immunostaining for AnkyrinG. Bottom: Calcium transient frequency plotted as a function of axon initial segment length. Each dot represents the transient frequency and axon initial segment length from a single neuron. Significance determined by Pearson correlation.

An *in vitro* model of ALS shows marked structural plasticity in the axon initial segment and reduction of intrinsic excitability

Though the ability to utilize an *in vitro* model of ALS would be incredibly advantageous in uncovering the mechanisms that underlie axon initial segment shortening seen *in vivo* in the $SOD1^{G93A}$ mouse model, it was unclear and even unexpected that ALS-model motor neurons in such a reduced environment would produce similar phenotypes to their *in vivo* counterparts. To evaluate the potential of *in vitro* ALS-model motor neurons to undergo axon initial segment structural changes, I used cultured motor neurons generated from transgenic murine ESCs. As considered in Chapter 2, stem cell differentiation yields a complex mixture of ventral spinal neurons, primarily composed of motor neurons, V3, V2a and V2b interneurons (Wichterle et al., 2002; Alaynick et al., 2011; Sternfeld et al., 2017). Motor neurons are identified in this milieu of spinal neurons by their expression of green or red fluorescent protein (GFP or RFP) driven off the motor neuron-specific promoter for the homeodomain protein Hb9 (Figure 4.4). These ESC lines, created in the Wichterle lab (Thams et al., 2018) expressed either the human $SOD1^{G93A}$ transgene or a human $SOD1^{WT}$ transgene, and were differentiated, dissociated and cultured using identical and simultaneous plating conditions (Wichterle and Peljto, 2008).

I looked for structural differences in the axon initial segment between $SOD1^{WT}$ and $SOD1^{G93A}$ motor neurons after one week in culture. After a week in culture, motor neurons elaborate complex processes, establish axon initial segments, and exhibit robust synaptic activity (Figure 2.1). To visualize the axon initial segment, I targeted the structural protein AnkyrinG (AnkG), master organizer of and densely clustered at the axon initial segment (Zhou et al., 1998; Yang et al., 2007; Song et al., 2009; Brachet et al., 2010; Kuba et al., 2014). Remarkably, the axon initial segment was found to be significantly shorter in the $SOD1^{G93A}$ motor neurons relative to $SOD1^{WT}$ motor neurons (Figure 4.4). This modification suggests that

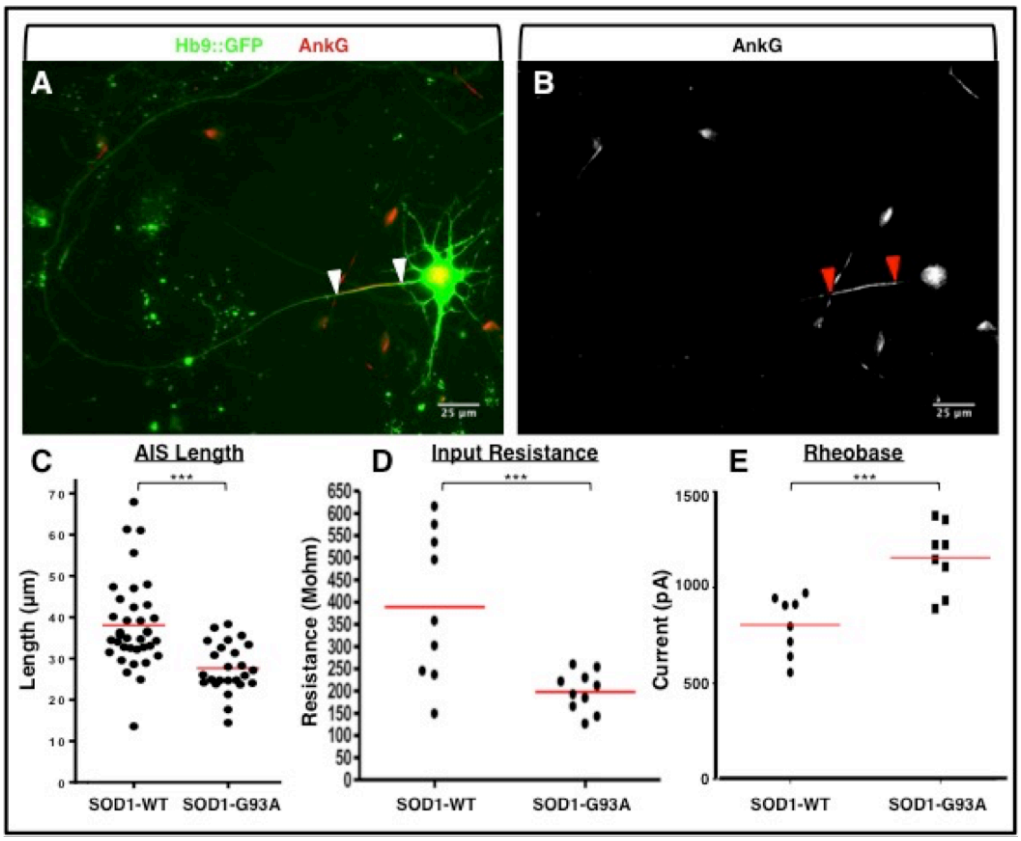

F	$SOD1^{WT}$ ± SEM	$SOD1^{G93A}$ ± SEM	Significance (red: $p < 0.05$)
Input Resistance (MOhm)	389 ± 56 $n = 9$	198 ± 14 $n = 10$	$p = 0.003$
Rheobase (pA; 2ms Stimulus)	806 ± 54 $n = 8$	1156 ± 63 $n = 8$	$p = 0.0008$
Capacitance (pF)	88 ± 9 $n = 9$	101 ± 6 $n = 10$	$p = 0.25$
Resting Membrane Potential (mV)	-56 ± 2 $n = 9$	-56 ± 2 $n = 8$	$p = 0.96$
Action Potential Duration (ms)	4.0 ± 0.3 $n = 9$	4.4 ± 0.3 $n = 10$	$p = 0.50$
Action Potential Overshoot (mV)	32 ± 2.3 $n = 9$	28.9 ± 2.0 $n = 10$	$p = 0.33$
Action Potential Max Rise Rate (mV/ms)	65 ± 4.4 $n = 9$	59 ± 4.8 $n = 10$	$p = 0.39$
Action Potential Max Fall Rate (mV/ms)	-14 ± 1.2 $n = 9$	-13 ± 0.9 $n = 10$	$p = 0.51$
Action Potential Threshold (mV)	-31 ± 0.6 $n = 9$	-32 ± 0.9 $n = 10$	$p = 0.59$
Max Number of Action Potentials	19.6 ± 2.7 $n = 9$	22.4 ± 1.3 $n = 10$	$p = 0.35$

Figure 4-4: *In vitro* $SOD1^{G93A}$ stem cell-derived motor neurons exhibit intrinsic hypoexcitability and reduced axon initial segment length

A and B) Representative images of an ESC-derived motor neuron plated 6-8 days after dissociation. Endogenously expressed GFP or RFP is used to identify motor neurons and the axon initial segment is visualized by immunostaining for AnkyrinG. C) Representative quantification from one differentiation. Similar results were seen between $SOD1^{WT}$ and $SOD1^{G93A}$ across multiple differentiations and using two different pairs of ESC lines, though the average length from differentiation to differentiation varied. D and E) Quantification of electrophysiological recordings from $SOD1^{WT}$ and $SOD1^{G93A}$ ESC-derived motor neurons from two different differentiations. F) Full table of current clamp recording data.

lower intrinsic excitability exists in the SOD1^{G93A} motor neurons, due to a reduced number of voltage-gated sodium channels in the shorter axon initial segment (Kuba et al., 2010).

To investigate this likelihood further, I used whole-cell electrophysiology and analyzed current-clamp recordings. In agreement with the axon initial segment data, I found lower intrinsic excitability in the SOD1^{G93A} motor neurons relative to SOD1^{WT} motor neurons, based on rheobase and input resistance (Figure 4.4). No significant changes were found in any of the other parameters tested including other passive properties, action potential characteristics and firing rates. Rheobase, which measures the propensity of a neuron to fire an action potential in response to a fixed-amplitude current injection, is higher in the SOD1^{G93A} motor neurons, a hallmark of reduced intrinsic excitability (Zengel et al., 1985). Furthermore, though somal size differences will influence input resistance (Fleshman et al., 1981; van Zundert et al., 2012), this is not the case here as studies in the lab have found no significant change in somal size between SOD1^{WT} and SOD1^{G93A} motor neurons. Additionally, there is no difference in capacitance, a measure that would also indicate a change in somal size and influence input resistance (Fleshman et al., 1981).

An *in vitro* model of ALS reveals an early increase in spontaneous action potential firing

I next asked whether the shortening of the axon initial segment is due to homeostatic mechanisms attempting to compensate for increased activity by reducing excitability in the SOD1^{G93A} motor neurons, or driving a reduction in activity through aberrant maturation of intrinsic physiology. To address this question, I loaded ESC-derived motor neurons, both 5 and 10 days after dissociation, with the calcium indicator Fluo-4 and again imaged the fluorescence intensity at a frequency of 5 Hz. Intriguingly, I found ESC-derived SOD1^{G93A} motor neurons have a significant increase in spontaneous calcium transients as compared to their SOD1^{WT}

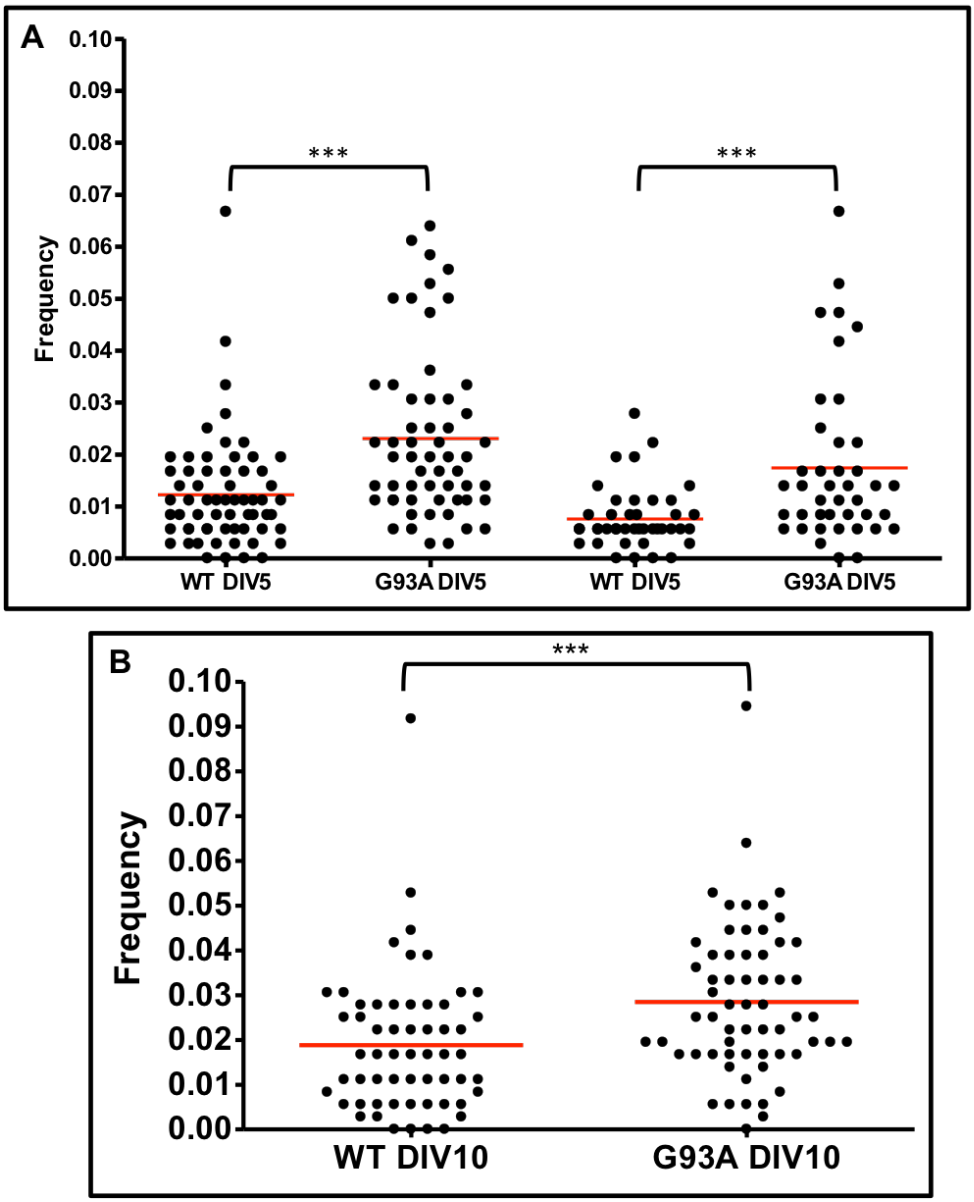

Figure 4-5: *In vitro* SOD1^{G93A} stem cell-derived motor neurons display increased calcium transient frequency as compared to SOD1^{WT}

A) Representative quantification of calcium transient frequency SOD1^{WT} and SOD1^{G93A} ESC-derived motor neurons from two different differentiations, 5 days after plating. Significance by students t-test. B) The same analysis as preformed in panel A, but on motor neurons 10 days after plating. Significance by students t-test.

counterparts (Figure 4.5). Additionally, as the ESC-derived motor neurons matured, both the $SOD1^{G93A}$ and $SOD1^{WT}$ increased in the frequency of spontaneous activity, however, the $SOD1^{G93A}$ still possessed increased activity as compared to $SOD1^{WT}$.

Spontaneous action potential output increases with maturation in *in vitro* $SOD1^{G93A}$ motor neurons

It is possible that the increased spontaneous activity seen in $SOD1^{G93A}$ ESC-derived motor neurons is an early, transient event, so I aimed to allow additional maturation time for the *in vitro* motor neuron cultures. Inopportunely though, murine ESC-derived motor neurons are difficult to culture on their own for longer than 10 days after dissociation. Though endogenous glial cells form during the differentiation process, they do not consistently become robust enough to be supportive of the culture. Therefore, it the use of a mouse primary cortical astrocyte co-culture to maintain the ESC-derived motor neurons is required. Primary astrocyte co-culture are known to be supportive of neuronal culture, synaptogenic and pro-maturation in general (Johnson et al., 2007; Tang et al., 2013; Muratore et al., 2014).

I attempted to use calcium imaging to evaluate activity of ESC-derived motor neurons on the primary astrocyte co-cultures, however, slow intrinsic calcium transients that occur in the astrocyte completely obscured the signal from the ESC-derived motor neurons. To circumvent this issue, I employed a loose-patch electrophysiological recording technique. Unlike the cell-attached configuration, a low electrical resistance seal (approx. 50 MΩ) is formed on each cell with a wide, 2-3 MΩ patch pipette (Figure 4.6). Although the throughput of this technique is not as high as with calcium imaging, it is much higher than conventional patch techniques as the same pipette can be used to record from multiple cells and the membrane remains intact. Moreover, it carries the distinct advantage of being able to resolve single action potentials.

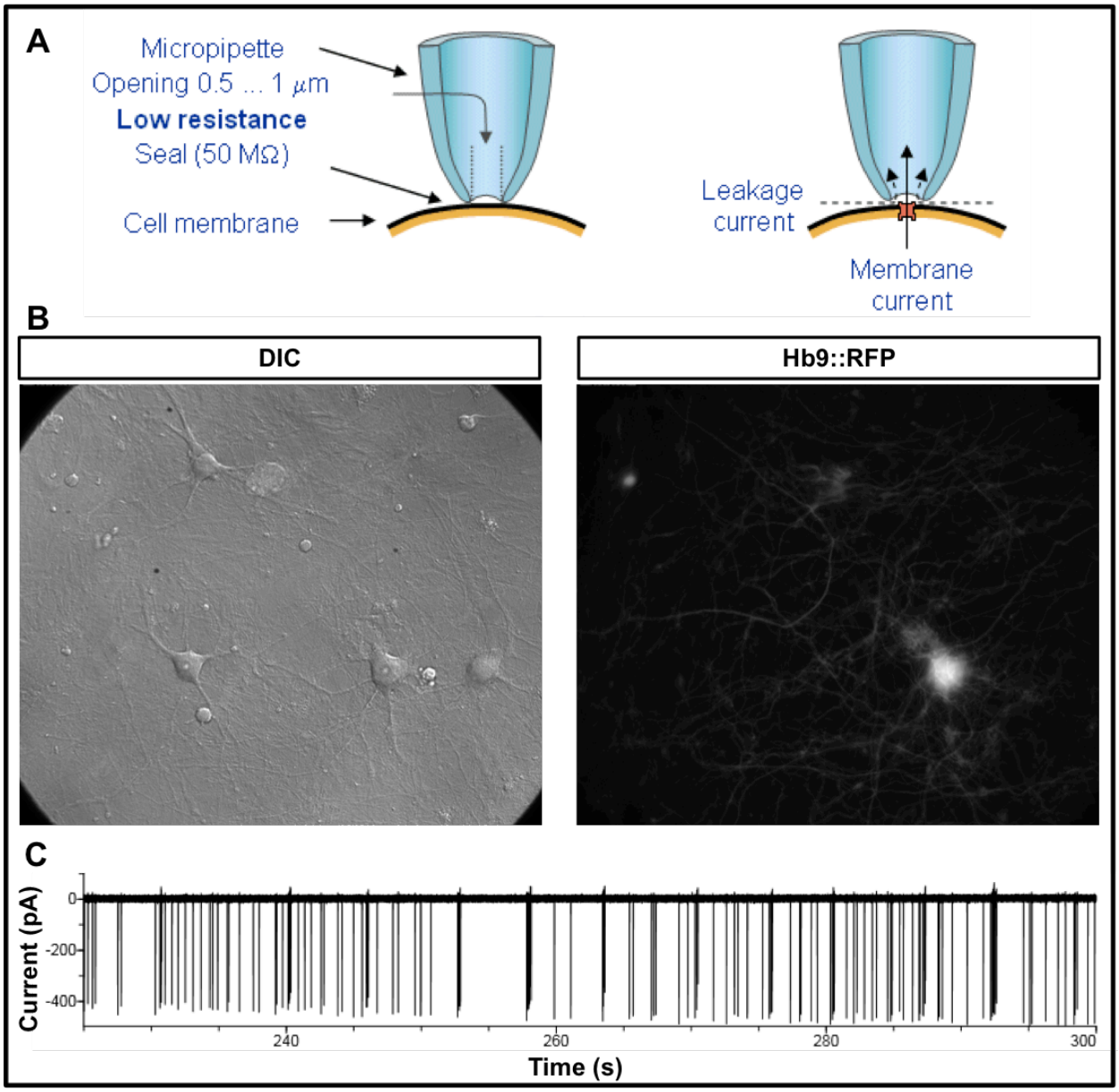

Figure 4-6: Loose patch electrophysiological recordings produce single action potential resolution and can mitigate issues that arise with calcium imaging

A) Rendition of a loose patch configuration, where a low resistance seal is formed allowing current leakage around the seal, yet still retaining enough current amplitude to record current flux. Though action potential amplitude has little meaning in this configuration, firing frequencies can be analyzed without disrupting the membrane or cytosolic ion concentrations. This technique also carries the advantage of not having to replace the pipette after each recording. Figure adapted from (Malmivuo and Plonsey, 1995). B) Representative DIC image and endogenous motor neuron reporter showing ESC-derived motor neurons, 16-18 days after plating, in a field to be analyzed by loose patch recording where the motor neuron can clearly be identified. C) Representative 5-minute loose patch recording where action potential waveforms in the voltage clamp configuration are similar to those of traditional extracellular recordings.

Using the loose patch technique in the voltage-clamp configuration, I recorded from SOD1^{G93A} and SOD1^{WT} ESC-derived motor neurons, 16-18 days after dissociation. I attempted to use this technique to record from younger ESC-derived motor neuron cultures, however, far fewer motor neurons were active at these ages rendering the technique ill-suited for gathering enough data at these time points. Of note, in addition to a greater fraction of ESC-derived motor neurons displaying spontaneous action potential firing, they also established a burst firing profile at the 16-18 day old time point (Figure 4.7A), arguing that these neurons were continuing to mature at that age. In agreement with the calcium imaging experiments, the loose-patch analysis revealed a significant increase in the number of spontaneous action potentials that were fired in the SOD1^{G93A} ESC-derived motor neurons as compared to SOD1^{WT} (Figure 4.7B). This technique also allowed for the quantification of intra-burst frequency in these motor neurons, measured as the number of action potentials within a burst over the total duration of the burst. Remarkably, in addition to the increased activity, the intra-burst frequency was two-fold higher in the SOD1^{G93A} ESC-derived motor neurons (Figure 4.7C).

Increased spontaneous activity in *in vitro* SOD1^{G93A} motor neurons is mediated by a cell-autonomous mechanism

To begin to address the mechanism behind the increased activity, I asked if it was due to increased firing in the presynaptic ALS interneurons or due to increased excitability cell intrinsic to ALS motor neurons. In an attempt to answer this question, I mixed non-transgenic ESC-derived motor neurons cultures with the SOD1^{WT} and SOD1^{G93A} cultures at a 10:1 ratio. This effectively dilutes any influence of the SOD1^{G93A} presynaptic neurons. Calcium imaging was then used to quantify the spontaneous activity of the SOD1^{WT} and the SOD1^{G93A} ESC-derived motor neurons. The cultures were then post fixed and stained for Hb9 to identify the non-

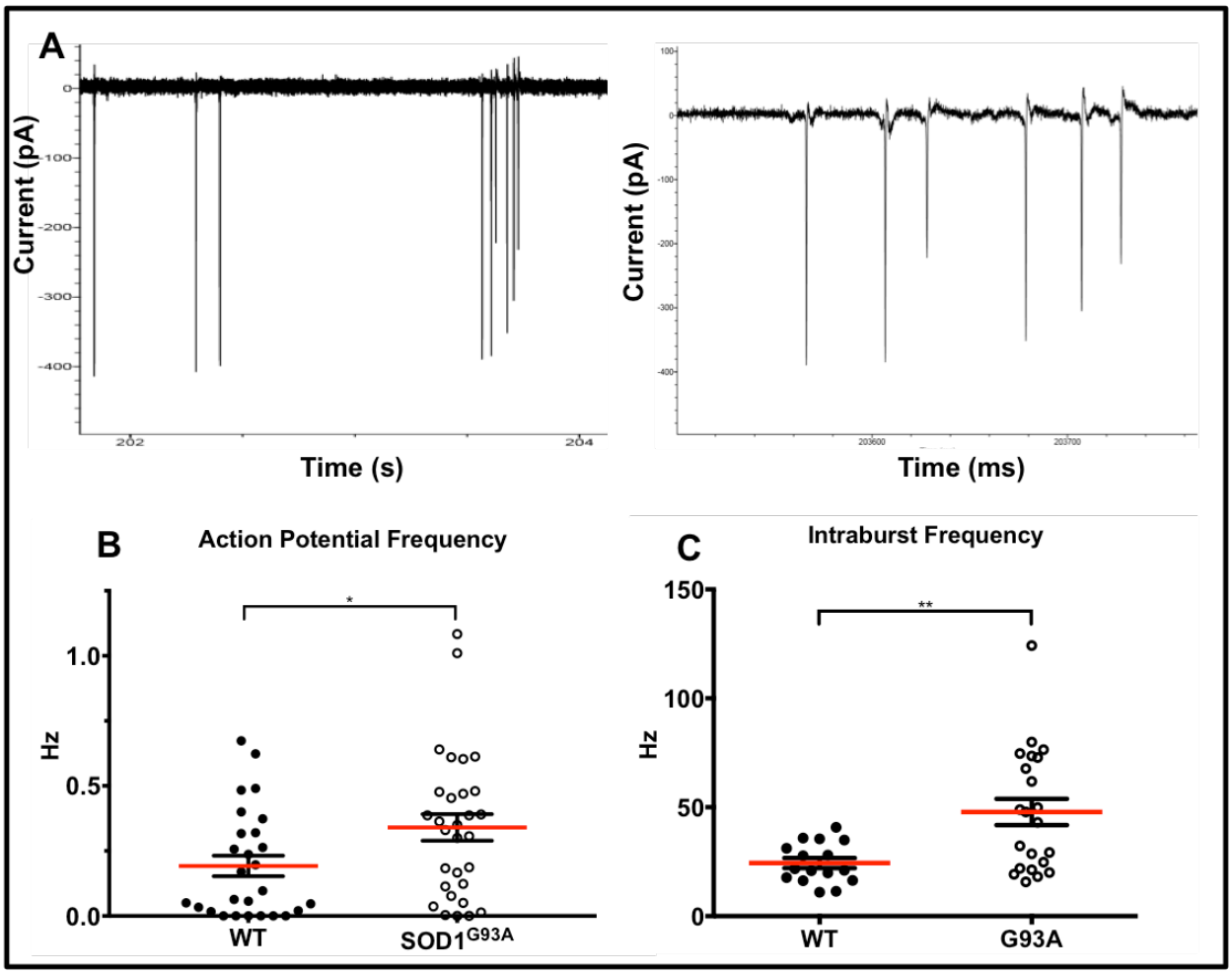

Figure 4-7: *In vitro* SOD1^{G93A} stem cell-derived motor neurons have persistently higher activity and develop higher burst frequencies

A) Two representative loose patch recordings with increasingly smaller time scales that show bursting properties of ESC-derived motor neurons, 16-18 days after plating. B) Action potential frequency was quantified from SOD1^{WT} and SOD1^{G93A} ESC-derived motor neurons from two different differentiations. C) From the same recordings quantified in panel B, intraburst frequencies were quantified. Bursts were identified by pClamp analysis software with a threshold for minimum number of action potentials set at >2. In the plots in B and C, each dot represents data from an individual motor neuron and the red line marks the mean with SEM. Significance determined by student's t-test.

transgenic ESC-derived motor neurons so their spontaneous activity could be analyzed as well. Interestingly, this allowed me to measure the frequency of spontaneous activity in non-transgenic and either the $SOD1^{WT}$ or $SOD1^{G93A}$ motor neurons within the same culture dish. This way, if the transgenic interneurons happened to still be influencing the synaptic network, it would be expected that the non-transgenic motor neurons would also be affected. Excitingly, the $SOD1^{G93A}$ motor neurons retained a significantly greater frequency of spontaneous activity, not only relative to the $SOD1^{WT}$ motor neurons in the other culture dishes, but also compared to the non-transgenic motor neurons they were co-cultured with (Figure 4.8). These data suggest the process underlying the increased spontaneous activity is indeed cell-autonomous. Considering the observation of decreased excitability and shorter axon initial segment in cultured ALS motor neurons, these results indicate that ALS motor neurons cell-autonomously elicit increased excitatory innervation that results in increased motor neuron activity and secondary compensatory decrease in motor neuron excitability.

Calcium permeability of AMPA receptors is reduced in *in vitro* $SOD1^{G93A}$ motor neurons

If motor neurons are attempting to compensate for increases in activity, multiple homeostatic mechanisms may be coming into play. In *in vivo* sections of spinal cords from neonatal ALS-model mice, a reduction of dendritic calcium was observed, likely due to L/T-type calcium transients (Quinlan et al., 2015). These findings provide possible further evidence of compensation for over-activation within spinal motor neurons. However, analysis of postmortem human spinal tissue showed an RNA editing defect that would lead to increases in calcium-permeable α-amino-3-hydroxy-5-methyl-4-isoxazolepropionic acid (AMPA) receptors (Kawahara et al., 2004). This would effectively increase the calcium flux into dendrites.

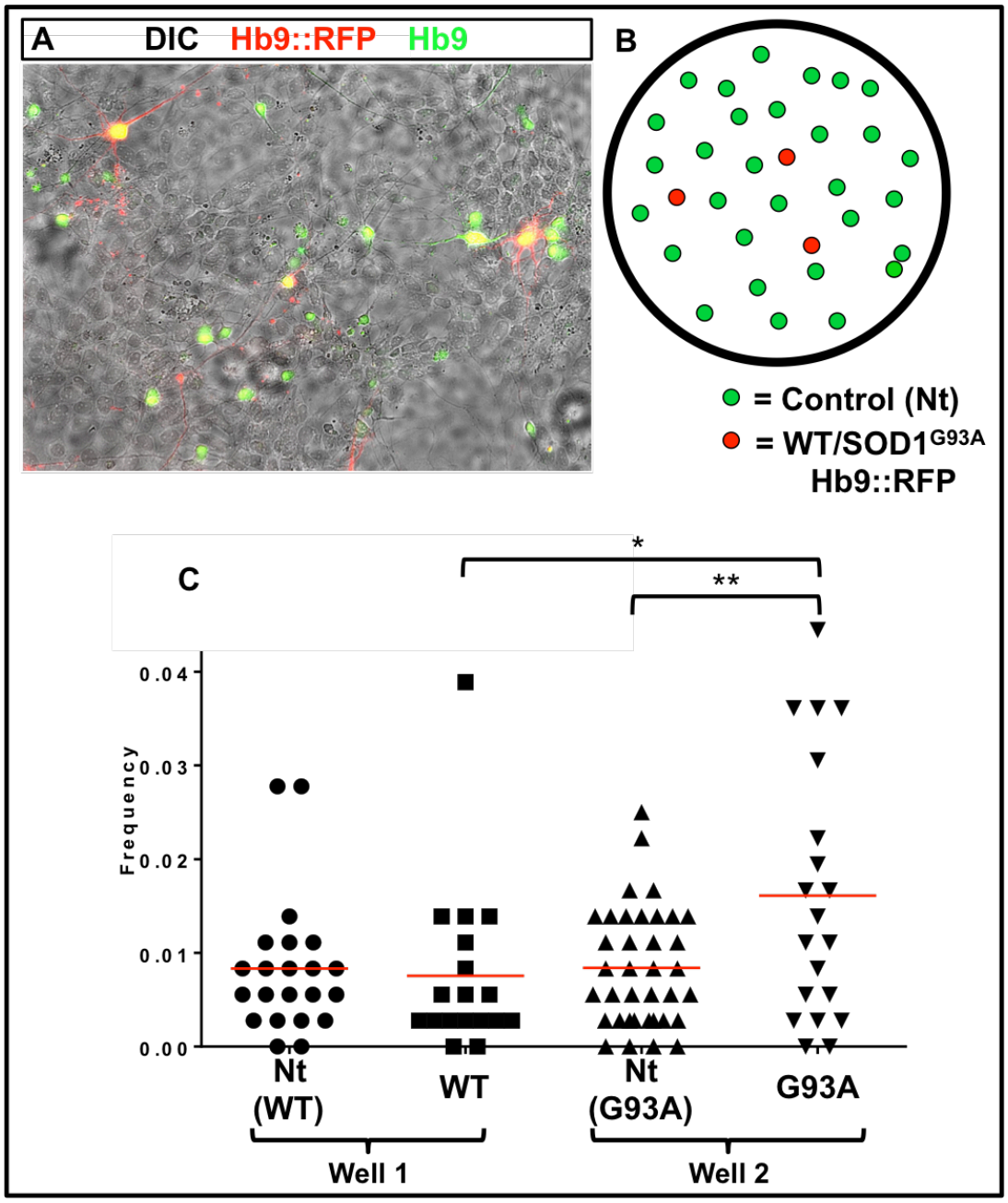

Figure 4-8: Increased activity in *in vitro* SOD1^{G93A} stem cell-derived motor neurons is mediated by a cell-autonomous mechanism

A) Representative calcium imaging field overlaying a DIC image, endogenous motor neuron-specific fluorescent reporter, and immunostaining of Hb9. B) SOD1^{WT} or SOD1^{G93A} ESC-derived motor neurons were diluted into non-transgenic ESC-derived motor neurons at a 1:10 ratio and separated into wells (eg Well 1- SOD1^{WT}+Nt 1:10; Well 2- SOD1^{G93A}+Nt 1:10). For each calcium imaging field, non-transgenic motor neurons were identified as positive for Hb9 immunostaining but negative for the endogenous reporter. Either SOD1^{WT} or SOD1^{G93A} ESC-derived motor neurons were identified by fluorescent reporters. Regions of interest were drawn around the soma for each neuron identified and calcium transients were quantified as described previously. C) Quantification of calcium transients for each of the example wells, where SOD1^{WT}+Nt motor neurons in well 1 do not differ in their calcium transient activity. In well 2, SOD1^{G93A} motor neurons display significantly higher calcium transient frequency relative to the Nt motor neurons that they are co-plated with, and relative to the SOD1^{WT} motor neurons in the opposing well. Each dot represents data from an individual motor neuron and the red line marks the mean. Significance determined by one-way ANOVA and Bonferroni post hoc analysis.

To investigate these possibilities in SOD1^{G93A} ESC-derived motor neurons, I first looked for RNA editing defects at the Q/R site of the AMPA subunit GluR2. GluR2 is the subunit of AMPA receptors that typically blocks calcium permeability, however, if RNA editing does not convert the encoded Glutamine residue to an Arginine, GluR2 no longer retains the ability to block calcium entry due to the loss of the positively charged residue (Whitney et al., 2008). Using an established protocol (Kawahara et al., 2003), I performed a *BbvI* restriction digest of the polymerase chain reaction (PCR) products from the region of GluR2 that contain the Q/R editing site. No such defect in GluR2 editing was observed using this method, indicating all GluR2 in the SOD1^{G93A} ESC-derived motor neurons was properly edited. Nevertheless, it is still possible that the GluR2 subunit was not incorporated into the AMPA receptors, still rendering them permeable to calcium.

I addressed this using an established electrophysiological protocol, as well as one of my own design. When analyzing the current-voltage relationship of AMPA channels, calcium-permeability results in strong inward rectification, due to the presence of the polyamine spermine in the internal recording solution (Isa et al., 1995; Morita et al., 2013). Therefore, I used whole-cell patch in the voltage clamp configuration to analyze the current-voltage relationship of AMPA channels in SOD1^{G93A} ESC-derived motor neurons as compared to SOD1^{WT}. In the presence of the voltage-gated sodium channel blocker TTX, I used a custom-made fast perfusion system to bath only the cell that was patched with the AMPA receptor agonist Kainate. Kainate is used as an agonist over glutamate or AMPA in this case as it maintains a steady current through AMPA receptors and does not induce channel desensitization (Seeburg, 1993). Kainate was applied while holding the membrane between -60 mV and +60 mV at 10 mV increments (Figure 4.9A, B). The current (I) was recorded at each voltage step and plotted as a function of that voltage, and the rectification index was calculated ($Rectification\ Index = \frac{I\ (50\ mV)}{I\ (-50\ mV)}$) for the recordings from both SOD1^{WT} and SOD1^{G93A} ESC-

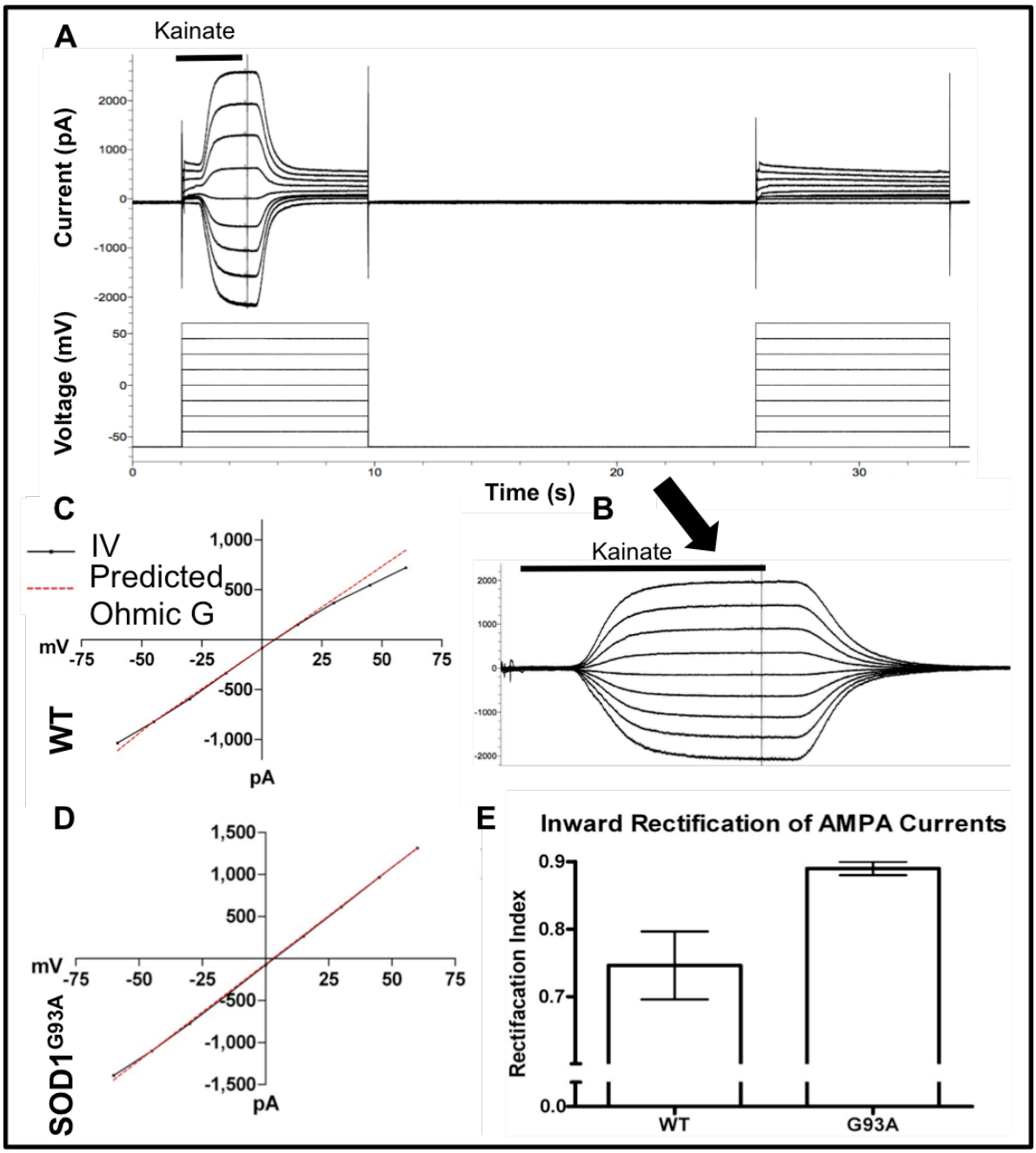

Figure 4-9: Fewer calcium-permeable AMPA channels may be present in *in vitro* SOD1^{G93A} stem cell-derived motor neurons

A) Using whole cell patch in the voltage clamp configuration, kainate-induced currents were recorded at depolarizing voltage steps followed by a non-perfused normalization step. Representative trace of whole cell recordings. B) Non-perfused normalization voltage step currents were subtracted from kainate-induced currents. The normalized currents were measured for each voltage step. C and D) Currents were plotted as a function of voltage for each voltage step and the rectification index calculated. E) Plotted rectification index for SOD1^{WT} or SOD1^{G93A} ESC-derived motor neurons. A total of 9 recordings were made over two differentiations. Statistics were not preformed due to the low number of recordings in this preliminary data.

derived motor neurons. Interestingly, I find the SOD1^{G93A} ESC-derived motor neurons have a lower rectification index, indicating a reduction in calcium-permeable AMPA channel (Figure 4.9C-E).

To investigate this further, I designed a more rapid analysis of the presence of calcium-permeable AMPA channels. While holding the in vitro motor neurons at -60 mV and applying Kainate as before, I also used the fast-perfusion system to deploy 1-naphthyl acetyl spermine (NASPM), another polyamine that selectively blocks calcium-permeable AMPA channels (Koike et al., 1997) (Figure 4.10A). As a control, I used the same small molecule application while holding the motor neurons at +60 mV, to ensure there were no off-target effects of the NASPM. I then quantified the lost current during the application of NASPM as a percentage of the total Kainate induced current. In agreement with the previous method, I find the SOD1^{G93A} ESC-derived motor neurons have a significant reduction in current through calcium-permeable AMPA channels as compared to SOD1^{WT}, indicating loss of membrane-incorporated calcium-permeable AMPA channels (Figure 4.10B, C).

Increased spontaneous action potential firing is driven by increased excitatory synaptic input

Data presented thus far in this chapter suggests that multiple homeostatic mechanisms are attempting to compensate for the increase of activity in the SOD1^{G93A} ESC-derived motor neurons. It also indicates that the increased firing is mediated by a cell-autonomous mechanism. Given that electrophysiological analyses have indicated that the SOD1^{G93A} ESC-derived motor neurons are intrinsically hypoexcitable, or less apt to fire an action potential, I hypothesized that these ALS-model motor neurons have increased net excitatory synaptic input.

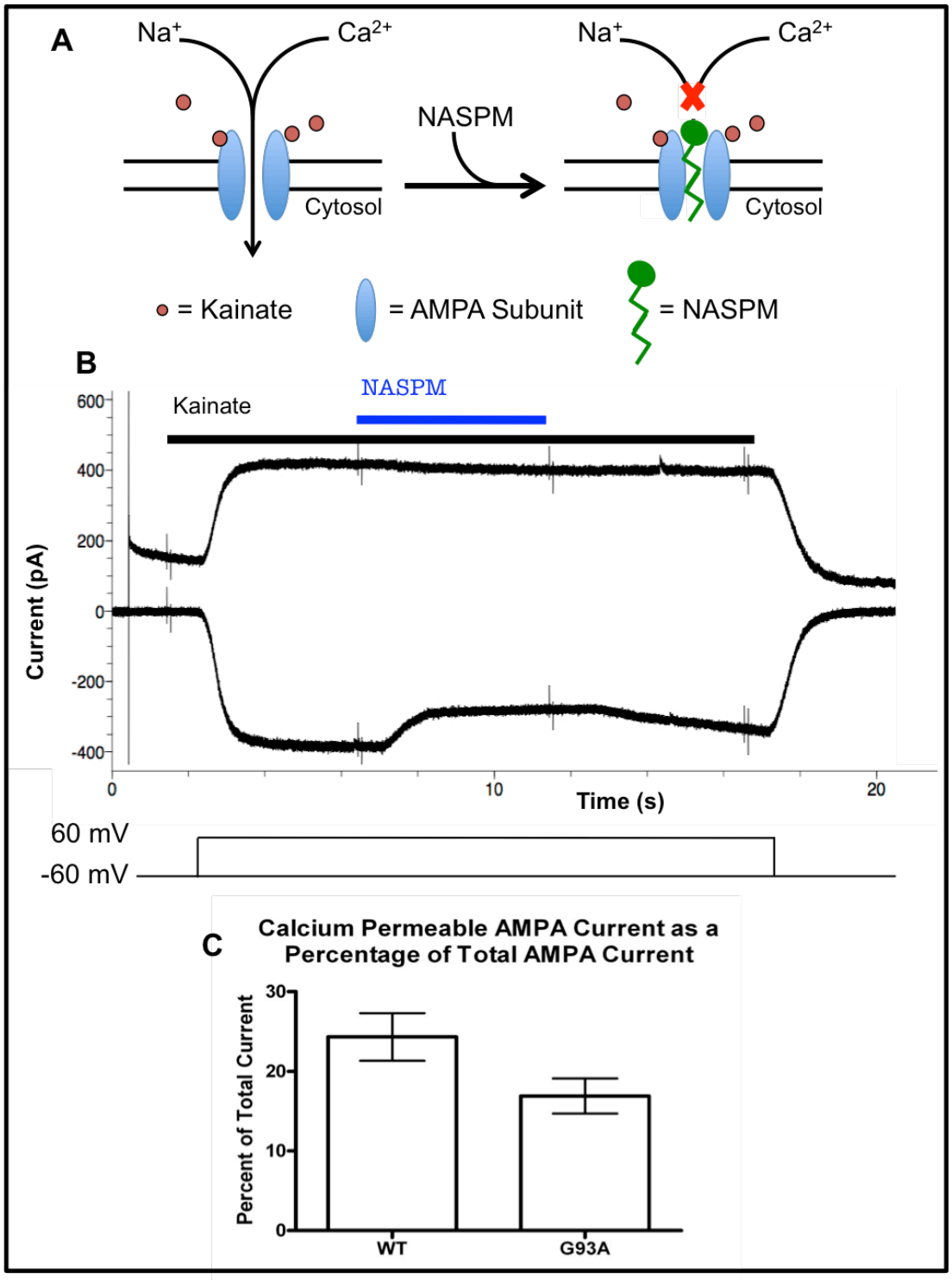

Figure 4-10: Further evidence of calcium-permeable AMPA channel reductions in *in vitro* SOD1^{G93A} stem cell-derived motor neurons

A) Rendition of the activity of NASPM, a polyamine that selectively blocks calcium permeable AMPA channels by plugging the pore. B) Representative trace of a whole cell patch recording in the voltage clamp configuration. Kainate was applied while holding the neuron at ± 60 mV, and a subsequent application of NASPM was deployed using a fast-perfusion system and allowed to partially wash. C) Quantification of the reduction of current blocked by NASPM as a percentage of the total kainate-evoked current.

I tested this possibility by analyzing miniature excitatory post-synaptic currents (mEPSCs) to observe synaptic activity in the $SOD1^{WT}$ and $SOD1^{G93A}$ ESC-derived motor neurons. Using whole-cell patch in the voltage clamp configuration, I recorded mEPSCs in the presence of TTX (Figure 4.11A, B). The mEPSCs were completely abolished by the glutamate receptor antagonist CNQX (Honoré et al., 1988) (Figure 4.11C), mimicking the EPSP and action potential block in Chapter 2 (Figure 4.11D). I used minianalysis software (Synaptosoft, Leonia, New Jersey) (Gu et al., 1998; Beaumont and Zucker, 2000) to analyze waveforms of the post-synaptic currents and to quantify the inter-event interval, or frequency of mEPSC events. In support of the hypothesis, I find increased mEPSC events in $SOD1^{G93A}$ ESC-derived motor neurons as compared to $SOD1^{WT}$, suggesting an increase in glutamatergic synaptic input onto these neurons (Figure 4.11E). Of note, while recording, I observed no evidence of inhibitory inputs onto motor neurons. Voltage steps between -80 and 40 mV were recorded for each neuron to verify the absence of these inputs (data not shown).

VGluT2-possitive synapses are increased onto *in vitro* $SOD1^{G93A}$ motor neurons

Through electrophysiological analyses presented in this thesis, as well as immunohistochemical analyses I have performed on these ESC-derived motor neurons, I see only excitatory inputs present. Specifically, I find only glutamatergic inputs marked by VGluT2 staining at the ages I have investigated. Therefore, I restricted my exploration here to focus on these inputs.

To further examine the possibility of an increase in glutamatergic input, I quantified the number of VGluT2 positive puncta onto $SOD1^{WT}$ and $SOD1^{G93A}$ ESC-derived motor neurons. I defined a circular region of interest of identical size, centered on each motor neuron soma. The puncta within the region were then counted. In agreement with the electrophysiological data,

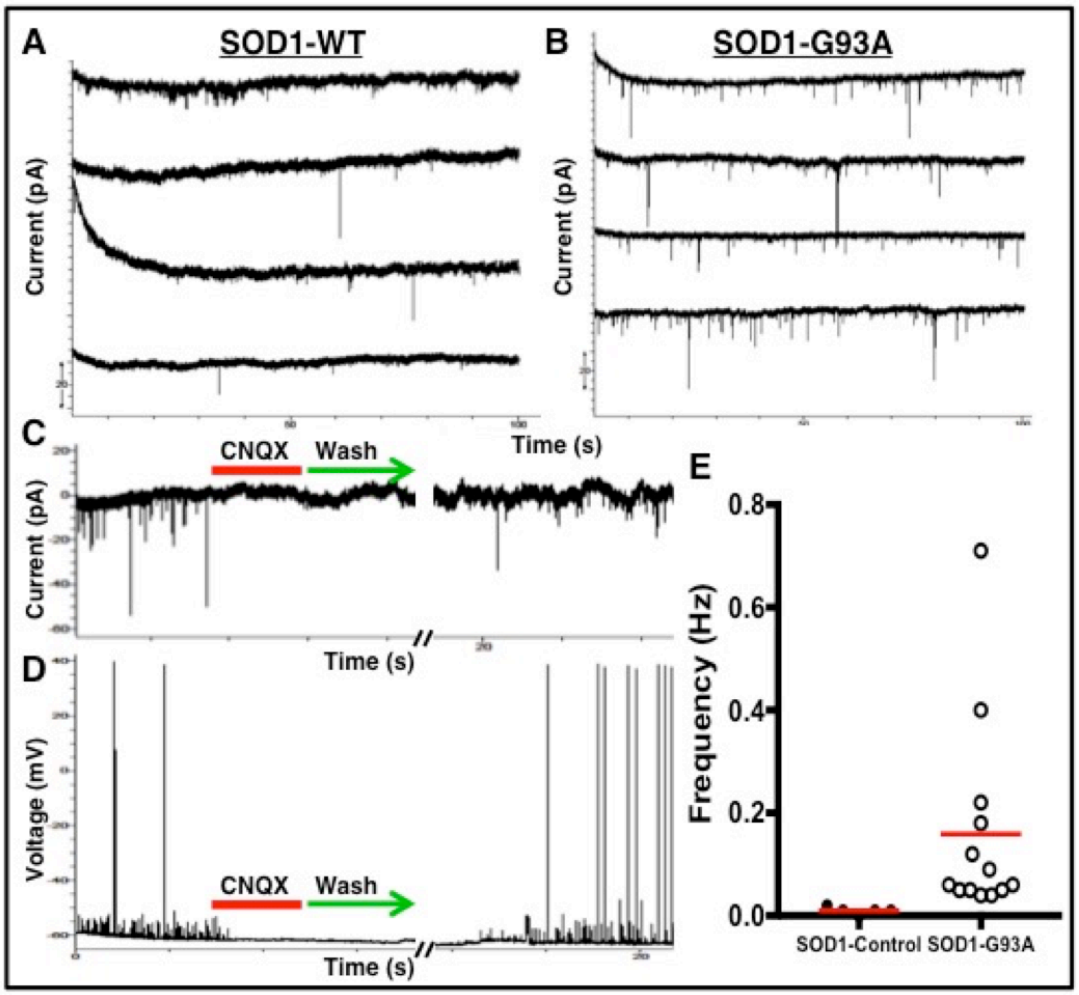

Figure 4-11: Increased numbers of excitatory synapses are found on *in vitro* SOD1^{G93A} stem cell-derived motor neurons

A and B) Representative recordings of miniature EPSC using whole cell patch in the voltage clamp configuration. Each trace is a recording from a single motor neuron. C) CNQX blocks miniature EPSCs, which return after a wash period. D) From figure 2.1, a similar CNQX block is seen in a recording of EPSPs. E) Quantification by the minianalysis software. Each dot reflects miniature EPSC frequency in a single motor neuron, red line represents the mean.

the number of VGluT2 synaptic puncta were two-fold greater on the $SOD1^{G93A}$ ESC-derived motor neurons as compared to $SOD1^{WT}$ (Figure 4.12).

V3 interneurons may be selectively enriched onto *in vitro* $SOD1^{G93A}$ motor neurons

Previous data presented in this chapter has suggested that cell-autonomous mechanisms in *in vitro* ALS-model motor neurons induce an increase in excitatory synapses onto motor neurons. It is possible that this could either be due to recruitment of greater numbers of neurons to make connections, or possibly an increase in sprouting of synapses for each monosynaptic connection. It is also unclear whether this affects all glutamatergic neurons or if there is specificity for a particular subtype of spinal interneuron.

To address the later part of those questions, I utilized new ESC lines that were transgenic for interneuronal reporters. Both a Chx10::tdTomato and a Sim1::tdTomato ESC line were used to identify V2a and V3 interneurons respectively (Alaynick et al., 2011; Sternfeld et al., 2017). I was able to optimize the concentration of Smoothened agonist to attain differentiation efficiencies of 12% for V2a interneurons and 30-40% for V3 interneurons, similar to the reported efficiencies and protocols (Sternfeld et al., 2017). For each well, I then plated 30,000 total cells from the enriched Chx10 or Sim1 cultures, and 20,000 total cells from the Hb9::GFP motor neuron culture (Figure 4.13). I matured these neurons for 5-6 days after dissociation, fixed with paraformaldehyde and visualized the axon initial segment by targeting AnkG. Remarkably, enrichment in excitatory V2a interneurons induced a reduction in axon initial segment length. Furthermore, the V3 interneurons selectively reduced the axon initial segment length of $SOD1^{G93A}$ ESC-derived motor neurons but not the $SOD1^{WT}$ (Figure 4.13).

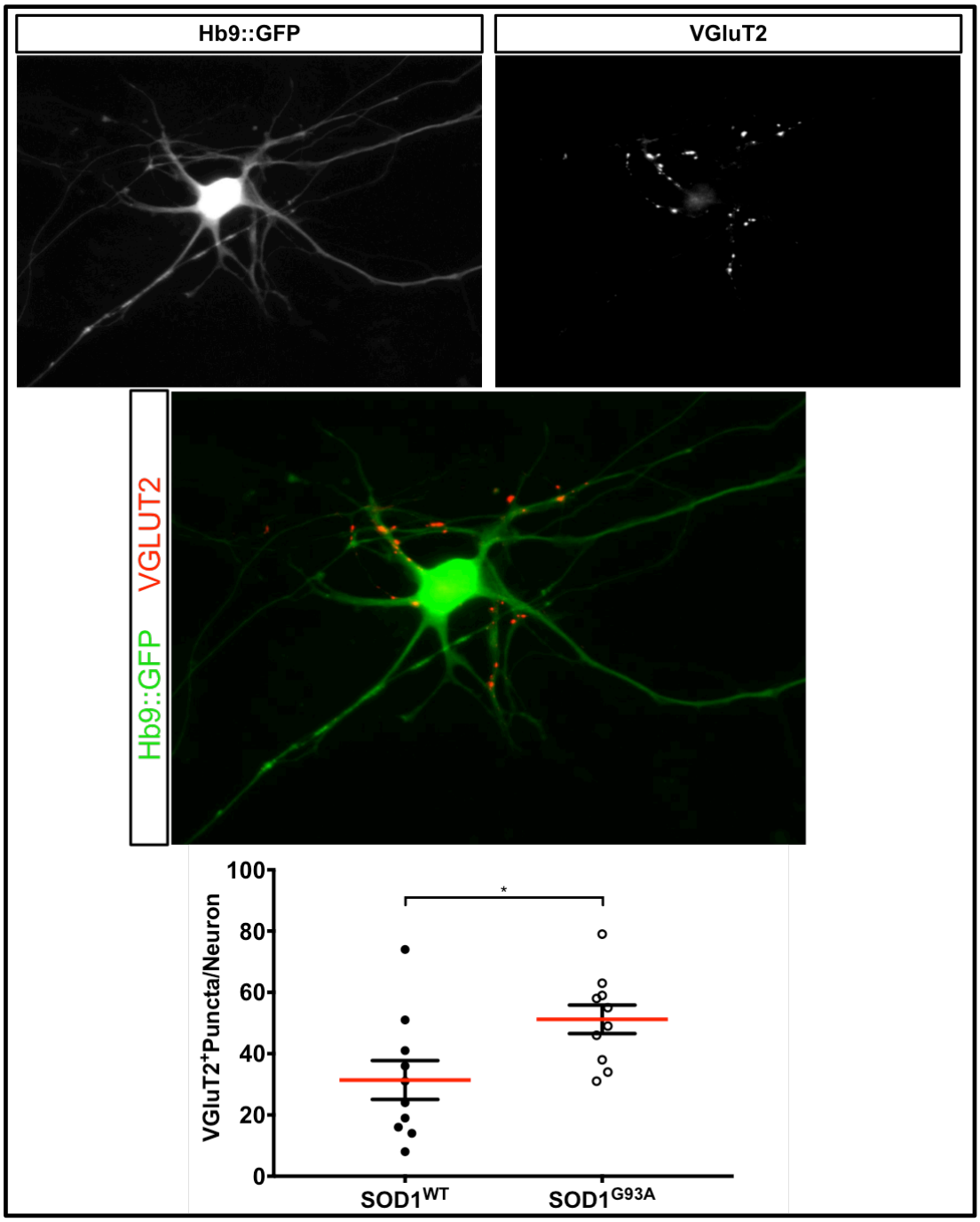

Figure 4-12: Increased numbers of VGluT2-possitive puncta are found on *in vitro* SOD1^{G93A} stem cell-derived motor neurons

Representative image of VGluT2 immunostaining in an ESC-derived motor neuron overlaid with the motor neuron-specific endogenous reporter. For this preliminary data, VGluT2-possitive puncta were counted within a defined radius from the center of each soma in a total of 20 motor neurons from a single differentiation. An almost two-fold increase in VGluT2-possitive puncta was found in on SOD1^{G93A} ESC-derived motor neurons as compared to SOD1^{WT}.

Discussion

Here, I show that the axon initial segment directly influences action potential kinetics in motor neurons and that motor neuron action potential firing frequency correlates with axon initial segment length. Remarkably, SOD1^{G93A} ESC-derived motor neurons are spontaneously hyperactive, while intrinsically hypoexcitable relative to the SOD1^{WT} ESC-derived motor neuron control. The SOD1^{G93A} ESC-derived motor neurons undergo multiple levels of compensation, including axon initial segment shortening, reduction in AMPA receptor-mediated calcium influx, and a shift in passive membrane properties. Downstream of these compensatory events, these motor neurons increase the burst frequency of action potentials, suggesting there may be more complex intrinsic responses to changes in excitatory input. In this *in vitro* model of ALS, the synaptically driven hyperexcitability is mediated by a cell-autonomous mechanism that modulates synaptic input. Furthermore, there may in fact be targeted effects on V3 interneurons in particular, where their enrichment shows no effect on SOD1^{WT} ESC-derived motor neurons, but reduces axon initial segment length in SOD1^{G93A} ESC-derived motor neurons.

Excitability vs. Activity

Astoundingly, the SOD1^{G93A} ESC-derived motor neurons appear to recapitulate the same axon initial segment phenotype that was observed in SOD1^{G93A} spinal motor neurons *in vivo*. Though difficulties exist in quantifying physiological synaptic activity *in vivo*, I clearly demonstrate that there is a significant increase in excitatory synaptic input on to SOD1^{G93A} ESC-derived motor neurons *in vitro*. The increase in input drives the motor neurons to compensate for the hyperactivity by becoming hypoexcitable. It is interesting that only passive membrane properties change with the shortening of the axon initial segment in these neurons. Unlike the action potential kinetic differences seen in Chapter 2 (Figure 2.1). One might expect that the

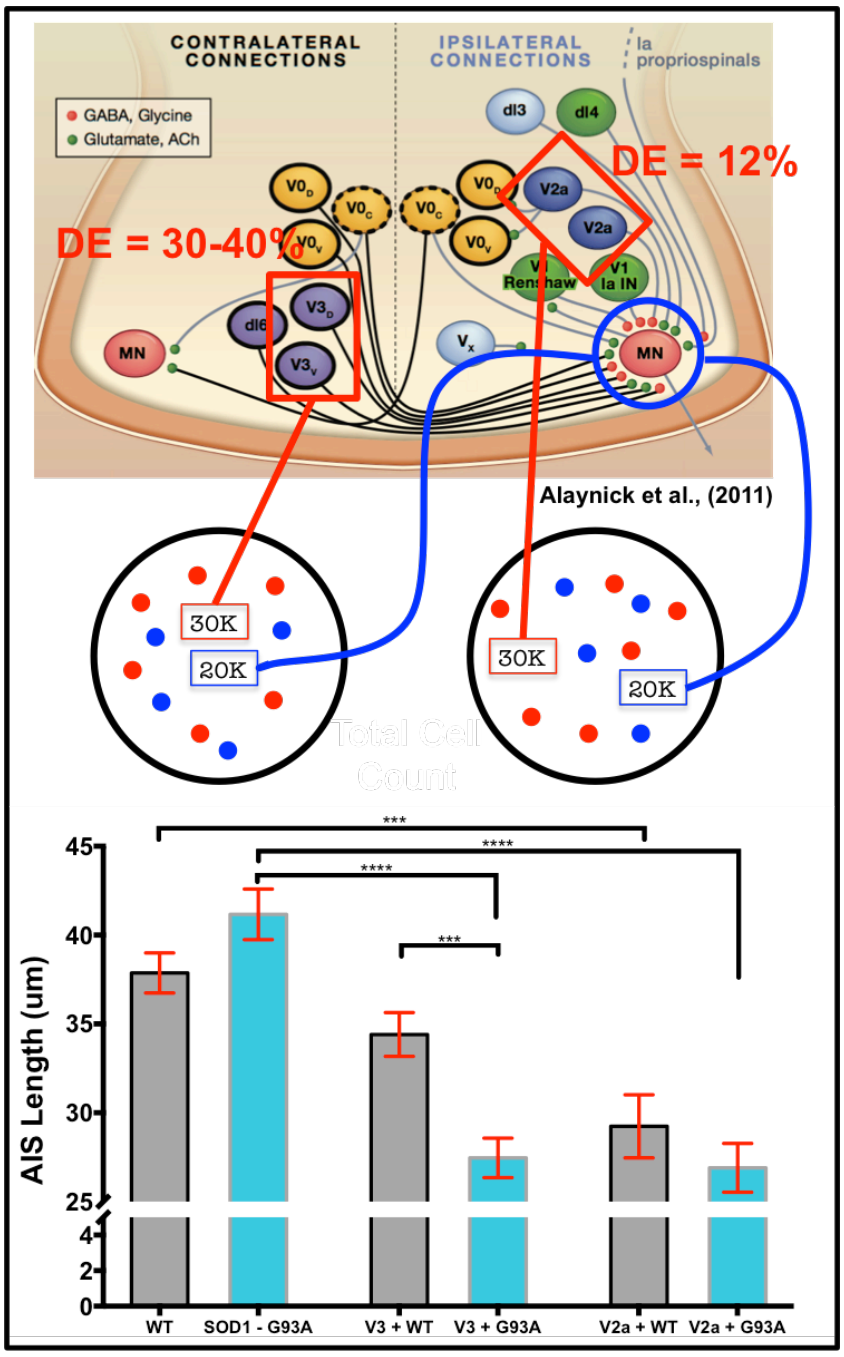

Figure 4-13: ***In vitro*** **SOD1^{G93A} stem cell-derived motor neurons exhibit axon initial segment shortening in response to enrichment of V3 interneurons in the surrounding culture.**

ESC lines were enriched for V3 interneurons or V2a interneurons. SOD1^{WT} or SOD1^{G93A} ESC-derived motor neurons were mixed with either the V3 or V2a enriched cultures at a 2:3 ratio. Cultures from three differentiation rounds were maintained for 5-6 days after dissociation and immunostained for ankyrinG. The axon initial segment length was quantified in each condition. Significance was determined by one-way ANOVA and Bonferroni post hoc analysis.

opposite action potential kinetic alterations would occur in the SOD1^{G93A} ESC-derived motor neurons as well. However, it is notable that the ESC-derived motor neurons analyzed in Chapter 2 were much older and cultured on astrocytes. It is also possible that there is an age-dependent effect on compensatory changes seen in neurons that respond to altered synaptic input, or, that the mutant SOD1 expression influences these mechanisms. Of note, there is a small survival phenotype seen in the motor neurons generated from the SOD1^{G93A} embryonic stem cells (Thams et al., 2018), however, this analysis was carried out at a very early age in these neurons. It could be interpreted that the motor neurons that die are the most vulnerable population and that those that are left represent more resistant subtypes. However, it could also be that the SOD1^{G93A} mutation confers an overall higher level of stress that confers a random increase of neuronal death in this population. Further analyses should be carried out across multiple ages in culture and in multiple plating conditions to differentiate between these possibilities and to make sure that enrichment of subtypes are not skewing the data.

The data, however, suggest that age-dependent physiological compensation may in fact occur. Though input resistance and rheobase measurements determined that SOD1^{G93A} ESC-derived motor neurons are intrinsically hypoexcitable, after almost 3-weeks in culture, intra-burst frequency is increased. It could be assumed from the data in Chapter 2 that a hyperactive neuron might try and decrease maximum firing rate, and this result seems contradictory to that. However, future analyses need to address the synaptic input more carefully. It could be that higher amplitude synaptic input is responsible for the increased intra-burst frequency. A more intriguing possibility is that synaptic input dictates, at least in part, subtype specific physiology in motor neurons. Fast α-motor neurons also show hypoexcitability but fire in high frequency bursts (Müller et al., 2014). The subtype specification for fast and slow α-motor neurons however, seems to be made after muscle contacts are made (Foehring et al., 1986). Perhaps, rather than a muscle-mediated signal, it is proprioceptive feedback to the local spinal circuitry and a subsequent alteration in synaptic drive that forces this final differentiation path. Of

course, a more detailed analysis will need to be performed but ESC-derived motor neurons prove to be a valuable model for synaptic network analysis and may help to provide these answers.

Cell-autonomous restructuring of the synaptic landscape

After observing the shortening in the axon initial segment, it was interesting but predicted that an increase in synaptic excitation might exist. However, a cell-autonomous mechanism in motor neurons that underlies this phenotype was not expected. Not only does this point to a potential pathophysiological mechanism that could be targeted in ALS, but it also uncovers possible mechanisms of synaptic recruitment relevant to basic motor neuron biology. Furthermore, it is an intriguing possibility that the alterations in synaptic input onto the $SOD1^{G93A}$ ESC-derived motor neurons may be mediated by V3 interneurons. This could provide understanding of a possible disease-relevant mechanism for ALS research, and may also prove an intriguing model for the study of synaptic recruitment and specification. That said, intensive future experimentation would need to show that this subtype specific recruitment actually occurs.

We have proposed several experiments for future analysis. First, one caveat in the present study is the lack of inhibitory, cholinergic and proprioceptive inputs in my culture conditions that may influence the synaptic landscape present on motor neurons. Given that the V2 interneurons exist in such low numbers in the regular motor neuron differentiation conditions (Sternfeld et al., 2017), I will enrich for V2b and V1 inhibitory interneurons to mix into the motor neuron cultures (Sternfeld et al., 2017; Hoang et al., 2018). Fluorescence activated cell sorting can be used to control the exact proportions of motor neurons and interneurons. Furthermore, astrocyte microislands (Lee et al., 2004; Joseph et al., 2010) can be utilized to isolate motor neurons and interneurons to ensure for monosynaptic connections. It is unclear from the present study whether increased synaptic inputs from a greater number of presynaptic

glutamatergic interneurons, induced synaptic sprouting for each monosynaptic input, or increased synaptic efficacy underlie the observed phenotype. The proposed experimental setup will hopefully answer that question.

Methods

Cell Culture

Mouse embryonic stem cells (ESCs) were cultured in EmbryoMax DMEM (EMD Millipore) supplemented with 15% embryonic stem cell screened fetal bovine serum (HyClone), 2mM L-glutamine (Life Technologies), 1x non-essential amino acids EmbryoMax MEM (EMD Millipore), 1x EmbryoMax nucleosides (EMD Millipore), 0.1mM β-mercapthoethanol (Sigma-Aldrich), 1000U/ml ESGRO Leukemia inhibitory factor (EMD Millipore), 1.25μM GSK-3 inhibitor XVI (EMD Millipore) and 100nM FGF receptor antagonist PD173074 (Tocris). All cells were determined to be negative for mycoplasma using the Venor GeM Mycoplasma detection kit (Sigma-Aldrich).

Motor neuron and interneuron differentiation

ESCs were differentiated into spinal neurons in embryoid bodies following established protocols (Wichterle et al., 2002; Wichterle and Peljto, 2008; Sternfeld et al., 2017). After 6 days of differentiation for motor neurons and 8 days of differentiation for interneurons, embryoid bodies were dissociated and neurons were plated on polyornithine/laminin/fibronectin coated plates in maturation media [Neurobasal medium (Life Technologies), 500μM L-glutamine (Life Technologies), 1x B-27 Supplement (serum free) (Life Technologies), 1:1000 β-mercapto ethanol (Chemicon ES-007-E), 2% heat-inactivated horse serum, containing neurotrophic factors (10ng/mL BDNF (R&D Systems), 10ng/mL GDNF (R&D Systems), 10ng/mL CNTF

(R&D Systems), 10ng/mL IGF-1 (R&D Systems), 10μM Forskolin (Sigma), and 100μM IBMX (R&D Systems)]. The media was replaced every 2-3 days starting from two days after plating. Motor neuron differentiations were consistently around 40% efficient.

Fixation and immunostaining

In vitro motor neurons were fixed with 4% paraformaldehyde (from 16% stock, 15710, Electron Microscopy Sciences) in phosphate-buffered saline (PBS) pH 7.4 (70011, ThermoFisher). Equal volume paraformaldehyde was first added to the media of each well and incubated for 2 minutes. This ~2% paraformaldehyde solution was then aspirated and the 4% paraformaldehyde added and incubated at 4°C for 20 minutes. After the incubation, three washes (>5 minutes each) in PBS were performed. Cultures were blocked for >30 minutes in PBS with 10% donkey serum (D9553, Sigma) and 0.1% Triton X-100 (T8787, Sigma). *In vitro* motor neurons were then were incubated at 4°C overnight in the above blocking buffer with primary antibodies [mouse monoclonal anti-vesicular glutamate transporter 2 (1:100; MAB5504, EMD Millipore or rabbit polyclonal anti-ankyrin G (Stock 0.2 μg/mL, 1:100; 386 003, Synaptic Systems)]. After the primary incubation, three washes (>5 minutes each) in PBS with 0.1% Triton were followed by a 1.5hr incubation at room temperature in the above wash buffer with donkey anti-mouse or anti-rabbit secondary antibodies (1.5 μg/mL; Jackson ImmunoResearch). After three more washes (as stated above), coverslips were mounted on microscope slides in Fluoromount G (OB100, ThermoFisher) and allowed to set for >12hrs.

Axon initial segment analysis

Motor neurons plated on polyornithine/laminin/fibronectin coated coverslips or primary cortical astrocytes were imaged using either a standard fluorescence microscope (Zeiss), or a laser-scanning confocal microscope (LSM 800, Zeiss) using a 40x oil-immersion objective. The settings were adjusted to prevent signal saturation and the confocal images were taken in z-

stacks with 1 μm steps. Z-stack images were projected into a single plane using maximum intensity projections and intensity across the length of the axon initial segment was quantified using the image analysis software Fiji (Schindelin et al., 2012). Briefly, two methods were used: 1) the start and end points were manually chosen and NeuronJ (Meijering et al., 2004) software determined the path length or 2) the cutoff intensity for axon initial segment start/end was 1/3 of the maximum intensity similar to methods used previously (Grubb and Burrone, 2010). AnkyrinG signal in the soma at times was quite high, therefore the axon initial segment starting point was manually determined.

Whole cell current clamp

Excitability was assessed using conventional whole cell current clamp technique. Briefly, astrocytes were prepared as previously described (Albuquerque et al., 2009) and plated on 15-mm diameter coverslips at a density of 100,000 cells per well in a 24-well plate. 4-6 days following astrocyte plating, non-sorted motor neurons added to the wells at a density of 50,000 total cells per well. Cultures were maintained for 5 days before recording. Membrane potential recordings were performed using a Multiclamp 700B amplifier and a Digidata 1550 digital-to-analog converter. Signals were recorded at a 10-kHz sample rate using pClamp 10 software (all equipment from Molecular Devices). Patch pipettes were fabricated with a P-97 pipette puller (Sutter Instruments) using 1.5 mm outer diameter, 1.28 mm inner diameter filamented capillary glass (World Precision Instruments). Pipette resistance was 2-5 MΩ when filled with the pipette solution. The external recording solution contained 145 mM NaCl, 5 mM KCl, 10 mM HEPES, 10 mM glucose, 2 mM $CaCl_2$ and 2 mM $MgCl_2$. The pH was adjusted to 7.3 using NaOH and the osmolality adjusted to 325 mOsm with sucrose. The pipette solution contained 130 mM CH_3KO_3S, 10 mM CH_3NaO_3S, 1 mM $CaCl_2$, 10 mM EGTA, 10 mM HEPES, 5 mM MgATP and 0.5 mM Na_2GTP (pH 7.3, 305 mOsm). Experiments were performed at room temperature (21–23 °C). During recordings, current was injected to hold the cells at -60 mV.

The liquid junction potential between pipette and external solutions was calculated empirically, and the correction applied before the experiment. Resting membrane potential was measured immediately following establishment of the whole-cell configuration. Membrane resistance and capacitance were calculated from the membrane potential changes in response to 1 s duration hyperpolarizing current steps that increased incrementally by 5 pA. Action potentials were evoked and rheobase obtained using 1 s duration depolarizing current steps that increased incrementally by 5 pA.

An action potential was defined as a transient depolarization of the membrane which had a minimum rise rate > 10 mV/ms and reached a peak amplitude > 0 mV. Action potential characteristics were measured from the first action potential at rheobase. The threshold potential was measured at the point where the voltage increases at a rate greater than 10 ms/mV. The duration was calculated from the full width at the half maximum voltage. For this calculation, the amplitude was measured from the threshold potential to the maximum potential. The maximum number of action potentials was measured from a 1 s current step. The amplitude of the step was dependent on the individual cell. Quantification was carried out using custom written scripts for Igor Pro v. 6 (Wavemetrics, USA). Outliers within Rheobase, Input Resistance, and Capacitance, that would indicate a poor seal, were identified using the ROUT method (Q = 0.5%) in GraphPad Prism version 7.0a for Mac, GraphPad Software, La Jolla California USA (www.graphpad.com). For each outlier detected, data from the entire neuron was removed from the analysis. Statistical comparisons were made using unpaired Student's t-test in GraphPad Prism. P-values < 0.05 were considered significant.

Whole cell voltage clamp

AMPA channel calcium conductance and the miniEPSC analysis were assessed using conventional whole cell voltage clamp techniques. Briefly, 15-mm diameter coverslips were coated with polyornithine/laminin/fibronectin. Non-sorted motor neurons were added to the wells

at a density of 50,000 total cells per well. Cultures were maintained for 5-6 days before recording. Recordings were performed using a Multiclamp 700B amplifier and a Digidata 1550 digital-to-analog converter. Signals were recorded at a 10-kHz sample rate using pClamp 10 software (all equipment from Molecular Devices). Patch pipettes were fabricated with a P-97 pipette puller (Sutter Instruments) using 1.5 mm outer diameter, 1.28 mm inner diameter filamented capillary glass (World Precision Instruments). Pipette resistance was 2-5 MΩ when filled with the pipette solution. The external recording solution contained 145 mM NaCl, 5 mM KCl, 10 mM HEPES, 10 mM glucose, 2 mM $CaCl_2$ and 2 mM $MgCl_2$. The pH was adjusted to 7.3 using NaOH and the osmolality adjusted to 325 mOsm with sucrose. Prior to the experiments, tetrodotoxin was added to the external recording solution for a final concentration of 500 nM. The pipette solution contained 130 mM CH_3CsO_3S, 10 mM CH_3NaO_3S, 1 mM $CaCl_2$, 10 mM EGTA, 10 mM HEPES, 0.1 mM Spermine, 5 mM MgATP and 0.5 mM Na_2GTP (pH 7.3, 305 mOsm). Experiments were performed at room temperature (21–23 °C). During the miniEPSC analysis, voltage was clamped at -60 mV.

Loose patch voltage clamp

Long-term action potential was assessed using a conventional whole cell voltage clamp configuration. Briefly, astrocytes were prepared as previously described (Albuquerque et al., 2009) and plated on 15-mm diameter coverslips at a density of 100,000 cells per well in a 24-well plate. 4-6 days following astrocyte plating, non-sorted motor neurons added to the wells at a density of 50,000 total cells per well. Cultures were maintained for 16-18 days before recording. Membrane current recordings were performed using a Multiclamp 700B amplifier and a Digidata 1550 digital-to-analog converter. Signals were recorded at a 10-kHz sample rate using pClamp 10 software (all equipment from Molecular Devices). Patch pipettes were fabricated with a P-97 pipette puller (Sutter Instruments) using 1.5 mm outer diameter, 1.28 mm inner diameter filamented capillary glass (World Precision Instruments). Pipette resistance was

1-3 MΩ when filled with the pipette solution. Both the external recording solution and the pipette solution contained 145 mM NaCl, 5 mM KCl, 10 mM HEPES, 10 mM glucose, 2 mM $CaCl_2$ and 2 mM $MgCl_2$. The pH was adjusted to 7.3 using NaOH and the osmolality adjusted to 325 mOsm with sucrose. A low resistance seal (~50 MΩ) was established and the voltage was clamped at 0 mV. 5-minute recordings of spontaneous action potential firing were taken for each neuron.

Calcium Imaging

Calcium transient frequency was assessed using a conventional calcium imaging technique. Briefly, 15-mm diameter coverslips were coated with polyornithine/laminin/fibronectin. Non-sorted motor neurons were added to the wells at a density of 50,000 total cells per well. Cultures were maintained for 5-6 days before imaging. The external imaging solution contained 145 mM NaCl, 5 mM KCl, 10 mM HEPES, 10 mM glucose, 2 mM $CaCl_2$ and 2 mM $MgCl_2$. The pH was adjusted to 7.3 using NaOH and the osmolality adjusted to 325 mOsm with sucrose. Calcium indicator (Fluo-4, F23917, ThermoFisher) was loaded into the cells using external solution supplemented with 2.5 μM Fluo-4 and 0.02% Pluronic acid, and incubating at room temperature for 30 minutes. A subsequent 30-minute wash in external solution was conducted. Coverslips were loaded into a slow perfusion chamber and imaged on a Nikon Eclipse TE300 inverted scope with a high numerical aperture 20x objective. An sCMOS camera was used to take a constant stream of images at 200 ms exposures for 5 minutes. Regions of interest based on fluorescent reporters were manually drawn in Fiji (Schindelin et al., 2012) and the florescence intensities for each image across the entire recording quantified. Waveforms of the intensity versus time plots were analyzed using custom written scripts for Igor Pro v. 6 (Wavemetrics, USA).

Chapter 5: Increasing STEM access to underprivileged high school students through the Science Matters Research Internship (SMRI)

Summary

Purpose

The existing disparities for low-income and underrepresented minority groups in the sciences underscore the need for outreach programs to help engage young men and women from low-income and minority families in scientific research. Inadequate resources throughout their K-12 years disadvantage students from low-income families who have the potential to succeed in STEM fields and, furthermore, many students are unaware of great career opportunities in STEM research.

The purpose of this internship is to encourage high-school students from low-income families to explore their potential in scientific research and to engage graduate students, postdocs and faculty who have been successful in scientific career tracks.

Internship

The Science Matters Research Internship (Figure 5.1) provides access to enhanced scientific learning and experience through a two-part yearlong program throughout an academic year. Our internship includes a “Bio Boot Camp” where Columbia University graduate students and postdocs deliver an eight part lecture series, as well as a three-month laboratory project where interns are mentored one-on-one.

Figure 5-1: Website for the Science Matters Research Internship

Participants

The target group for the internship is high achieving low-income high school juniors that attend underfunded schools. These students are vetted by the established national non-profit organization, Minds Matter NYC. They must maintain a minimum 3.0 GPA (their average is 3.4). 90% of the low-income students are from underrepresented minority groups and the mean family income is $23,000 per year.

Introduction

Problem

The National Academies, U.S. Congress Joint Economic Committee, Bureau of Labor Statistics, and President Obama's Council of Advisors on Science and Technology have all cautioned that increases in need for STEM professionals will not be met by current rates of U.S. citizen enrollment in STEM graduate schools. Of additional concern is the disparity between low-income/minority students, and their more affluent counterparts when it comes to entrance and completion of STEM degrees. Research by Change the Equation suggests that highest-poverty communities welcome and benefit from top-quality afterschool STEM programs that fill gaps left from underfunded high schools.

Solution

SMRI provides a two-step approach to increase success within low-income communities. Our interns join with varying backgrounds in science. Underfunded schools can lack means to provide substantial science and math courses, and often do not offer AP courses for their high achieving students. To ensure a level starting point, SMRI provides access to a college-level cellular and molecular biology text, and lectures on biochemistry, neuroscience,

biology, and development. This bio boot camp garners enthusiasm for learning in a collegiate setting, and prepares the interns for a high-paced laboratory project requiring rapid syntheses of knowledge.

Secondly, the interns dive into their laboratory projects. Spending two to three evenings a week (6-10 hrs), they work one-on-one with their mentor, a senior graduate student or postdoc. SMRI interns practice the scientific method, and importantly, experience how their coursework applies to real-world careers. In addition to developing skills in a variety of scientific techniques, the interns obtain valuable networks of prominent professionals in the sciences. It will prove most valuable to have gained experience and to yield letters of recommendations from these sources.

SMRI Interns

SMRI interns are selected from rising juniors who participate in the Minds Matter NYC program. This has proven a valuable collaboration that provides students within our target population, as well as support for those students throughout their high school career. Minds Matter also ensures access to tracking information for our interns who have gone on to attend STEM programs at institutions including Washington University, Smith College, Johns Hopkins and MIT. See attached information regarding Minds Matter NYC.

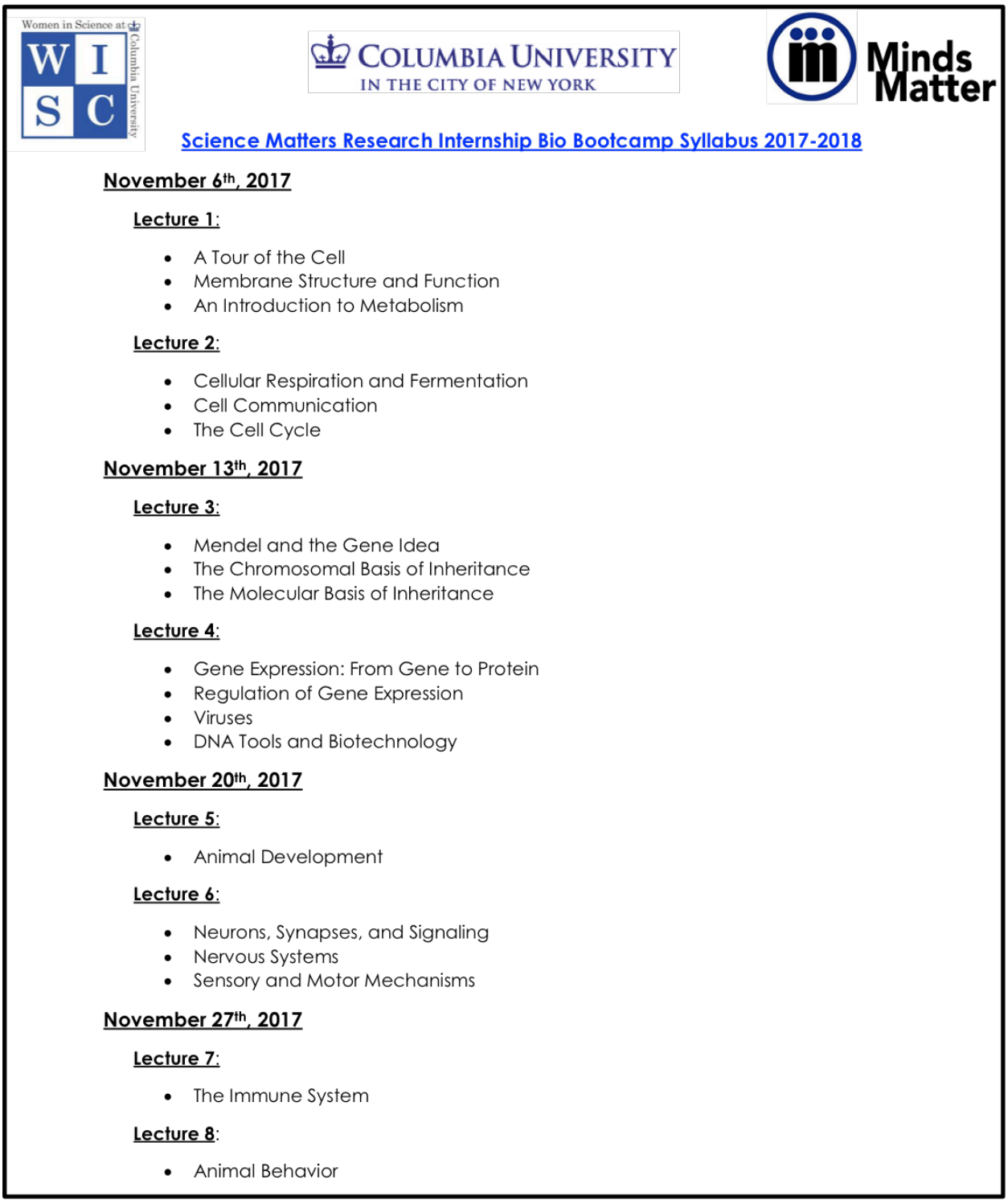

Science Matters Research Internship Bio Bootcamp Syllabus 2017-2018

November 6th, 2017

Lecture 1:

- A Tour of the Cell
- Membrane Structure and Function
- An Introduction to Metabolism

Lecture 2:

- Cellular Respiration and Fermentation
- Cell Communication
- The Cell Cycle

November 13th, 2017

Lecture 3:

- Mendel and the Gene Idea
- The Chromosomal Basis of Inheritance
- The Molecular Basis of Inheritance

Lecture 4:

- Gene Expression: From Gene to Protein
- Regulation of Gene Expression
- Viruses
- DNA Tools and Biotechnology

November 20th, 2017

Lecture 5:

- Animal Development

Lecture 6:

- Neurons, Synapses, and Signaling
- Nervous Systems
- Sensory and Motor Mechanisms

November 27th, 2017

Lecture 7:

- The Immune System

Lecture 8:

- Animal Behavior

Figure 5-2: Sample syllabus for the SMRI Bio Bootcamp

Results

Principal Members

- Oversight
  - John Smerdon – Founding Director
  - Katherine Xu – Founding Director
  - CUMC Graduate Affairs
  - Women in Science @ Columbia
- Current Directors
  - Elise Flynn
  - Christian Garcia

Internship Framework

- Application and admission
  - Applications are accepted from rising juniors within the Minds Matter NYC program. After an interview session and application review, students are selected based on merit and interest in the STEM fields.

- Mentor selection and intern pairing
  - Mentors volunteer and are selected based on experience and a group interview. Students are paired with a mentor whose expertise lies within their field of prospective interest.

- Kick-off meeting and mentor/intern introductions

- Bio Boot Camp, an eight-part lecture series on cellular and molecular biology (Figure 5.2)

- Orientation day
  - Final exam to gauge students understanding of the lecture material
  - EH&S training
  - ID card issuance
  - Laboratory orientation

- Research project
  - Working with a mentor one-on-one, the interns preform a three-month project from February through April where they must form a hypothesis, perform applicable experiments, and interpret the results.

- Biotech Field Trip
  - Interns take part in a daylong trip to Regeneron Pharmaceuticals where they tour multiple facilities on the Regeneron campus as well as take part in open discussions with current Regeneron scientists.

- Oral presentations and final symposium
  - Interns perform a mid-project practice presentation to introduce their project, as well as a final presentation during the SMRI symposium

Discussion

The Science Matters Research internship has successfully mentored 25 high school juniors over the past 4 years. Now in its 5th year, SMRI and its nine current interns will mark half a decade of training for underprivileged New York youth. Our partnership with Minds Matter NYC provides detailed tracking information for the students through their completion of their bachelor's degrees. Though our first cohort has not yet graduated, we will soon start compiling data that will allow us to analyze our success empirically. Qualitatively, all of our interns thus far have enrolled in science or premedical programs at their undergraduate institutions. Many of them have received full scholarships, including to Washington University in St. Louis, to the Neuroscience program at Smith College, and to the Massachusetts Institute of Technology. SMRI looks forward to monitoring all of the interns' future STEM career success.

Chapter 6: Conclusions and Future Directions

The goal of presenting and discussing the data in this thesis was to uncover potential pathophysiology in ALS that may help to elucidate disease-relevant mechanisms. Amyotrophic lateral sclerosis was described well over a century ago and the first mouse model created more than two decades ago, and yet, we still have a poor understanding of the pathophysiology in the disease. It seems likely that motor neuron non-autonomous pathways exacerbate the disease, however, it is unclear whether these pathways are involved in the pathogenesis of ALS. To that point, there is a coincidence between ALS and frontal temporal dementia, and indeed, there may be some cell-autonomous mechanistic overlap (Ferrari et al., 2011). Alternately, it is possible for non-autonomous mechanisms, such as neuroinflammation, to be initiated by one disease but then aggravate the neurodegenerative processes in other neuronal subtypes. In fact, it seems that many of the cell non-autonomous pathways reported may not occur until post-symptomatic stages and therefore they may be downstream effects. These hypotheses are difficult to investigate though, as researchers have little access to pre-symptomatic patients. For the effects of neuroinflammatory pathways, however, it has been reported in patients and in the SOD1 mouse models that motor neuron dysfunction precedes the onset of these cell-nonautonomous effectors (Boillée et al., 2006; Oeckl et al., 2018). Regardless, intrinsic mechanisms specific to vulnerable motor neurons would have to either be selectively responsive to these extrinsic stressors, or they underlie the main driving element to ALS pathogenesis. Thus, I have focused on these intrinsic mechanisms for my investigations into ALS pathophysiology.

Homeostatic mechanisms

As humans and other species age, up to 40% of muscle mass is lost, resulting in a reduction of force output (Brooks and Faulkner, 1994) and a concurrent loss of motor neurons.

However, the loss of muscle mass is not equally divided amongst the different subtypes of muscle fibers. Interestingly, in rats it was found that type II fibers are lost first in aging, and at least in rats, is accompanied by a loss in the α-motor neuron subtype (Kadhiresan et al., 1996). Furthermore, compensatory sprouting of motor neurons that innervate type I fibers occurs attempting to maintain functionality of the motor system. This process of homeostatic compensation displays far from subtle similarities to the clinical presentations in ALS. That is not to say that the underlying mechanisms are the same, but certainly the homeostatic process of maintaining motor functionality in aging may parallel was is seen in the disease. It is also worth considering that some of the mechanisms involved in ageing are simply sped up in ALS.

Throughout this thesis, I have discussed homeostasis in motor neurons as an indicator of aberrant synaptic input. Yet, these mechanisms may have an even larger role in ALS pathogenesis. The data in this thesis would argue that increased synaptic excitation is pushing a hypoexcitable response in spinal motor neurons that manifests as a structural change in the axon initial segment. There are some clues from the ESC-derived motor neurons as to the other intrinsic changes in excitability that may coincide with the axon initial segment shortening/lengthening; however, it is unclear if the mature adult motor neurons *in vivo* will undergo the exact same responses. Similar to the titration plot of a buffer, homeostatic mechanisms likely have a range in which they work well, where rapid and devastating effects for the neurons reside outside that range, a concept predicted by modeling (Nijhout et al., 2014). Regardless, pushing homeostatic mechanisms to engage more robustly would likely place a greater metabolic demand on a cell, at the very least.

Furthermore, axon initial segment disruption may have direct consequences on motor neurons in ALS. In previous analyses however, where the axon initial segment length was increased by two-fold, there was a somewhat modest consequence on action potential threshold (Kuba et al., 2010). For the small shift in motor neuron axon initial segment length in ALS reported here, I would not expect to find a measurable shift in threshold. That is not to say

that subtle effects on threshold or action potential kinetics would not be important, but they would likely not be measurable. It is also possible that plasticity in the axon initial segment is coupled to shifts in ion channel subtype compositions that could elicit a more pronounced effect on action potential kinetics and threshold, but such mechanism have not yet been reported. Of additional interest is the shift in intra-burst frequency observed in the loose-patch recordings presented in Chapter 4. This result suggests motor neurons increase their firing frequency in response to increased excitation. Though they are otherwise intrinsically hypoexcitable, they elicit higher frequency bursts that may lead to a greater influx of calcium. If this response reflects physiological mechanism in *in vivo* motor neurons, it could exacerbate excitotoxicity. It also may point toward mechanisms used in subtype specification between fast and slow α-motor neurons. As described in the introduction, fast α-motor neurons are hypoexcitable but fire in high frequency bursts (Müller et al., 2014). It has also been shown that the boundary between these two subtypes is plastic, where after axotomy, they dedifferentiate and then redifferentiate after reinnervation (Foehring et al., 1986). It is possible that the redifferentiation process is driven by circuit feedback after muscle innervation where the motor neurons innervating type II fibers receive greater excitatory input that evokes a physiological response toward a fast α-motor neuron profile. Future studies that control input to ESC-derived motor neurons may uncover such a mechanism.

Another intriguing possibility surrounding the structural changes in the axon initial segment is the effect it might have on neuronal polarity. There is evidence in Alzheimer's disease that the axon initial segment is poorly maintaining polarity (Sun et al., 2014a). While in ALS, neurofilament accumulations at the hillock and axonal transport defects have both been reported (Sasaki and Maruyama, 1992; Sasaki et al., 2005). Of interest in these reports is that they observed an increased diameter of the hillock region. It could be argued that shortening of the axon initial segment might occur if the axon is of greater diameter to maintain a similar number of ion channels. However, it would likely be more complicated as a larger diameter

would also increase capacitance and therefore a larger number of sodium channels would need to be present to maintain a similar threshold. This is also complicated by the cranial data where the axon initial segment increases in length. Nevertheless, investigation of the diameter of the axon initial segment would be an interesting direction for future analysis. Also for future study, and one that may be well suited for ESC-derived neurons, would be to investigate whether long-term homeostatic plasticity in the axon initial segment disrupts neuronal polarity.

Lastly, more systematic analysis of homeostatic mechanisms within the local spinal circuitry is warranted. Amazingly, symptoms do not present in ALS until over 30% of the motor neurons have degenerated (Brownstone and Lancelin, 2018), evidence of significant reorganization in the spinal circuitry. Plasticity in spinal circuitry is well documented and clinically exploited in treatment programs such as neuromuscular reeducation (Judd et al., 2016), used by physical therapists to reprogram firing order of particular muscle groups. So, it seems feasible that the profound homeostatic circuit level changes are in play long before the first muscle weakness is detected in ALS patients. Interestingly, it has been reported in symptomatic SOD1 mice that remaining alpha and gamma motor neurons lose over a third of their synaptic inputs (Zang et al., 2005). This finding is supported by what is seen in the axon initial segment data presented in Chapter 2 showing that in P65 $SOD1^{G93A}$ mice, both the "normal" α-motor neurons as well as the γ-motor neurons have longer axon initial segments. However, all of these dynamic changes are occurring late in the disease, after neuromuscular junction retraction and as motor neuron degeneration is emerging. The presence of circuit level defects observed in these later stages, then, are not surprising. Nor would it be unanticipated that they may exacerbate the already existent pathophysiology. The remaining question here is whether the early circuit level changes predicted by the data presented in this thesis contribute to the pathogenesis of ALS. However, using these data to support the hypothesis of excitotoxicity is complicated by the opposite nature of the circuit level changes in cranial motor neurons.

The cranial quandary

Perhaps the most perplexing finding in these studies was the phenotypic heterogeneity that was observed in the cranial motor neurons. Considering all of the discussion of homeostatic changes in spinal motor neurons examined in the previous section, these results clearly complicate any support to an excitotoxicity hypothesis. Though structural changes in either direction still support an early shift in synaptic excitation. Furthermore, the disruptions to neuronal polarity addressed in the previous section may still apply here. Nevertheless, this unexpected result suggests that ALS-vulnerable cranial motor neurons undergo a decrease in net excitation.

Considering the more widespread heterogeneity in ALS phenotypes that I observed in the cranial motor neurons, it could be argued that cranial and spinal motor neurons exhibit distinct pathophysiology from one another. Certainly, there are distinct functional differences between cranial and spinal motor neurons (Chandrasekhar, 2004) that may underlie this phenomenon, but to my knowledge, it is not a hypothesis that has been previously proposed. It could also be argued that some of these phenotypes do not underlie the pathophysiology in ALS, at least for p62 aggregation and excitotoxicity. Since vacuole formation still occurs in the neuropil, it was not included in this list. Certainly, if the axon initial segment changes are accepted to be a proxy for excitation in motor neurons, then it has to be assumed that ALS-vulnerable cranial motor neurons have lower net excitation, and therefore unlikely to suffer from excitotoxic effects. Another caveat here, however, is that the ESC-derived motor neurons used to verify a compensatory response of axon initial segment plasticity, are models of spinal motor neurons. It is a possibility that the axon initial segment in cranial motor neurons does not respond to excitation in the same way, though it would be extremely unlikely as such behavior is unprecedented in all other excitatory neurons investigated thus far.

It should also be noted that the hypoglossal motor neurons exhibit a shorter neonatal axon initial segment, before becoming longer as a young adult. This is interesting bearing in mind the increased synaptic input reported in neonatal hypoglossal motor neurons, as well as other electrophysiological differences seen that would lead to hyperactivity in this population (van Zundert et al., 2012). Hypoglossal motor neurons may be unique here due to the importance of early circuit formation required for suckling (Fukushima et al., 2007). Perhaps this early shift in excitation is evidence of abnormalities in local circuitry that occur during development, or that like corticospinal neurons, corticobulbar neurons are also hyperactive at that age. The shift in axon initial segment from short to long relative to the Nt littermates may reflect the dynamic development of dendritic morphology in the first two to three postnatal weeks (Kanjhan et al., 2016). Nevertheless, this shift may reflect interesting developmental mechanisms unique hypoglossal motor neurons.

Consistent with other reports, oculomotor neurons were spared from most of the phenotypes investigated in this report. Interestingly, there is a shortening of the axon initial segment in the oculomotor neurons at later disease stages. As discussed in the introduction, oculomotor neurons are likely quite resistant to excitotoxicity, but this is still a surprising result that suggests these neurons have increased net excitation. A late change in axon initial segment length in γ-motor neurons is understandable considering its intimate link with α-motor neuron circuitry. However, oculomotor neurons seem relatively isolated from the other cranial motor nuclei. Perhaps axon initial segment shortening in these motor neurons is a reflection of hyperactive premotor circuitry, or an effect of the astrogliosis and microgliosis in the glia surrounding their nucleus (An et al., 2014). It would be worth further investigation to verify an increase in synaptic input and to understand the driving mechanism.

Excitability and activity in ALS

The most basic question asked by this thesis was if adult motor neurons in ALS suffer from hyperactivity that could lead to excitotoxicity. For spinal motor neurons, I would argue that this might be the case. Very early in the disease, just after circuitry maturation, I have observed a shortening in the axon initial segment, indicative of higher levels of net excitation. Behavioral assays would show major alterations in motor neuron firing, therefore, it would seem that the spinal motor neurons are able to compensate for the change in input. However, the act of compensation itself may be putting undue stress on the motor neurons. Additionally, increased calcium influx from subthreshold depolarization (Magee et al., 1995) may also be adding to an excitotoxic effect, though it would seem unlikely to produce the calcium influx required to elicit toxicity. Regardless, these data would support that hyperexcitation exists in ALS-vulnerable spinal motor neurons, though it cannot be concluded that this is contributing to excitotoxicity. Furthermore, as discussed in the previous section, it seems the opposite, hypoexcitation, exists in ALS-vulnerable cranial motor neurons. It is important to note that axon initial segment plasticity occurs long before motor neuron death in these mice (Turner and Talbot, 2008), and is therefore reflecting true changes throughout the entire population of motor neurons.

I discussed the controversy over excitability in depth in the introduction. My data has addressed this question indirectly in adult motor neurons at different ages throughout the ALS disease course. Interestingly in neonates, I do not find a difference in axon initial segment length in ALS, though they are longer than adult suggestive of lower activity and excitation. This might agree with recent reports that have claimed neonatal α-motor neurons are not hyperexcitable in and that early intrinsic excitability does not contribute to ALS pathophysiology (Leroy and Zytnicki, 2015). Though I would agree with their overall conclusions, some of the assumptions made are somewhat problematic considering contradictions throughout the literature. The first assumption, is that slow and fast α-motor neurons undergo the same pathogenic pathway that leads to degeneration. Heterogeneity shown here in the phenotypic

presentation of ALS in cranial motor neurons might question whether that assumption is appropriate, and perhaps further analysis should establish this to be true. Second, they claim most of the previously reported electrophysiological data must be inaccurate, as these reports do not take into account differential sensitivities of motor neuron subtypes. This claim implies that intrinsic hyperexcitability reported in these studies may be skewed by the influence of data from multiple motor neuron subtypes. Yet, for subtype specific intrinsic excitability to have a major influence across most of these studies, then there would have to be a significant number of slow α-motor neurons represented in the recordings from the random picking of neurons to patch. In their study, there was good correlation between their electrophysiological categorization of slow and fast α-motor neurons using the fast α-motor neuron specific expression of chondrolectin (Leroy et al., 2014). However, reports have shown that there are limited numbers of type I muscle fibers in small mammals such as mice (Peters et al., 1999), indicating that the total number of slow α-motor neurons may be quite small in the spinal population. For example, the majority of the muscles innervated by motor neurons that originate in Lumbar segments 4-5 (L4-5) are reported to be almost entirely type II fibers (Burkholder et al., 1994; Augusto et al., 2004; Bácskai et al., 2014). A commonly used source muscle for slow α-motor neuron innervation is the soleus muscle (Kaplan et al., 2014). This crural muscle innervated by L4-5 motor neurons is well known for its composition of ~50% type I fibers (Peters et al., 1999), the highest proportion of all L4-5 muscles, however, one report suggests that ~20 slow α-motor neurons innervating the soleus muscle (Fladby and Jansen, 1987). If this were true, then it would be unlikely that the studies reporting changes in intrinsic excitability are simply being influenced by a preponderance of slow α-motor neuron contamination in their data. However, given the paradoxical literature of high numbers of slow α-motor neurons yet low numbers of Type I fibers, it is possible that slow α-motor neuron numbers may not directly correlate with the fiber composition and indeed be skewing the electrophysiological data. This is also important when interpreting the axon initial segment data. It would not be appropriate to

compare structural changes in the axon initial segment from one subtype to another in order to make conclusions regarding the intrinsic excitability. For instance, γ-motor neurons are considerably smaller than α-motor neurons and have known differences in their intrinsic excitability, yet the axon initial segment length in these two subtypes are the same length. It would seem that the utility of this sub-cellular structure is tuned to the demands of the particular neuronal subtype. Given the uncertainty in the fast and slow α-motor neuron composition in these mice, it could mark a caveat in the axon initial segment length comparisons between non-transgenic and ALS-model mice. This would hold especially true at later stages of the disease if fast α-motor neurons are first to degenerate, leaving an enrichment of the slow α-motor neuron subtype. This could in fact be an interesting possibility considering that the motor neurons at postnatal day 65 that were deemed "normal" had longer axon initial segments as compared to the non-transgenic animals (Figure 2.6). Future studies should probe the contradictory findings between fiber types and electrophysiological analyses to uncover the basis of these inconsistencies.

It seems possible, however, that the discrepancies found in many of the electrophysiological analyses are due to the variety of models being used and differences in the experimental parameters employed. Dissociation into primary cultures and spinal sectioning are known to have major detrimental effects on motor neurons (Bucchia et al., 2018) and therefore may be skewing results. Additionally, it is difficult to reconcile how changes reported in immature motor neurons will manifest as the neurons mature. I have also posed the question of how intrinsic excitability is interpreted. Many studies view intrinsic excitability as a driving force of activity. However, as pointed out by the many studies looking into axon initial segment plasticity including those presented in this thesis, it seems that intrinsic excitability dynamics are compensatory in response to changes in input. So it may be appropriate to consider that intrinsic excitability may reflect homeostatic shifts in response to excitation, rather than underlie the driving force, thus inversely proportional to their amplitude of excitation.

Though this thesis did not serve as the final answer to an ongoing debate over excitability and activity in ALS patients, the experiments presented here do support an early change in motor circuitry and intrinsic excitability. It would be misrepresentative to conclude that the early circuit level defects contribute to the pathophysiology that leads to motor neuron degeneration, though the association between these circuitry defects and neuronal stress in the spinal motor neurons posits this as an intriguing possibility. However, the divergent changes in net excitation between spinal and cranial motor neurons extrapolated from the analyses presented in this thesis are unharmonious with the simple view of excitotoxicity postulated decades ago.

References

Alaynick WA, Jessell TM, Pfaff SL (2011) SnapShot: Spinal Cord Development. Cell 146:178–178.e1.

Albuquerque C, Joseph DJ, Choudhury P, MacDermott AB (2009) Dissection, plating, and maintenance of cortical astrocyte cultures. Cold Spring Harb Protoc 2009:pdb.prot5273.

Amendola J, Durand J (2008) Morphological differences between wild-type and transgenic superoxide dismutase 1 lumbar motoneurons in postnatal mice. The Journal of Comparative Neurology 511:329–341.

Amendola J, Gueritaud JP, Lamotte d'Incamps B, Bories C, Liabeuf S, Allene C, Pambo-Pambo A, Durand J (2007) Postnatal electrical and morphological abnormalities in lumbar motoneurons from transgenic mouse models of amyotrophic lateral sclerosis. Arch Ital Biol 145:311–323.

An T, Shi P, Duan W, Zhang S, Yuan P, Li Z, Wu D, Xu Z, Li C, Guo Y (2014) Oxidative stress and autophagic alteration in brainstem of SOD1-G93A mouse model of ALS. Mol Neurobiol 49:1435–1448.

Arber S (2012) Motor circuits in action: specification, connectivity, and function. Neuron 74:975–989.

Arimura N, Kaibuchi K (2007) Neuronal polarity: from extracellular signals to intracellular mechanisms. Nat Rev Neurosci 8:194–205.

Arlotta P, Molyneaux BJ, Chen J, Inoue J, Kominami R, Macklis JD (2005) Neuronal subtype-specific genes that control corticospinal motor neuron development in vivo. Neuron 45:207–221.

Augusto V, Padovani CR, Campos GER (2004) Skeletal muscle fiber types in C57BL6J mice. Braz J morphol Sci 21:89–94.

Baalman KL, Cotton RJ, Rasband SN, Rasband MN (2013) Blast Wave Exposure Impairs Memory and Decreases Axon Initial Segment Length. Journal of Neurotrauma 30:741–751.

Banci L, Bertini I, Boca M, Girotto S, Martinelli M, Valentine JS, Vieru M (2008) SOD1 and Amyotrophic Lateral Sclerosis: Mutations and Oligomerization Koutsopoulos S, ed. PLoS ONE 3:e1677.

Bácskai T, Rusznák Z, Paxinos G, Watson C (2014) Musculotopic organization of the motor neurons supplying the mouse hindlimb muscles: a quantitative study using Fluoro-Gold retrograde tracing. Brain Struct Funct 219:303–321.

Bean BP (2007) The action potential in mammalian central neurons. Nat Rev Neurosci 8:451–465.

Beaumont V, Zucker RS (2000) Enhancement of synaptic transmission by cyclic AMP

modulation of presynaptic Ih channels. Nat Neurosci 3:133–141.

Beers DR, Ho BK, Siklós L, Alexianu ME, Mosier DR, Mohamed AH, Otsuka Y, Kozovska ME, McAlhany RE, Smith RG, Appel SH (2001) Parvalbumin overexpression alters immune-mediated increases in intracellular calcium, and delays disease onset in a transgenic model of familial amyotrophic lateral sclerosis. J Neurochem 79:499–509.

Bellingham MC (2011) A review of the neural mechanisms of action and clinical efficiency of riluzole in treating amyotrophic lateral sclerosis: what have we learned in the last decade? CNS Neurosci Ther 17:4–31.

Bensimon G, Lacomblez L, Meininger V (1994) A controlled trial of riluzole in amyotrophic lateral sclerosis. ALS/Riluzole Study Group. N Engl J Med 330:585–591.

Bergemalm D, Jonsson PA, Graffmo KS, Andersen PM, Brännström T, Rehnmark A, Marklund SL (2006) Overloading of stable and exclusion of unstable human superoxide dismutase-1 variants in mitochondria of murine amyotrophic lateral sclerosis models. J Neurosci 26:4147–4154.

Blizzard CA, Southam KA, Dawkins E, Lewis KE, King AE, Clark JA, Dickson TC (2015) Identifying the primary site of pathogenesis in amyotrophic lateral sclerosis - vulnerability of lower motor neurons to proximal excitotoxicity. Dis Model Mech 8:215–224.

Boillée S, Yamanaka K, Lobsiger CS, Copeland NG, Jenkins NA, Kassiotis G, Kollias G, Cleveland DW (2006) Onset and progression in inherited ALS determined by motor neurons and microglia. Science 312:1389–1392.

Bories C, Amendola J, Lamotte d'Incamps B, Durand J (2007) Early electrophysiological abnormalities in lumbar motoneurons in a transgenic mouse model of amyotrophic lateral sclerosis. Eur J Neurosci 25:451–459.

Bosco DA, Morfini G, Karabacak NM, Song Y, Gros-Louis F, Pasinelli P, Goolsby H, Fontaine BA, Lemay N, McKenna-Yasek D, Frosch MP, Agar JN, Julien J-P, Brady ST, Brown RH (2010) Wild-type and mutant SOD1 share an aberrant conformation and a common pathogenic pathway in ALS. Nat Neurosci 13:1396–1403.

Boulting GL, Kiskinis E, Croft GF, Amoroso MW, Oakley DH, Wainger BJ, Williams DJ, Kahler DJ, Yamaki M, Davidow L, Rodolfa CT, Dimos JT, Mikkilineni S, MacDermott AB, Woolf CJ, Henderson CE, Wichterle H, Eggan K (2011) A functionally characterized test set of human induced pluripotent stem cells. Nat Biotechnol 29:279–286.

Brachet A, Leterrier C, Irondelle M, Fache M-P, Racine V, Sibarita J-B, Choquet D, Dargent B (2010) Ankyrin G restricts ion channel diffusion at the axonal initial segment before the establishment of the diffusion barrier. J Cell Biol 191:383–395.

Brockington A, Ning K, Heath PR, Wood E, Kirby J, Fusi N, Lawrence N, Wharton SB, Ince PG, Shaw PJ (2013) Unravelling the enigma of selective vulnerability in neurodegeneration: motor neurons resistant to degeneration in ALS show distinct gene expression characteristics and decreased susceptibility to excitotoxicity. Acta Neuropathologica 125:95–109.

Brooks SV (2003) Current Topics for Teaching Sekeletal Muscle Physiology. Advances in Physiology Education 27:171–182.

Brooks SV, Faulkner JA (1994) Skeletal muscle weakness in old age: underlying mechanisms. Med Sci Sports Exerc 26:432–439.

Brownstone RM, Lancelin C (2018) Escape from homeostasis: spinal microcircuits and progression of amyotrophic lateral sclerosis. J Neurophysiol 119:1782–1794.

Bruijn LI, Houseweart MK, Kato S, Anderson KL, Anderson SD, Ohama E, Reaume AG, Scott RW, Cleveland DW (1998) Aggregation and motor neuron toxicity of an ALS-linked SOD1 mutant independent from wild-type SOD1. Science 281:1851–1854.

Bucchia M, Merwin SJ, Re DB, Kariya S (2018) Limitations and Challenges in Modeling Diseases Involving Spinal Motor Neuron Degeneration in Vitro. Front Cell Neurosci 12:61.

Burkholder TJ, Fingado B, Baron S, Lieber RL (1994) Relationship Between Muscle Fiber Types and Sizes and Muscle Architectural Properties in the Mouse Hindlimb. Journal of Morphology 221:177–190.

Carp JS, Wolpaw JR (2010) Motor Neurons and Spinal Control of Movement. Chichester, UK: John Wiley & Sons, Ltd.

Carriedo SG, Yin HZ, Weiss JH (1996) Motor neurons are selectively vulnerable to AMPA/kainate receptor-mediated injury in vitro. Journal of Neuroscience 16:4069–4079.

Chand AN, Galliano E, Chesters RA, Grubb MS (2015) A distinct subtype of dopaminergic interneuron displays inverted structural plasticity at the axon initial segment. J Neurosci 35:1573–1590.

Chandrasekhar A (2004) Turning heads: development of vertebrate branchiomotor neurons. Dev Dyn 229:143–161.

Chang Q, Martin LJ (2009) Glycinergic innervation of motoneurons is deficient in amyotrophic lateral sclerosis mice: a quantitative confocal analysis. Am J Pathol 174:574–585.

Chang Q, Martin LJ (2011) Glycine receptor channels in spinal motoneurons are abnormal in a transgenic mouse model of amyotrophic lateral sclerosis. J Neurosci 31:2815–2827.

Chang Q, Martin LJ (2014) Motoneuron subtypes show specificity in glycine receptor channel abnormalities in a transgenic mouse model of amyotrophic lateral sclerosis. Channels 5:299–303.

Chiu AY, Zhai P, Dal Canto MC, Peters TM, Kwon YW, Prattis SM, Gurney ME (1995) Age-dependent penetrance of disease in a transgenic mouse model of familial amyotrophic lateral sclerosis. Mol Cell Neurosci 6:349–362.

Clarke KA, Still J (2001) Development and consistency of gait in the mouse. Physiol Behav 73:159–164.

Colbert CM, Johnston D (1996) Axonal action-potential initiation and Na+ channel densities in

the soma and axon initial segment of subicular pyramidal neurons. Journal of Neuroscience 16:6676–6686.

Colbert CM, Pan E (2002) Ion channel properties underlying axonal action potential initiation in pyramidal neurons. Nat Neurosci 5:533–538.

Comley L, Allodi I, Nichterwitz S, Nizzardo M, Simone C, Corti S, Hedlund E (2015) Motor neurons with differential vulnerability to degeneration show distinct protein signatures in health and ALS. Neuroscience 291:216–229.

COOMBS JS, CURTIS DR, ECCLES JC (1957) The interpretation of spike potentials of motoneurones. The Journal of Physiology 139:198–231.

Dal Canto MC, Gurney ME (1994) Development of central nervous system pathology in a murine transgenic model of human amyotrophic lateral sclerosis. Am J Pathol 145:1271–1279.

De Vos KJ, Hafezparast M (2017) Neurobiology of axonal transport defects in motor neuron diseases: Opportunities for translational research? Neurobiology of Disease 105:283–299.

Deng H-X, Shi Y, Furukawa Y, Zhai H, Fu R, Liu E, Gorrie GH, Khan MS, Hung W-Y, Bigio EH, Lukas T, Dal Canto MC, O'Halloran TV, Siddique T (2006) Conversion to the amyotrophic lateral sclerosis phenotype is associated with intermolecular linked insoluble aggregates of SOD1 in mitochondria. Proc Natl Acad Sci USA 103:7142–7147.

Di Giorgio FP, Carrasco MA, Siao MC, Maniatis T, Eggan K (2007) Non-cell autonomous effect of glia on motor neurons in an embryonic stem cell-based ALS model. Nat Neurosci 10:608–614.

Dodge FA, Cooley JW (1973) Action Potential of the Motorneuron. IBM J Res Develop 17:219–229.

Duflocq A, Chareyre F, Giovannini M, Couraud F, Davenne M (2011) Characterization of the axon initial segment (AIS) of motor neurons and identification of a para-AIS and a juxtapara-AIS, organized by protein 4.1B. BMC Biol 9:66.

Elbasiouny SM, Quinlan KA, Eissa TL, Heckman CJ (2012) Electrophysiological Abnormalities in SOD1 Transgenic Models in Amyotrophic Lateral Sclerosis: The Commonalities and Differences. Amyotroph Lateral Scler 6:157–174. DOI: 10.5772/30711

Ellaway PH, Taylor A, Durbaba R (2015) Muscle spindle and fusimotor activity in locomotion. J Anat 227:157–166.

Esteban J, Rosen DR, Bowling AC, Sapp P, McKenna-Yasek D, O'Regan JP, Beal MF, Horvitz HR, Brown RH (1994) Identification of two novel mutations and a new polymorphism in the gene for Cu/Zn superoxide dismutase in patients with amyotrophic lateral sclerosis. Hum Mol Genet 3:997–998.

Evans MD, Sammons RP, Lebron S, Dumitrescu AS, Watkins TBK, Uebele VN, Renger JJ, Grubb MS (2013) Calcineurin signaling mediates activity-dependent relocation of the axon initial segment. Journal of Neuroscience 33:6950–6963.

Ferrari R, Kapogiannis D, Huey ED, Momeni P (2011) FTD and ALS: a tale of two diseases. Curr Alzheimer Res 8:273–294.

Ferri A, Cozzolino M, Crosio C, Nencini M, Casciati A, Gralla EB, Rotilio G, Valentine JS, Carrì MT (2006) Familial ALS-superoxide dismutases associate with mitochondria and shift their redox potentials. Proc Natl Acad Sci USA 103:13860–13865.

Ferrucci M, Spalloni A, Bartalucci A, Cantafora E, Fulceri F, Nutini M, Longone P, Paparelli A, Fornai F (2010) Neurobiology of Disease. Neurobiology of Disease 37:370–383.

Filipchuk AA, Durand J (2012) Postnatal dendritic development in lumbar motoneurons in mutant superoxide dismutase 1 mouse model of amyotrophic lateral sclerosis. Neuroscience 209:144–154.

Fischer LR, Culver DG, Tennant P, Davis AA, Wang M, Castellano-Sanchez A, Khan J, Polak MA, Glass JD (2004) Amyotrophic lateral sclerosis is a distal axonopathy: evidence in mice and man. Exp Neurol 185:232–240.

Fischer LR, Li Y, Asress SA, Jones DP, Glass JD (2012) Absence of SOD1 leads to oxidative stress in peripheral nerve and causes a progressive distal motor axonopathy. Exp Neurol 233:163–171.

Fladby T, Jansen JK (1987) Postnatal loss of synaptic terminals in the partially denervated mouse soleus muscle. Acta Physiol Scand 129:239–246.

Fleshman JW, Munson JB, Sypert GW (1981) Rheobase, input resistance, and motor-unit type in medial gastrocnemius motoneurons in the cat. Journal of ….

Flood DG, Reaume AG, Gruner JA, Hoffman EK, Hirsch JD, Lin YG, Dorfman KS, Scott RW (1999) Hindlimb motor neurons require Cu/Zn superoxide dismutase for maintenance of neuromuscular junctions. Am J Pathol 155:663–672 Available at: https://www.sciencedirect.com/science/article/pii/S0002944010651620/pdfft?md5=165c548918fbff2fd511c9b23c1e63cc&pid=1-s2.0-S0002944010651620-main.pdf [Accessed December 18, 2018].

Foehring RC, Sypert GW, Munson JB (1986) Properties of self-reinnervated motor units of medial gastrocnemius of cat. II. Axotomized motoneurons and time course of recovery. J Neurophysiol 55:947–965.

Foran E, Bogush A, Goffredo M, Roncaglia P, Gustincich S, Pasinelli P, Trotti D (2011) Motor neuron impairment mediated by a sumoylated fragment of the glial glutamate transporter EAAT2. Glia 59:1719–1731.

Frakes AE, Ferraiuolo L, Haidet-Phillips AM, Schmelzer L, Braun L, Miranda CJ, Ladner KJ, Bevan AK, Foust KD, Godbout JP, Popovich PG, Guttridge DC, Kaspar BK (2014) Microglia induce motor neuron death via the classical NF-κB pathway in amyotrophic lateral sclerosis. Neuron 81:1009–1023.

Frey D, Schneider C, Xu L, Borg J, Spooren W, Caroni P (2000) Early and selective loss of neuromuscular synapse subtypes with low sprouting competence in motoneuron diseases. J Neurosci 20:2534–2542.

Fukushima N, Yokouchi K, Kawagishi K, Kakegawa A, Ezawa N, Moriizumi T (2007) Neural plasticity of neonatal hypoglossal nerve for effective suckling. J Neurosci Res 85:2518–2526.

FUORTES MG, FRANK K, BECKER MC (1957) Steps in the production of motoneuron spikes. J Gen Physiol 40:735–752.

Gandevia SC, Macefield G, Burke D, McKenzie DK (1990) Voluntary activation of human motor axons in the absence of muscle afferent feedback. The control of the deafferented hand. Brain 113 (Pt 5):1563–1581.

Gianino S, Stein SA, Li H, Lu X, Biesiada E, Ulas J, Xu XM (1999) Postnatal growth of corticospinal axons in the spinal cord of developing mice. Brain Res Dev Brain Res 112:189–204.

Grubb MS, Burrone J (2010) Activity-dependent relocation of the axon initial segment fine-tunes neuronal excitability. Nature 465:1070–1074.

Gu JG, Bardoni R, Magherini PC, MacDermott AB (1998) Effects of the P2-purinoceptor antagonists suramin and pyridoxal-phosphate-6-azophenyl-2“,4-”disulfonic acid on glutamatergic synaptic transmission in rat dorsal horn neurons of the spinal cord. Neurosci Lett 253:167–170.

Guareschi S, Cova E, Cereda C, Ceroni M, Donetti E, Bosco DA, Trotti D, Pasinelli P (2012) An over-oxidized form of superoxide dismutase found in sporadic amyotrophic lateral sclerosis with bulbar onset shares a toxic mechanism with mutant SOD1. Proceedings of the National Academy of Sciences 109:5074–5079.

Gurney ME, Fleck TJ, Himes CS, Hall ED (1998) Riluzole preserves motor function in a transgenic model of familial amyotrophic lateral sclerosis. Neurology 50:62–66.

Gurney ME, Pu H, Chiu AY, Dal Canto MC, Polchow CY, Alexander DD, Caliendo J, Hentati A, Kwon YW, Deng HX (1994) Motor neuron degeneration in mice that express a human Cu,Zn superoxide dismutase mutation. Science 264:1772–1775.

Gustafsson B, Pinter MJ (1984) An investigation of threshold properties among cat spinal alpha-motoneurones. The Journal of Physiology 357:453–483.

Haenggeli C, Kato AC (2002) Differential vulnerability of cranial motoneurons in mouse models with motor neuron degeneration. Neurosci Lett 335:39–43.

Haidet-Phillips AM, Hester ME, Miranda CJ, Meyer K, Braun L, Frakes A, Song S, Likhite S, Murtha MJ, Foust KD, Rao M, Eagle A, Kammesheidt A, Christensen A, Mendell JR, Burghes AHM, Kaspar BK (2011) Astrocytes from familial and sporadic ALS patients are toxic to motor neurons. Nat Biotechnol 29:824–828.

Hamada MS, Kole MHP (2015) Myelin loss and axonal ion channel adaptations associated with gray matter neuronal hyperexcitability. J Neurosci 35:7272–7286.

Harty RC, Kim TH, Thomas EA, Cardamone L, Jones NC, Petrou S, Wimmer VC (2013) Axon initial segment structural plasticity in animal models of genetic and acquired epilepsy.

Epilepsy Res 105:272–279.

Heckman CJ, Johnson M, Mottram C, Schuster J (2008) Persistent Inward Currents in Spinal Motoneurons and Their Influence on Human Motoneuron Firing Patterns. Neuroscientist 14:264–275.

Hedstrom KL, Ogawa Y, Rasband MN (2008) AnkyrinG is required for maintenance of the axon initial segment and neuronal polarity. J Cell Biol 183:635–640.

Hideyama T, Yamashita T, Suzuki T, Tsuji S, Higuchi M, Seeburg PH, Takahashi R, Misawa H, Kwak S (2010) Induced Loss of ADAR2 Engenders Slow Death of Motor Neurons from Q/R Site-Unedited GluR2. Journal of Neuroscience 30:11917–11925.

Higgins CMJ, Jung C, Xu Z (2003) ALS-associated mutant SOD1G93A causes mitochondrial vacuolation by expansion of the intermembrane space and by involvement of SOD1 aggregation and peroxisomes. BMC Neurosci 4:16.

Hoang PT, Chalif JI, Bikoff JB, Jessell TM, Mentis GZ, Wichterle H (2018) Subtype Diversification and Synaptic Specificity of Stem Cell-Derived Spinal Interneurons. Neuron 100:135–149.e137.

Hodgkin AL (1948) The local electric changes associated with repetitive action in a non-medullated axon. The Journal of Physiology 107:165–181.

Honoré T, Davies SN, Drejer J, Fletcher EJ, Jacobsen P, Lodge D, Nielsen FE (1988) Quinoxalinediones: potent competitive non-NMDA glutamate receptor antagonists. Science 241:701–703.

Hossaini M, Cardona Cano S, van Dis V, Haasdijk ED, Hoogenraad CC, Holstege JC, Jaarsma D (2011) Spinal inhibitory interneuron pathology follows motor neuron degeneration independent of glial mutant superoxide dismutase 1 expression in SOD1-ALS mice. J Neuropathol Exp Neurol 70:662–677.

Hu W, Tian C, Li T, Yang M, Hou H, Shu Y (2009) Distinct contributions of Na (v)1.6 and Na (v)1.2 in action potential initiation and backpropagation. Nat Neurosci 12:996–1002.

Huang CY-M, Rasband MN (2018) Axon initial segments: structure, function, and disease. Ann N Y Acad Sci 1420:46–61.

Huang Y-M, Rasband MN (2016) Organization of the axon initial segment: Actin like a fence. J Cell Biol 215:9–11.

Hugon J, Vallat JM, Spencer PS, Leboutet MJ, Barthe D (1989) Kainic acid induces early and delayed degenerative neuronal changes in rat spinal cord. Neurosci Lett 104:258–262.

Hulliger M (2005) The mammalian muscle spindle and its central control. In: Reviews of Physiology, pp 1–110 Reviews of Physiology, Biochemistry and Pharmacology. Berlin, Heidelberg: Springer Berlin Heidelberg.

Igoudjil A, Magrane J, Fischer LR, Kim HJ, Hervias I, Dumont M, Cortez C, Glass JD, Starkov AA, Manfredi G (2011) In Vivo Pathogenic Role of Mutant SOD1 Localized in the

Mitochondrial Intermembrane Space. J Neurosci 31:15826–15837.

Ikonomidou C, Qin YQ, Labruyere J, Olney JW (1996) Motor neuron degeneration induced by excitotoxin agonists has features in common with those seen in the SOD-1 transgenic mouse model of amyotrophic lateral sclerosis. J Neuropathol Exp Neurol 55:211–224.

Isa T, Iino M, Itazawa S, Ozawa S (1995) Spermine mediates inward rectification of Ca (2+)-permeable AMPA receptor channels. Neuroreport 6:2045–2048.

Jacko M, Weyn-Vanhentenryck SM, Smerdon JW, Yan R, Feng H, Williams DJ, Pai J, Xu K, Wichterle H, Zhang C (2018) Rbfox Splicing Factors Promote Neuronal Maturation and Axon Initial Segment Assembly. Neuron 97:853–868.e856.

Jaiswal MK, Zech W-D, Goos M, Leutbecher C, Ferri A, Zippelius A, Carrì MT, Nau R, Keller BU (2009) Impairment of mitochondrial calcium handling in a mtSOD1 cell culture model of motoneuron disease. BMC Neurosci 10:64.

Jiang M, Schuster JE, Fu R, Siddique T, Heckman CJ (2009) Progressive changes in synaptic inputs to motoneurons in adult sacral spinal cord of a mouse model of amyotrophic lateral sclerosis. J Neurosci 29:15031–15038.

Johnson MA, Weick JP, Pearce RA, Zhang S-C (2007) Functional neural development from human embryonic stem cells: accelerated synaptic activity via astrocyte coculture. J Neurosci 27:3069–3077.

Jones SL, Svitkina TM (2016) Axon Initial Segment Cytoskeleton: Architecture, Development, and Role in Neuron Polarity. Neural Plast 2016:6808293.

Joseph DJ, Choudhury P, MacDermott AB (2010) An in vitro assay system for studying synapse formation between nociceptive dorsal root ganglion and dorsal horn neurons. J Neurosci Methods 189:197–204.

Judd DL, Winters JD, Stevens-Lapsley JE, Christiansen CL (2016) Effects of neuromuscular reeducation on hip mechanics and functional performance in patients after total hip arthroplasty: A case series. Clin Biomech (Bristol, Avon) 32:49–55.

Kadhiresan VA, Hassett CA, Faulkner JA (1996) Properties of single motor units in medial gastrocnemius muscles of adult and old rats. The Journal of Physiology 493.2:543–552.

Kanjhan R, Fogarty MJ, Noakes PG, Bellingham MC (2016) Developmental changes in the morphology of mouse hypoglossal motor neurons. Brain Struct Funct 221:3755–3786.

Kanning KC, Kaplan A, Henderson CE (2010) Motor neuron diversity in development and disease. Annu Rev Neurosci 33:409–440.

Kapfhamer D, Miller DE, Lambert S, Bennett V, Glover TW, Burmeister M (1995) Chromosomal localization of the ankyrinG gene (ANK3/Ank3) to human 10q21 and mouse 10. Genomics 27:189–191.

Kaphzan H, Buffington SA, Jung JI, Rasband MN, Klann E (2011) Alterations in intrinsic membrane properties and the axon initial segment in a mouse model of Angelman

syndrome. J Neurosci 31:17637–17648.

Kaphzan H, Buffington SA, Ramaraj AB, Lingrel JB, Rasband MN, Santini E, Klann E (2013) Genetic reduction of the α1 subunit of Na/K-ATPase corrects multiple hippocampal phenotypes in Angelman syndrome. Cell Rep 4:405–412.

Kaplan A, Spiller KJ, Towne C, Kanning KC, Choe GT, Geber A, Akay T, Aebischer P, Henderson CE (2014) Neuronal matrix metalloproteinase-9 is a determinant of selective neurodegeneration. Neuron 81:333–348.

Kawahara Y, Ito K, Sun H, Aizawa H, Kanazawa I, Kwak S (2004) Glutamate receptors: RNA editing and death of motor neurons. Nature 427:801.

Kawahara Y, Ito K, Sun H, Kanazawa I, Kwak S (2003) Low editing efficiency of GluR2 mRNA is associated with a low relative abundance of ADAR2 mRNA in white matter of normal human brain. Eur J Neurosci 18:23–33.

Kiernan MC, Vucic S, Cheah BC, Turner MR, Eisen A, Hardiman O, Burrell JR, Zoing MC (2011) Amyotrophic lateral sclerosis. The Lancet 377:942–955.

Kihira T, Yoshida S, Yoshimasu F, Wakayama I, Yase Y (1997) Involvement of Onuf's nucleus in amyotrophic lateral sclerosis. J Neurol Sci 147:81–88.

Kim J, Hughes EG, Shetty AS, Arlotta P, Goff LA, Bergles DE, Brown SP (2017) Changes in the Excitability of Neocortical Neurons in a Mouse Model of Amyotrophic Lateral Sclerosis Are Not Specific to Corticospinal Neurons and Are Modulated by Advancing Disease. J Neurosci 37:9037–9053.

King AE, Dickson TC, Blizzard CA, Foster SS, Chung RS, West AK, Chuah MI, Vickers JC (2007) Excitotoxicity mediated by non-NMDA receptors causes distal axonopathy in long-term cultured spinal motor neurons. Eur J Neurosci 26:2151–2159.

Koike M, Iino M, Ozawa S (1997) Blocking effect of 1-naphthyl acetyl spermine on Ca (2+)-permeable AMPA receptors in cultured rat hippocampal neurons. Neurosci Res 29:27–36.

Kole MHP, Ilschner SU, Kampa BM, Williams SR, Ruben PC, Stuart GJ (2008) Action potential generation requires a high sodium channel density in the axon initial segment. Nat Neurosci 11:178–186.

Kole MHP, Letzkus JJ, Stuart GJ (2007) Axon initial segment Kv1 channels control axonal action potential waveform and synaptic efficacy. Neuron 55:633–647.

Kole MHP, Stuart GJ (2008) Is action potential threshold lowest in the axon? Nat Neurosci 11:1253–1255.

Kole MHP, Stuart GJ (2012) Signal processing in the axon initial segment. Neuron 73:235–247.

Komatsu M, Kageyama S, Ichimura Y (2012) p62/SQSTM1/A170: Physiology and pathology - ScienceDirect. Pharmacological research.

Kong J, Xu Z (1998) Massive mitochondrial degeneration in motor neurons triggers the onset of

amyotrophic lateral sclerosis in mice expressing a mutant SOD1. Journal of Neuroscience 18:3241–3250.

Kuba H, Adachi R, Ohmori H (2014) Activity-dependent and activity-independent development of the axon initial segment. J Neurosci 34:3443–3453.

Kuba H, Oichi Y, Ohmori H (2010) Presynaptic activity regulates Na (+) channel distribution at the axon initial segment. Nature 465:1075–1078.

Kuo JJ, Schonewille M, Siddique T, Schults ANA, Fu R, Bär PR, Anelli R, Heckman CJ, Kroese ABA (2004) Hyperexcitability of cultured spinal motoneurons from presymptomatic ALS mice. J Neurophysiol 91:571–575.

Kuo JJ, Siddique T, Fu R, Heckman CJ (2005) Increased persistent Na (+) current and its effect on excitability in motoneurones cultured from mutant SOD1 mice. The Journal of Physiology 563:843–854.

Lalancette-Hebert M, Sharma A, Lyashchenko AK, Shneider NA (2016) Gamma motor neurons survive and exacerbate alpha motor neuron degeneration in ALS. Proceedings of the National Academy of Sciences.

Larkindale J, Yang W, Hogan PF, Simon CJ, Zhang Y, Jain A, Habeeb-Louks EM, Kennedy A, Cwik VA (2014) Cost of illness for neuromuscular diseases in the United States. Muscle Nerve 49:431–438.

Lawton KJ, Perry WM, Yamaguchi A, Zornik E (2017) Motor Neurons Tune Premotor Activity in a Vertebrate Central Pattern Generator. J Neurosci 37:3264–3275.

Le Bras B, Fréal A, Czarnecki A, Legendre P, Bullier E, Komada M, Brophy PJ, Davenne M, Couraud F (2013) In vivo assembly of the axon initial segment in motor neurons. Brain Struct Funct.

Lee CJ, Labrakakis C, Joseph DJ, MacDermott AB (2004) Functional similarities and differences of AMPA and kainate receptors expressed by cultured rat sensory neurons. Neuroscience 129:35–48.

Leroy F, Lamotte d'Incamps B, Imhoff-Manuel RD, Zytnicki D (2014) Early intrinsic hyperexcitability does not contribute to motoneuron degeneration in amyotrophic lateral sclerosis. Elife 3.

Leroy F, Zytnicki D (2015) Is hyperexcitability really guilty in amyotrophic lateral sclerosis? Neural Regen Res 10:1413–1415.

Lewinski von F, Keller BU (2005) Ca2+, mitochondria and selective motoneuron vulnerability: implications for ALS. Trends Neurosci 28:494–500.

Li M, Ona VO, Guégan C, Chen M, Jackson-Lewis V, Andrews LJ, Olszewski AJ, Stieg PE, Lee JP, Przedborski S, Friedlander RM (2000) Functional role of caspase-1 and caspase-3 in an ALS transgenic mouse model. Science 288:335–339.

Li Y, Balasubramanian U, Cohen D, Zhang P-W, Mosmiller E, Sattler R, Maragakis NJ,

Rothstein JD (2015) A comprehensive library of familial human amyotrophic lateral sclerosis induced pluripotent stem cells. PLoS ONE 10:e0118266.

Liu H, Dai C, Fan Y, Guo B, Ren K, Sun T, Wang W (2017) From autophagy to mitophagy: the roles of P62 in neurodegenerative diseases. J Bioenerg Biomembr 49:413–422.

Liu J, Lillo C, Jonsson PA, Vande Velde C, Ward CM, Miller TM, Subramaniam JR, Rothstein JD, Marklund S, Andersen PM, Brännström T, Gredal O, Wong PC, Williams DS, Cleveland DW (2004) Toxicity of familial ALS-linked SOD1 mutants from selective recruitment to spinal mitochondria. Neuron 43:5–17.

Longair MH, Baker DA, Armstrong JD (2011) Simple Neurite Tracer: open source software for reconstruction, visualization and analysis of neuronal processes. Bioinformatics 27:2453–2454.

Lorenzo L-E, Barbe A, Portalier P, Fritschy J-M, Bras H (2006) Differential expression of GABAA and glycine receptors in ALS-resistant vs. ALS-vulnerable motoneurons: possible implications for selective vulnerability of motoneurons. Eur J Neurosci 23:3161–3170.

Lorincz A, Nusser Z (2008) Cell-type-dependent molecular composition of the axon initial segment. J Neurosci 28:14329–14340.

Lutz C (2018) Mouse models of ALS: Past, present and future. Brain Res 1693:1–10.

Lüthi A, McCormick DA (1998) H-current: properties of a neuronal and network pacemaker. Neuron 21:9–12.

Macefield VG, Gandevia SC, Bigland-Ritchie B, Gorman RB, Burke D (1993) The firing rates of human motoneurones voluntarily activated in the absence of muscle afferent feedback. The Journal of Physiology 471:429–443.

Magee JC, Christofi G, Miyakawa H, Christie B, Lasser-Ross N, Johnston D (1995) Subthreshold synaptic activation of voltage-gated Ca2+ channels mediates a localized Ca2+ influx into the dendrites of hippocampal pyramidal neurons. J Neurophysiol 74:1335–1342.

Maier A, DeSantis M, Eldred E (1974) The occurrence of muscle spindles in extraocular muscles of various vertebrates. Journal of Morphology 143:397–408.

Malmivuo J, Plonsey R (1995) Bioelectromagnetism. Oxford University Press, USA.

Martin E, Cazenave W, Cattaert D, Branchereau P (2013) Embryonic alteration of motoneuronal morphology induces hyperexcitability in the mouse model of amyotrophic lateral sclerosis. Neurobiology of Disease 54:116–126.

Martin LJ (2010) Mitochondrial and Cell Death Mechanisms in Neurodegenerative Diseases. Pharmaceuticals (Basel) 3:839–915.

Martin LJ, Chang Q (2012) Inhibitory synaptic regulation of motoneurons: a new target of disease mechanisms in amyotrophic lateral sclerosis. Mol Neurobiol 45:30–42.

Martin LJ, Liu Z, Chen K, Price AC, Pan Y, Swaby JA, Golden WC (2007) Motor neuron degeneration in amyotrophic lateral sclerosis mutant superoxide dismutase-1 transgenic mice: mechanisms of mitochondriopathy and cell death. The Journal of Comparative Neurology 500:20–46.

Martinez-Silva M de L, Imhoff-Manuel RD, Sharma A, Heckman CJ, Shneider NA, Roselli F, Zytnicki D, Manuel M (2018) Hypoexcitability precedes denervation in the large fast-contracting motor units in two unrelated mouse models of ALS. Elife 7.

Mattiazzi M, D'Aurelio M, Gajewski CD, Martushova K, Kiaei M, Beal MF, Manfredi G (2002) Mutated human SOD1 causes dysfunction of oxidative phosphorylation in mitochondria of transgenic mice. J Biol Chem 277:29626–29633.

McGown A, McDearmid JR, Panagiotaki N, Tong H, Mashhadi Al S, Redhead N, Lyon AN, Beattie CE, Shaw PJ, Ramesh TM (2013) Early interneuron dysfunction in ALS: insights from a mutant sod1 zebrafish model. Annals of Neurology 73:246–258.

Meehan CF, Moldovan M, Marklund SL, Graffmo KS, Nielsen JB, Hultborn H (2010) Intrinsic properties of lumbar motor neurones in the adult G127insTGGG superoxide dismutase-1 mutant mouse in vivo: evidence for increased persistent inward currents. Acta Physiol (Oxf) 200:361–376.

Meijering E, Jacob M, Sarria J-CF, Steiner P, Hirling H, Unser M (2004) Design and validation of a tool for neurite tracing and analysis in fluorescence microscopy images. Cytometry A 58:167–176.

Miles GB, Yohn DC, Wichterle H, Jessell TM, Rafuse VF, Brownstone RM (2004) Functional properties of motoneurons derived from mouse embryonic stem cells. J Neurosci 24:7848–7858.

Miller RG, Bouchard JP, Duquette P, Eisen A, Gelinas D, Harati Y, Munsat TL, Powe L, Rothstein J, Salzman P, Sufit RL (1996) Clinical trials of riluzole in patients with ALS. ALS/Riluzole Study Group-II. Neurology 47:S86–90–discussionS90–2.

Mitra P, Brownstone RM (2012) An in vitro spinal cord slice preparation for recording from lumbar motoneurons of the adult mouse. J Neurophysiol 107:728–741.

Molinari M (2009) Plasticity properties of CPG circuits in humans: impact on gait recovery. Brain Res Bull 78:22–25.

Monster AW, Chan H, O'Connor D (1978) Activity patterns of human skeletal muscles: relation to muscle fiber type composition. Science 200:314–317.

MOORE JW, Stockbridge N, Westerfield M (1983) On the site of impulse initiation in a neurone. The Journal of Physiology 336:301–311.

Morita D, Rah JC, Isaac JTR (2013) Incorporation of inwardly rectifying AMPA receptors at silent synapses during hippocampal long-term potentiation. Philosophical Transactions of the Royal Society B: Biological Sciences 369:20130156–20130156.

Muir J, Kittler JT (2014) Plasticity of GABAA receptor diffusion dynamics at the axon initial

segment. Front Cell Neurosci 8:151.

Muller FL, Song W, Liu Y, Chaudhuri A, Pieke-Dahl S, Strong R, Huang T-T, Epstein CJ, Roberts LJ, Csete M, Faulkner JA, Van Remmen H (2006) Absence of CuZn superoxide dismutase leads to elevated oxidative stress and acceleration of age-dependent skeletal muscle atrophy. Free Radic Biol Med 40:1993–2004.

Muratore CR, Srikanth P, Callahan DG, Young-Pearse TL (2014) Comparison and optimization of hiPSC forebrain cortical differentiation protocols. PLoS ONE 9:e105807.

Murphy PR, Martin HA (1993) Fusimotor discharge patterns during rhythmic movements. Trends Neurosci 16:273–278.

Müller D, Cherukuri P, Henningfeld K, Poh CH, Wittler L, Grote P, Schlüter O, Schmidt J, Laborda J, Bauer SR, Brownstone RM, Marquardt T (2014) Dlk1 promotes a fast motor neuron biophysical signature required for peak force execution. Science 343:1264–1266.

NARAHASHI T, MOORE JW, SCOTT WR (1964) TETRODOTOXIN BLOCKAGE OF SODIUM CONDUCTANCE INCREASE IN LOBSTER GIANT AXONS. J Gen Physiol 47:965–974.

Nicholls DG (2002) Mitochondrial function and dysfunction in the cell: its relevance to aging and aging-related disease. Int J Biochem Cell Biol 34:1372–1381.

Niechwiej-Szwedo E, González E, Bega S, Verrier MC, Wong AM, Steinbach MJ (2006) Proprioceptive role for palisade endings in extraocular muscles: evidence from the Jendrassik Maneuver. Vision Res 46:2268–2279.

Nieto-Gonzalez JL, Moser J, Lauritzen M, Schmitt-John T, Jensen K (2011) Reduced GABAergic inhibition explains cortical hyperexcitability in the wobbler mouse model of ALS. Cereb Cortex 21:625–635.

Nihei K, McKee AC, Kowall NW (1993) Patterns of neuronal degeneration in the motor cortex of amyotrophic lateral sclerosis patients. Acta Neuropathologica 86:55–64.

Nijhout HF, Best J, Reed MC (2014) Escape from homeostasis. Math Biosci 257:104–110.

Nijssen J, Comley LH, Hedlund E (2017) Motor neuron vulnerability and resistance in amyotrophic lateral sclerosis. Acta Neuropathologica 133:863–885.

Nimchinsky EA, Young WG, Yeung G, Shah RA, Gordon JW, Bloom FE, Morrison JH, Hof PR (2000) Differential vulnerability of oculomotor, facial, and hypoglossal nuclei in G86R superoxide dismutase transgenic mice. The Journal of Comparative Neurology 416:112–125.

Nishimura K, Ohta M, Saito M, Morita-Isogai Y, Sato H, Kuramoto E, Yin DX, Maeda Y, Kaneko T, Yamashiro T, Takada K, Oh SB, Toyoda H, Kang Y (2018) Electrophysiological and Morphological Properties of α and γ Motoneurons in the Rat Trigeminal Motor Nucleus. Front Cell Neurosci 12:9.

O'Reilly PM, FitzGerald MJ (1990) Fibre composition of the hypoglossal nerve in the rat. J Anat 172:227–243.

Oeckl P et al. (2018) Different neuroinflammatory profile in amyotrophic lateral sclerosis and frontotemporal dementia is linked to the clinical phase. J Neurol Neurosurg Psychiatr 90:4–10.

Olney JW (1969) Brain lesions, obesity, and other disturbances in mice treated with monosodium glutamate. Science 164:719–721.

Oskarsson B, Gendron TF, Staff NP (2018) Amyotrophic Lateral Sclerosis: An Update for 2018. Mayo Clin Proc 93:1617–1628.

Pambo-Pambo A, Durand J, Gueritaud J-P (2009) Early excitability changes in lumbar motoneurons of transgenic SOD1G85R and SOD1G (93A-Low) mice. J Neurophysiol 102:3627–3642.

Paré B, Lehmann M, Beaudin M, Nordström U, Saikali S, Julien J-P, Gilthorpe JD, Marklund SL, Cashman NR, Andersen PM, Forsberg K, Dupré N, Gould P, Brännström T, Gros-Louis F (2018) Misfolded SOD1 pathology in sporadic Amyotrophic Lateral Sclerosis. Sci Rep 8:14223.

Parone PA, Da Cruz S, Han JS, McAlonis-Downes M, Vetto AP, Lee SK, Tseng E, Cleveland DW (2013) Enhancing Mitochondrial Calcium Buffering Capacity Reduces Aggregation of Misfolded SOD1 and Motor Neuron Cell Death without Extending Survival in Mouse Models of Inherited Amyotrophic Lateral Sclerosis. Journal of Neuroscience 33:4657–4671.

Personius KE, Balice-Gordon RJ (2001) Loss of correlated motor neuron activity during synaptic competition at developing neuromuscular synapses. Neuron 31:395–408.

Peters T, Kubis HP, Wetzel P, Sender S, Asmussen G, Fons R, Jürgens KD (1999) Contraction parameters, myosin composition and metabolic enzymes of the skeletal muscles of the etruscan shrew Suncus etruscus and of the common European white-toothed shrew Crocidura russula (Insectivora: soricidae). J Exp Biol 202:2461–2473.

Pfanner N, Craig EA, Hönlinger A (1997) Mitochondrial preprotein translocase. Annu Rev Cell Dev Biol 13:25–51.

Pieri M, Albo F, Gaetti C, Spalloni A, Bengtson CP, Longone P, Cavalcanti S, Zona C (2003) Altered excitability of motor neurons in a transgenic mouse model of familial amyotrophic lateral sclerosis. Neurosci Lett 351:153–156.

Pieri M, Carunchio I, Curcio L, Mercuri NB, Zona C (2009) Increased persistent sodium current determines cortical hyperexcitability in a genetic model of amyotrophic lateral sclerosis. Exp Neurol 215:368–379.

Pinter MJ, Curtis RL, Hosko MJ (1983) Voltage threshold and excitability among variously sized cat hindlimb motoneurons. J Neurophysiol 50:644–657.

Prescott SA, De Koninck Y, Sejnowski TJ (2008) Biophysical basis for three distinct dynamical mechanisms of action potential initiation. PLoS Comput Biol 4:e1000198.

Prochazka A, Hulliger M, Zangger P, Appenteng K (1985) “Fusimotor set”: new evidence for alpha-independent control of gamma-motoneurones during movement in the awake cat.

Brain Res 339:136–140.

Pun S, Santos AF, Saxena S, Xu L, Caroni P (2006) Selective vulnerability and pruning of phasic motoneuron axons in motoneuron disease alleviated by CNTF. Nat Neurosci 9:408–419.

Quinlan KA, Lamano JB, Samuels J, Heckman CJ (2015) Comparison of dendritic calcium transients in juvenile wild type and SOD1 (G93A) mouse lumbar motoneurons. Front Cell Neurosci 9:139.

Quinlan KA, Schuster JE, Fu R, Siddique T, Heckman CJ (2011) Altered postnatal maturation of electrical properties in spinal motoneurons in a mouse model of amyotrophic lateral sclerosis. The Journal of Physiology 589:2245–2260.

Rakhit R, Crow JP, Lepock JR, Kondejewski LH, Cashman NR, Chakrabartty A (2004) Monomeric Cu,Zn-superoxide dismutase is a common misfolding intermediate in the oxidation models of sporadic and familial amyotrophic lateral sclerosis. J Biol Chem 279:15499–15504.

Rasband MN (2010) The axon initial segment and the maintenance of neuronal polarity. Nat Rev Neurosci 11:552–562.

Re DB, Le Verche V, Yu C, Amoroso MW, Politi KA, Phani S, Ikiz B, Hoffmann L, Koolen M, Nagata T, Papadimitriou D, Nagy P, Mitsumoto H, Kariya S, Wichterle H, Henderson CE, Przedborski S (2014) Necroptosis Drives Motor Neuron Death in Models of Both Sporadic and Familial ALS. Neuron 81:1001–1008.

Reaume AG, Elliott JL, Hoffman EK, Kowall NW, Ferrante RJ, Siwek DF, Wilcox HM, Flood DG, Beal MF, Brown RH, Scott RW, Snider WD (1996) Motor neurons in Cu/Zn superoxide dismutase-deficient mice develop normally but exhibit enhanced cell death after axonal injury. Nat Genet 13:43–47.

Reiner A, Medina L, Figueredo-Cardenas G, Anfinson S (1995) Brainstem motoneuron pools that are selectively resistant in amyotrophic lateral sclerosis are preferentially enriched in parvalbumin: evidence from monkey brainstem for a calcium-mediated mechanism in sporadic ALS. Exp Neurol 131:239–250.

Rekling JC, Funk GD, Bayliss DA, Dong XW, Feldman JL (2000) Synaptic control of motoneuronal excitability. Physiol Rev 80:767–852.

Robinson DA (1970) Oculomotor Unit Behavior in the Monkey. J Neurophysiol 33:393–403.

Rothstein JD (2009) Current hypotheses for the underlying biology of amyotrophic lateral sclerosis. Annals of Neurology 65 Suppl 1:S3–S9.

Rothstein JD, Martin LJ, Kuncl RW (1992) Decreased glutamate transport by the brain and spinal cord in amyotrophic lateral sclerosis. N Engl J Med 326:1464–1468.

Rothstein JD, Tsai G, Kuncl RW, Clawson L, Cornblath DR, Drachman DB, Pestronk A, Stauch BL, Coyle JT (1990) Abnormal Excitatory Armno Acid Metabolism in Amyotrophc Lateral Sclerosis. Annals of Neurology 28:18–25.

Rudnick ND, Griffey CJ, Guarnieri P, Gerbino V, Wang X, Piersaint JA, Tapia JC, Rich MM, Maniatis T (2017) Distinct roles for motor neuron autophagy early and late in the SOD1 (G93A) mouse model of ALS. Proceedings of the National Academy of Sciences 114:E8294–E8303.

Saba L, Viscomi MT, Caioli S, Pignataro A, Bisicchia E, Pieri M, Molinari M, Ammassari-Teule M, Zona C (2016) Altered Functionality, Morphology, and Vesicular Glutamate Transporter Expression of Cortical Motor Neurons from a Presymptomatic Mouse Model of Amyotrophic Lateral Sclerosis. Cereb Cortex 26:1512–1528.

Saito M, Tomonaga M, Narabayashi H (1978) Histochemical study of the muscle spindles in parkinsonism, motor neuron disease and myasthenia. An examination of the pathological fusimotor endings by the acetylcholinesterase technic. J Neurol 219:261–271.

Sareen D et al. (2013) Targeting RNA foci in iPSC-derived motor neurons from ALS patients with a C9ORF72 repeat expansion. Sci Transl Med 5:208ra149.

Sasaki S, Iwata M (1996) Ultrastructural study of the synapses of central chromatolytic anterior horn cells in motor neuron disease. J Neuropathol Exp Neurol 55:932–939.

Sasaki S, Maruyama S (1992) Increase in diameter of the axonal initial segment is an early change in amyotrophic lateral sclerosis. J Neurol Sci 110:114–120.

Sasaki S, Warita H, Abe K, Iwata M (2005) Impairment of axonal transport in the axon hillock and the initial segment of anterior horn neurons in transgenic mice with a G93A mutant SOD1 gene. Acta Neuropathologica 110:48–56.

Sasaki S, Warita H, Komori T, Murakami T, Abe K, Iwata M (2006) Parvalbumin and calbindin D-28k immunoreactivity in transgenic mice with a G93A mutant SOD1 gene. Brain Res 1083:196–203.

Saxena S, Cabuy E, Caroni P (2009) A role for motoneuron subtype–selective ER stress in disease manifestations of FALS mice. Nat Neurosci 12:627–636.

Schafer DP, Jha S, Liu F, Akella T, McCullough LD, Rasband MN (2009) Disruption of the axon initial segment cytoskeleton is a new mechanism for neuronal injury. J Neurosci 29:13242–13254.

Schindelin J, Arganda-Carreras I, Frise E, Kaynig V, Longair M, Pietzsch T, Preibisch S, Rueden C, Saalfeld S, Schmid B, Tinevez J-Y, White DJ, Hartenstein V, Eliceiri K, Tomancak P, Cardona A (2012) Fiji: an open-source platform for biological-image analysis. Nat Methods 9:676–682.

Seeburg PH (1993) The TiPS/TINS lecture: the molecular biology of mammalian glutamate receptor channels. Trends Pharmacol Sci 14:297–303.

Sen I, Nalini A, Joshi NB, Joshi PG (2005) Cerebrospinal fluid from amyotrophic lateral sclerosis patients preferentially elevates intracellular calcium and toxicity in motor neurons via AMPA/kainate receptor. J Neurol Sci 235:45–54.

Shneider NA, Brown MN, Smith CA, Pickel J, Alvarez FJ (2009) Gamma motor neurons

express distinct genetic markers at birth and require muscle spindle-derived GDNF for postnatal survival. Neural Dev 4:42.

Song A-H, Wang D, Chen G, Li Y, Luo J, Duan S, Poo M-M (2009) A selective filter for cytoplasmic transport at the axon initial segment. Cell 136:1148–1160.

Sternfeld MJ, Hinckley CA, Moore NJ, Pankratz MT, Hilde KL, Driscoll SP, Hayashi M, Amin ND, Bonanomi D, Gifford WD, Sharma K, Goulding M, Pfaff SL (2017) Speed and segmentation control mechanisms characterized in rhythmically-active circuits created from spinal neurons produced from genetically-tagged embryonic stem cells. Elife 6.

Stifani N (2014) Motor neurons and the generation of spinal motor neuron diversity. Front Cell Neurosci 8:293.

Sugiyama K, Tanaka K (2018) Spinal cord-specific deletion of the glutamate transporter GLT1 causes motor neuron death in mice. Biochem Biophys Res Commun 497:689–693.

Sun X, Wu Y, Gu M, Liu Z, Ma Y, Li J, Zhang Y (2014a) Selective filtering defect at the axon initial segment in Alzheimer's disease mouse models. Proceedings of the National Academy of Sciences 111:14271–14276.

Sun X, Wu Y, Gu M, Zhang Y (2014b) miR-342-5p Decreases Ankyrin G Levels in Alzheimer's Disease Transgenic Mouse Models. Cell Rep.

Swash M, Fox KP (1974) The pathology of the human muscle spindle: effect of denervation. J Neurol Sci 22:1–24.

Swinnen B, Robberecht W (2014) The phenotypic variability of amyotrophic lateral sclerosis. Nat Rev Neurol 10:661–670.

Tang X, Zhou L, Wagner AM, Marchetto MCN, Muotri AR, Gage FH, Chen G (2013) Astroglial cells regulate the developmental timeline of human neurons differentiated from induced pluripotent stem cells. Stem Cell Res 11:743–757.

Thams S, Lowry ER, Larraufie M-H, Spiller KJ, Li H, Williams DJ, Hoang P, Jiang E, Williams LA, Sandoe J, Eggan K, Lieberam I, Kanning KC, Stockwell BR, Henderson CE, Wichterle H (2018) A Stem Cell-Based Screening Platform Identifies Compounds that Desensitize Motor Neurons to Endoplasmic Reticulum Stress. Mol Ther.

Turner BJ, Lopes EC, Cheema SS (2003) Neuromuscular accumulation of mutant superoxide dismutase 1 aggregates in a transgenic mouse model of familial amyotrophic lateral sclerosis. Neurosci Lett 350:132–136.

Turner BJ, Talbot K (2008) Transgenics, toxicity and therapeutics in rodent models of mutant SOD1-mediated familial ALS. Prog Neurobiol 85:94–134.

Turner MR, Bowser R, Bruijn L, Dupuis L, Ludolph A, McGrath M, Manfredi G, Maragakis N, Miller RG, Pullman SL, Rutkove SB, Shaw PJ, Shefner J, Fischbeck KH (2013) Mechanisms, models and biomarkers in amyotrophic lateral sclerosis. Amyotroph Lateral Scler Frontotemporal Degener 14 Suppl 1:19–32.

Urban PP, Vogt T, Hopf HC (1998) Corticobulbar tract involvement in amyotrophic lateral sclerosis. Brain 121:1099–1108.

van Zundert B, Izaurieta P, Fritz E, Alvarez FJ (2012) Early pathogenesis in the adult-onset neurodegenerative disease amyotrophic lateral sclerosis. Journal of Cellular Biochemistry 113:3301–3312.

van Zundert B, Peuscher MH, Hynynen M, Chen A, Neve RL, Brown RH, Constantine-Paton M, Bellingham MC (2008) Neonatal neuronal circuitry shows hyperexcitable disturbance in a mouse model of the adult-onset neurodegenerative disease amyotrophic lateral sclerosis. J Neurosci 28:10864–10874.

Vande Velde C, Miller TM, Cashman NR, Cleveland DW (2008) Selective association of misfolded ALS-linked mutant SOD1 with the cytoplasmic face of mitochondria. Proceedings of the National Academy of Sciences 105:4022–4027.

Vanselow BK, Keller BU (2000) Calcium dynamics and buffering in oculomotor neurones from mouse that are particularly resistant during amyotrophic lateral sclerosis (ALS)-related motoneurone disease. The Journal of Physiology 525 Pt 2:433–445.

Venugopal S, Hsiao C-F, Sonoda T, Wiedau-Pazos M, Chandler SH (2015a) Homeostatic dysregulation in membrane properties of masticatory motoneurons compared with oculomotor neurons in a mouse model for amyotrophic lateral sclerosis. J Neurosci 35:707–720.

Venugopal S, Wiedau-Pazos M, Chandler SH (2015b) Early dysregulation of trigeminal motor poolexcitability in a mouse model forneurodegenerative motoneuron disease. BMC Neurosci 16:P31.

Vijayvergiya C, Beal MF, Buck J, Manfredi G (2005) Mutant superoxide dismutase 1 forms aggregates in the brain mitochondrial matrix of amyotrophic lateral sclerosis mice. J Neurosci 25:2463–2470.

Vinsant S, Mansfield C, Jimenez-Moreno R, Del Gaizo Moore V, Yoshikawa M, Hampton TG, Prevette D, Caress J, Oppenheim RW, Milligan C (2013) Characterization of early pathogenesis in the SOD1 (G93A) mouse model of ALS: part II, results and discussion. Brain Behav 3:431–457.

Vucic S, Nicholson GA, Kiernan MC (2008) Cortical hyperexcitability may precede the onset of familial amyotrophic lateral sclerosis. Brain 131:1540–1550.

Vucic S, Rothstein JD, Kiernan MC (2014) Advances in treating amyotrophic lateral sclerosis: insights from pathophysiological studies. Trends Neurosci 37:433–442.

Vucic S, Ziemann U, Eisen A, Hallett M, Kiernan MC (2013) Transcranial magnetic stimulation and amyotrophic lateral sclerosis: pathophysiological insights. J Neurol Neurosurg Psychiatr 84:1161–1170.

Wainger BJ, Kiskinis E, Mellin C, Wiskow O, Han SSW, Sandoe J, Perez NP, Williams LA, Lee S, Boulting G, Berry JD, Brown RH, Cudkowicz ME, Bean BP, Eggan K, Woolf CJ (2014) Intrinsic Membrane Hyperexcitability of Amyotrophic Lateral Sclerosis Patient-Derived Motor

Neurons. Cell Rep.

Wang J, Xu G, Borchelt DR (2002) High molecular weight complexes of mutant superoxide dismutase 1: age-dependent and tissue-specific accumulation. Neurobiology of Disease 9:139–148.

Watts CR, Vanryckeghem M (2001) Laryngeal dysfunction in Amyotrophic Lateral Sclerosis: a review and case report. BMC Ear Nose Throat Disord 1:1.

Wefelmeyer W, Cattaert D, Burrone J (2015) Activity-dependent mismatch between axo-axonic synapses and the axon initial segment controls neuronal output. Proceedings of the National Academy of Sciences 112:9757–9762.

Whitehead J, Keller-Peck C, Kucera J, Tourtellotte WG (2005) Glial cell-line derived neurotrophic factor-dependent fusimotor neuron survival during development. Mech Dev 122:27–41.

Whitney NP, Peng H, Erdmann NB, Tian C, Monaghan DT, Zheng JC (2008) Calcium-permeable AMPA receptors containing Q/R-unedited GluR2 direct human neural progenitor cell differentiation to neurons. The FASEB Journal 22:2888–2900.

Wichterle H, Lieberam I, Porter JA, Jessell TM (2002) Directed Differentiation of Embryonic Stem Cells into Motor Neurons. Cell.

Wichterle H, Peljto M (2008) Differentiation of mouse embryonic stem cells to spinal motor neurons. Curr Protoc Stem Cell Biol Chapter 1:Unit1H.1.1–1H.1.9.

Witts EC, Zagoraiou L, Miles GB (2014) Anatomy and function of cholinergic C bouton inputs to motor neurons. J Anat 224:52–60.

Wong PC, Pardo CA, Borchelt DR, Lee MK, Copeland NG, Jenkins NA, Sisodia SS, Cleveland DW, Price DL (1995) An adverse property of a familial ALS-linked SOD1 mutation causes motor neuron disease characterized by vacuolar degeneration of mitochondria. Neuron 14:1105–1116.

Wootz H, Enjin A, Wallén-Mackenzie A, Lindholm D, Kullander K (2010) Reduced VGLUT2 expression increases motor neuron viability in Sod1 (G93A) mice. Neurobiology of Disease 37:58–66.

Wootz H, Fitzsimons-Kantamneni E, Larhammar M, Rotterman TM, Enjin A, Patra K, André E, van Zundert B, Kullander K, Alvarez FJ (2013) Alterations in the motor neuron-renshaw cell circuit in the Sod1 (G93A) mouse model. The Journal of Comparative Neurology 521:1449–1469.

Xu H, Sakiyama-Elbert SE (2015) Directed Differentiation of V3 Interneurons from Mouse Embryonic Stem Cells. Stem Cells Dev 24:2723–2732.

Yang Y, Ogawa Y, Hedstrom KL, Rasband MN (2007) betaIV spectrin is recruited to axon initial segments and nodes of Ranvier by ankyrinG. J Cell Biol 176:509–519.

Yoshimura T, Rasband MN (2014) Axon initial segments: diverse and dynamic neuronal

compartments. Curr Opin Neurobiol 27C:96–102.

Yue Z-W, Wang Y-L, Xiao B, Feng L (2018) Axon Initial Segment Structural Plasticity is Involved in Seizure Susceptibility in a Rat Model of Cortical Dysplasia. Neurochem Res 43:878–885.

Zang DW, Lopes EC, Cheema SS (2005) Loss of synaptophysin-positive boutons on lumbar motor neurons innervating the medial gastrocnemius muscle of the SOD1G93A G1H transgenic mouse model of ALS. J Neurosci Res 79:694–699.

Zang DW, Yang Q, Wang HX, Egan G, Lopes EC, Cheema SS (2004) Magnetic resonance imaging reveals neuronal degeneration in the brainstem of the superoxide dismutase 1 transgenic mouse model of amyotrophic lateral sclerosis. Eur J Neurosci 20:1745–1751.

Zengel JE, Reid SA, Sypert GW, Munson JB (1985) Membrane electrical properties and prediction of motor-unit type of medial gastrocnemius motoneurons in the cat. J Neurophysiol 53:1323–1344.

Zhou D, Lambert S, Malen PL, Carpenter S, Boland LM, Bennett V (1998) AnkyrinG is required for clustering of voltage-gated Na channels at axon initial segments and for normal action potential firing. J Cell Biol 143:1295–1304.

Zhu C, Beck MV, Griffith JD, Deshmukh M, Dokholyan NV (2018) Large SOD1 aggregates, unlike trimeric SOD1, do not impact cell viability in a model of amyotrophic lateral sclerosis. Proceedings of the National Academy of Sciences 115:4661–4665.